Deciphering the Toxicity Effects of 5′-Methylthioadenosine Accumulation in *Arabidopsis thaliana*

by

SAEER AHMAD ADEEL

A thesis
presented to the University of Waterloo
in fulfillment of the
thesis requirement for the degree of
Master of Science
in
Biology

Waterloo, Ontario, Canada, 2021

© Saeer Ahmad Adeel 2021

Author's Declaration

I hereby declare that I am the sole author of this thesis. This is a true copy of the thesis, including any required final revisions, as accepted by my examiners.

I understand that my thesis may be made electronically available to the public.

Abstract

Metabolic constraints imposed by extreme environmental fluctuations are an inescapable reality for sessile organisms such as plants. To survive, they finely tune their metabolic activity to adapt their growth to the surrounding environment. For example, plants couple photosynthesis with the assimilation of sulfate into cysteine, methionine, and S-adenosylmethionine (SAM). They also effectively recycle the sulfur-containing by-product 5′-methylthioadenosine (MTA), which arises from SAM-dependent reactions using MTA nucleosidase (MTN). *Arabidopsis thaliana* mutants deficient in MTN activity have numerous developmental and metabolic abnormalities due to MTA accumulation. In an attempt to understand the molecular basis of this complex phenotype, a genetic screen was carried out using the single mutant, *mtn1-1*. This mutant develops a short root phenotype when grown with MTA as the sole sulfur source, and this screen aims to find genetic changes that suppress this phenotype. By identifying and characterizing the dominant genetic suppressor, this study seeks to detail the physiological impacts of MTA accumulation.

The mutation, designated as *MTA RESISTANT 11* (*mtar11*), is located in a transcription factor, bZIP29. This transcription factor regulates a plethora of processes in plant development, including genes involved in stress, osmosensory responses, and several core cell cycle genes. bZIP29's genetic targets are defined by its interaction with other proteins like the TOR complex and other bZIPs resulting in a pleiotropic regulation of plant growth. This suppressor mutant suggests the overall down-regulation of growth caused by MTA accumulation.

In addition to overcoming the MTA metabolic pressure, the *mtar11* mutation results in the increase of plant growth and fertility in the *mtn1-1* background. *mtar11* was also commonly found in domesticated plants after a preliminary assessment of its conservation. These two findings led to a more detailed investigation revealing that the *mtar11* mutation is more associated with domesticated species. In fact, non-conservative amino acid changes at several other residues within bZIP29 were also associated with domesticated species. A phylogenetic analysis of the 461 homologs of bZIP29 and the 173 plant species these homologs belong to uncovered several instances of independent evolution of these residues and lateral gene transfers. Both these findings reveal a novel evolutionary pressure behind bZIP29.

Furthermore, *mtn1-1mtn2-1mtar11* plants recover the low TOR activity of the double mutant while significantly increasing it compared to WT. The lack of TOR activity in the double mutant indicates that the majority of growth defects from MTA accumulation arise from the impairment of TOR signaling in plant development. This finding also suggests a novel interaction between bZIP29 and the TOR complex in growth regulation, mostly restricting cell proliferation.

The results gathered in this work are assembled into a model that seeks to explain the effects of MTA accumulation on plant physiology. The detailed analysis of *mtar11* has revealed further complexity to the tight coordination between plant productivity and sulfur metabolism.

Acknowledgements

First and foremost, I would like Dr. Barbara Moffatt and Dr. Andrew Doxey for taking a chance on me as a student and allowing me to pursue my love of biology. Barb, you have been a wonderful mentor in my life and my science career. You have provided me with every opportunity to branch out in our field, encouraged me to attend conferences, and gave me the confidence to present my work outside our bubble. While my ideas have not always been well thought out or coherent, you still listened, considered my ideas, troubleshot experiments, and have been a tremendous help editing and providing feedback on this thesis.

Andrew, you have been a tremendous mentor ever since you were my second reader for my 499. Thank you for all your support, especially when I thought I was not moving forward with my bioinformatics projects. You always took time out of your busy schedule to discuss ideas and problems. I would also like to thank you for being so inclusive with your lab resources and computer infrastructure, which I utilized many times during my project. Thank you for allowing me into your lab group and develop friendships I cherish today.

Thank you to Dr. Susan Lolle for igniting my passion for science back when you took a chance on me as a 499 student. You provided me with my first opportunity to be a part of a special project and introduced me to many members of our department, including Barb and Andrew. Thank you for being instrumental in my development as a biologist and for the guidance and support you have provided me.

Thank you to Dr. Simon Chuong for always being willing to teach my new techniques and providing guidance on the many facets of plant physiology. Your advice and support allowed me to pursue many histological experiments that proved crucial in understanding our complex mutants.

I am also grateful for my collaborators, Drs. Yihan Dong (University of Strasbourg, Institut de Biologie Moléculaire des Plantes) and Neil Emery and Anna Kisiała (Trent University, Peterborough, Canada). Thank you, Dr. Dong, for performing the TOR assays that proved critical to my work and your helpful insights into TOR signaling and its regulation of the cell cycle. Thank you to Drs. Emery and Kisiała for performing and assisting me in

profiling the phytohormones of the MTN-deficient mutants. Your insights into metabolomics and hormone measurements were invaluable and vital in understanding our mutants.

Next, I would like to thank a few faculty members that have helped me. Thank you, Dr. Barbara Katzenback, for allowing me to use both your qPCR machine and helping me with my flow cytometry experiment. My experiments always took a long time, but you always supported them, so thank you. Thank you to Dr. Bruce Reed and Dr. Mungo Marsden for allowing me to use your microscopes, and the education on microscopy was priceless. Finally, thank you to Dr. Vivan Choh (Optometry) for allowing me to use your lab and equipment to section my tissue. Thank you for helping me troubleshot my experiments on the vibratome.

I am also very grateful to Benjamin Tremblay for guiding me early in my Master's and for the constant support. Much of my project is attributed to your fine work at the Moffatt lab, and I thank you for all the advice you have given me these past few years.

I would not have accomplished what I had without the support and contributions of the many lab members of the Moffatt Lab. Thank you to Fanxi Dong, Jiyoung Shin, Allison Szenasi, and Johnny Alkhoury for being the constant in the lab and helping me with a lot of the grunt work involved in my project. Much of the results I report in this thesis were because of your hard work. Thank you to Kyle Symonds, John Steele, Vlad Bularca, Patrick Cort, Isabelle Simpson, and Kelvin Chang for taking up some of my projects and progressing them to a place I could not have done independently.

Thank you to my friends and colleagues for supporting me and providing me a life outside the lab. Thank you to Amanda Clark, Nilanth Yogadasan, Therese Francom, Alyssa Overton, Delaney Nash, Dr. Michael Mansfield, Quinn Abram, and many others.

Finally, thank you to my family for your unconditional support and for providing me an escape outside of work. I am grateful for all you do for me, especially during this degree, and your unwavering love.

Table of Contents

List of Figures

List of Tables

List of Abbreviations

1/2MS Half-strength Murashige and Skoog.

ABA Abscisic acid.

ACC 1-aminocyclopropane-1-carboxylic acid.

ACL5 ACAULIS 5 EC 2.5.1.79.

ACO 1-aminocyclopropane-1-carboxylic oxidase EC 1.14.17.4.

APR Adenosine 5′-phosphosulfate reductase EC 1.8.99.2.

APS Adenosine 5′-phosphosulfate.

Arabidopsis *Arabidopsis thaliana*.

ARF5 AUXIN RESPONSE FACTOR 5.

ATPS Adenosine 5′-triphosphate sulfurylase EC 2.7.7.4.

BELL BEL1-like.

bZIP29 Basic-Leucine Zipper 29.

CBL Cystathionine β-lyase EC 4.4.1.8.

CDK CYCLIN DEPENDENT KINASE.

CGS Cystathionine γ-synthase EC 4.4.1.1.

CK Cytokinin.

CLV CLAVATA.

CYC Cyclins.

Cys Cysteine.

DAS Days after stratification.

dcSAM Decarboxylate S-adenosylmethionine.

dkml DRINK ME-LIKE.

DP DIMERISATION PARTNER.

eIF2α eukaryotic INITIATION FACTOR 2.

EMS Ethyl methanesulfonate.

FLC FLOWERING LOCUS C.

FT FLOWERING LOCUS T.

GA Gibberellic acid.

GCN2 GENERAL CONTROL NON-REPRESSIBLE 2.

GLS Glucosinolate.

GSH Glutathione.

GUS β-glucuronidase.

HCys Homocysteine.

IAA Indole-3-acetic acid.

IAN Indole-3-acetonitrile.

ITC Isothiocyanates.

LFY LEAFY.

LST8 LETHAL with SEC13 PROTEIN 8.

Met Methionine.

MPK3 Mitogen-Activated Protein Kinase.

MS Methionine synthase EC 2.1.1.13.

MTA 5′-methylthioadenosine.

MTAR 5′-METHYLTHIOADENOSINE RESISTANT.

MTN 5′-methylthioadenosine nucleosidase EC 3.2.2.9.

MTR 5′-methylthioribose.

NA Nicotianamine.

NAS Nicotianamine synthase EC 2.5.1.43.

NSP1 Nitrile-specifier protein 1.

OAS *O*-acetylserine.

PAPS Phosphoadenosine 5′-phosphosulfate.

PCA Principle component analysis.

PCR Polymerase chain reaction.

PNF POUNDFOOLISH.

PNY PENNYWISE.

PYL PYR1/PYL/RCAR.

QC Quiescent center.

RAPTOR Regulatory-associated protein of TOR.

RBR RETINOBLASTOMA-RELATED.

S6K PROTEIN-SERINE KINASE 6.

SAH S-adenosylhomocysteine.

SAM S-adenosylmethionine.

SIR Sulfite reductase EC 1.8.7.1.

SMR SIAMESE-RELATED.

SNP Single nucleotide polymorphisms.

SnRK2 SUC NON-FERMENTING 1-RELATED KINASE 2.

SOC1 SUPPRESSOR OF OVEREXPRESSION OF CONSTANS1.

Spd Spermidine.

SPDS Spermidine synthase EC 2.5.1.16.

Spm Spermine.

SPMS Spermine synthase EC 2.5.1.16.

STM SHOOT MERISTEMLESS.

TOR TARGET OF RAPAMYCIN.

TORC TOR complex.

TSF TWIN SISTER OF FT.

Tspm Thermospermine.

VIP1 VirE2-interacting protein 1.

WGS Whole-genome sequencing.

WOX5 WUSCHEL-RELATED HOMEOBOX 5.

WT Wild type.

WUS WUSCHEL.

YAK1 YET ANOTHER KINASE 1.

Chapter 1

General Introduction

1.1 Sulfur assimilation and methionine metabolism

Sulfur is a required element for all life forms, and cycles through the ecosystem in many forms. Unfortunately, environmental fluctuations and extreme shifts of available sulfur are an inescapable reality for sessile organisms such as plants. They have adapted to these fluctuations by coordinating their metabolism and growth to their surrounding environments. To that effect, they play a crucial role as primary producers of organic sulfur compounds and the recycling of elemental sulfur. Furthermore, they synthesize various sulfur-containing metabolites, each with distinct properties and biological functions (Saito, 2004).

Sulfur is present in specific cell wall, and cell membrane sulfolipids forming a substantial part of polar lipids. In addition, plant phytohormones brassinosteroids and jasmonate are both deactivated by sulfation (Gidda et al., 2003). Glucosinolates are also essential secondary sulfur metabolites that act as defense compounds against predators while also being beneficial to humans (Bednarek et al., 2009). Given the importance of sulfur to a plant's physiology, elucidating the contribution of central sulfur metabolism pathways is critical to understanding the links between metabolism and growth in changing environments.

1.1.1 Sulfur assimilation in plants

Sulfate is the most common form of sulfur found in nature. Plants use proton/sulfate symporters to mediate the influx of sulfate into cells (Smith et al., 1995; Gigolashvili and Kopriva, 2014). Once inside a cell, sulfur assimilation begins in the plastid with the activation of sulfate by adenosine 5′-triphosphate sulfurylase (ATPS; EC 2.7.7.4) to form adenosine 5′-phosphosulfate (APS; Figure 1.1). From there, sulfur assimilation takes one of two paths. The first involves the phosphorylation of APS by APS kinase (APK; EC 2.7.1.25) to form phosphoadenosine 5′-phosphosulfate (PAPS). Many sulfation reactions use PAPS as a substrate to synthesize secondary metabolites, including glucosinolate biosynthesis (Figure 1.1). However, APS may also be reduced into sulfite by APS reductase (APR; EC 1.8.99.2), and sulfite is then further reduced to sulfide by ferredoxin-dependent sulfite

reductase (SIR; EC 1.8.7.1). Sulfide is incorporated into O-acetylserine (OAS) to form cysteine (Cys). As a result, Cys biosynthesis is pivotal in understanding sulfur assimilation (Leustek et al., 2000; Takahashi et al., 2011).

The regulation of Cys biosynthesis has been an active area of research as it is considered the central regulator for the entire process of sulfur assimilation. The Cys synthase complex catalyzes the formation of Cys and OAS and acts as a sensor of sulfide in the cell (Wirtz et al., 2004). Multifaceted regulatory signals from this complex result in transcriptional changes to sulfur transport and enzyme activities responsible for sulfate reduction (Wirtz et al., 2004; Wirtz and Hell, 2006). In addition to being the central regulatory element, Cys is the starting point for glutathione (GSH), methionine (Met), and S-adenosylmethionine (SAM) synthesis. Cys and O-phosphohomoserine are then substrates for the synthesis of cystathionine by cystathionine γ-synthase (CGS; EC 4.4.1.1) and subsequently cleaved to produce homocysteine (HCys) by cystathionine β-lyase (CBL; EC 4.4.1.8). Met synthase (MS; EC 2.1.1.13) then methylates HCys to produce Met (Figure 1.2).

1.1.2 Methionine metabolism in plants

Three different biochemical pathways contribute to the *de novo* synthesis of Met: the carbon backbone originates from aspartate, the sulfur atom comes from Cys, and the methyl group from the β-carbon of serine (Mondal et al., 1996). *de novo* synthesis of Met occurs in both the chloroplast and the cytosol (Ravanel et al., 2004).

Met plays many important roles in the biosynthetic processes of macromolecules. In addition to protein synthesis, it serves as the primary methyl donor in many methyltransferase systems through the intermediary of SAM. Since SAM is an energetically costly metabolite, it is regenerated via S-adenosylhomocysteine (SAH) and eventually back into HCys through a series of biochemical reactions conventionally referred to as the SAM cycle (Ravanel et al., 1998; Figure 1.2). A subsequent set of reactions utilize SAM to produce physiologically important metabolites but produce 5′-methylthioadenosine (MTA) as a byproduct rather than SAH (Bürstenbinder et al., 2010).
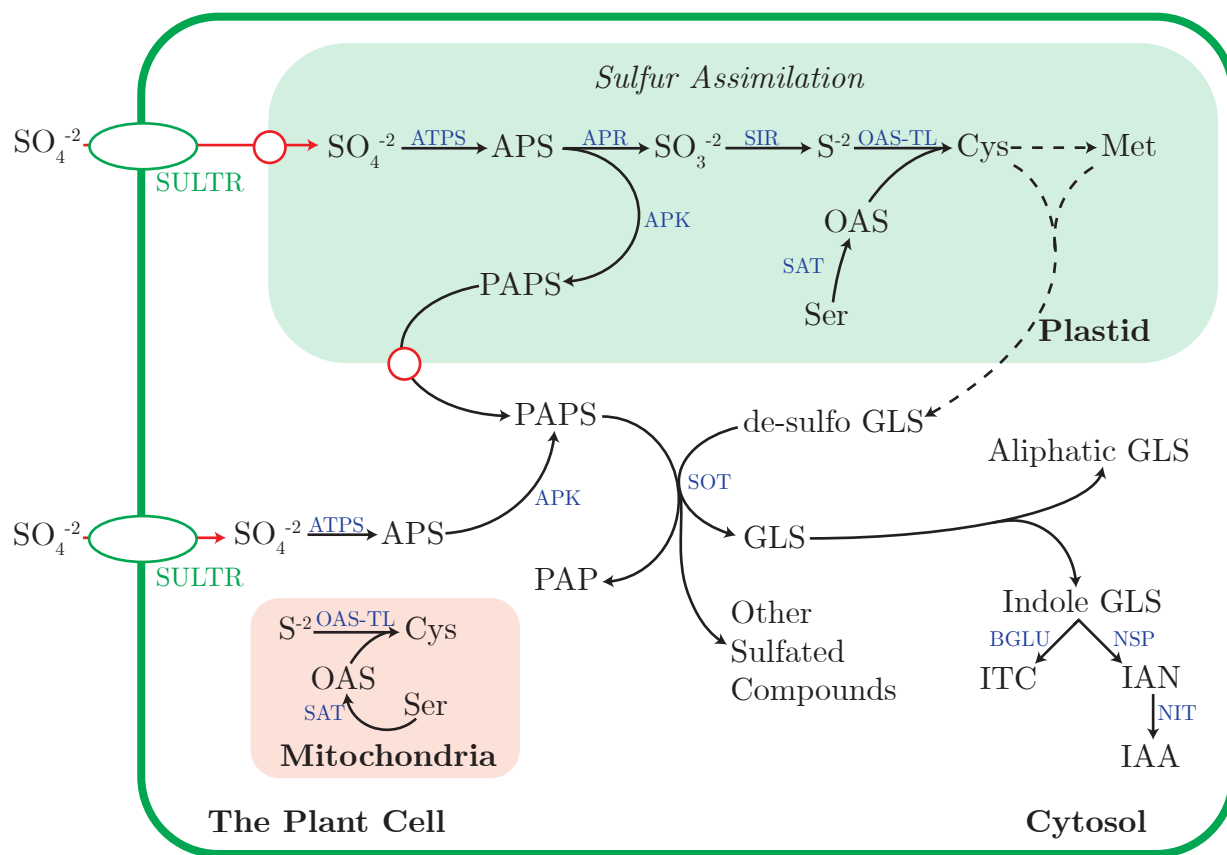
Figure 1.1: Cellular organization of sulfur assimilation and sulfation reactions in plant cells.

SULTR mediates the influx of sulfate into both the cytosol and plastids, where ATPS activates sulfate to form APS. APS is either phosphorylated or reduced to produce PAPS or sulfite by APK or APR, respectively. Sulfur assimilation proceeds forward with sulfite to produce the terminal metabolite, Cys. Cys biosynthesis occurs in both the mitochondria and the plastid. Sulfation reactions utilize PAPS to form several sulfated compounds as well as GLS in the cytosol. Enzymes are in red, while dashed lines depict summarized pathways. *APK, APS kinase; APR, APS reductase; APS, adenosine 5′-phosphosulfate; ATPS, APS sulfurylase; BGLU, BETA GLUCOSIDASE; Cys, cysteine; GLS, glucosinolate; IAA, indole-3-acetic acid; IAN, indole-3-acetonitrile; ITC, isothiocyanates; Met, methionine; NIT, nitrilase; NSP, nitrile-specifier protein; OAS, O-acetylserine; OAS-TL, OAS(thiol)lyase; PAP, 5′-phosphoadenosine 3′-phosphate; PAPS, phosphoadenosine 5′-phosphosulfate; SIR, sulfite reductase; SAT, serine acetyltransferase; Ser, serine; SOT, sulfotransferase; SULTR, sulfate transporter.*

There are two subsets of biochemical reactions that utilize SAM. The first uses SAM to produce 1-aminocyclopropane-1-carboxylic acid (ACC) and nicotianamine (NA; Figure 1.2). The former, a precursor for the plant hormone ethylene (Pattyn et al., 2021) and the latter, a metal ion chelator (Schuler et al., 2012). ACC is converted into ethylene by the enzyme 1-aminocyclopropane-1-carboxylic oxidase (ACO; EC 1.14.17.4) in the cytosol or the plasma membrane. Ethylene has many essential roles in a plant's development, including senescence and responses to stress (Iqbal et al., 2017). Nicotianamine synthase (NAS; EC 2.5.1.43) catalyzes the biosynthesis of NA in the cytosol and plastids (Mizuno et al., 2003). Plant roots secrete NA into the rhizosphere to chelate and dissolve a wide range of metal ions, including iron and zinc. These NA-metal ion complexes allow for the reabsorption of heavy metals through specialized transporters on the plasma membrane (Curie et al., 2001; Schuler et al., 2012). The enzymes that catalyze the formation of ACC and NA produce MTA as a byproduct (Figure 1.2). While a single molecule of MTA is produced for every ACC made, three molecules of MTA are produced for every NA synthesized.

The other subset of reactions that rely on the SAM pool start with its decarboxylation producing decarboxylate SAM (dcSAM; Figure 1.2). Using dcSAM as a precursor, spermidine synthase (SPDS; EC 2.5.1.16), spermine synthase (SPMS; EC 2.5.1.16), and ACAULIS 5 (ACL5; EC 2.5.1.79) produce the polyamines spermidine (Spd), spermine (Spm), and thermospermine (Tspm), respectively (Figure 1.2). Of the three polyamines, only Spd is essential in plants as its removal results in embryo arrest (Imai et al., 2004). The role of polyamines in plants is unresolved and complex: they are essential in moderating growth, regulating plant vascular development, and translational gene regulation amongst other roles (Imai et al., 2006). The biosynthesis of each polyamine produces a single molecule of MTA as a byproduct (Figure 1.2).

Adenine

MTR

MTA

MTN

Met Salvage Cycle

ET

Tpsm

Met

NA

MS

SAMS

NAS

ACL5

GSH

Spm

Cys

Transsulfuration Pathway

HCys

SAM Cycle

SAM

SAMDC

dcSAM

SPMS

CGS

CBL

Cyst

SPDS

Spd

SAHH

Put

SAH
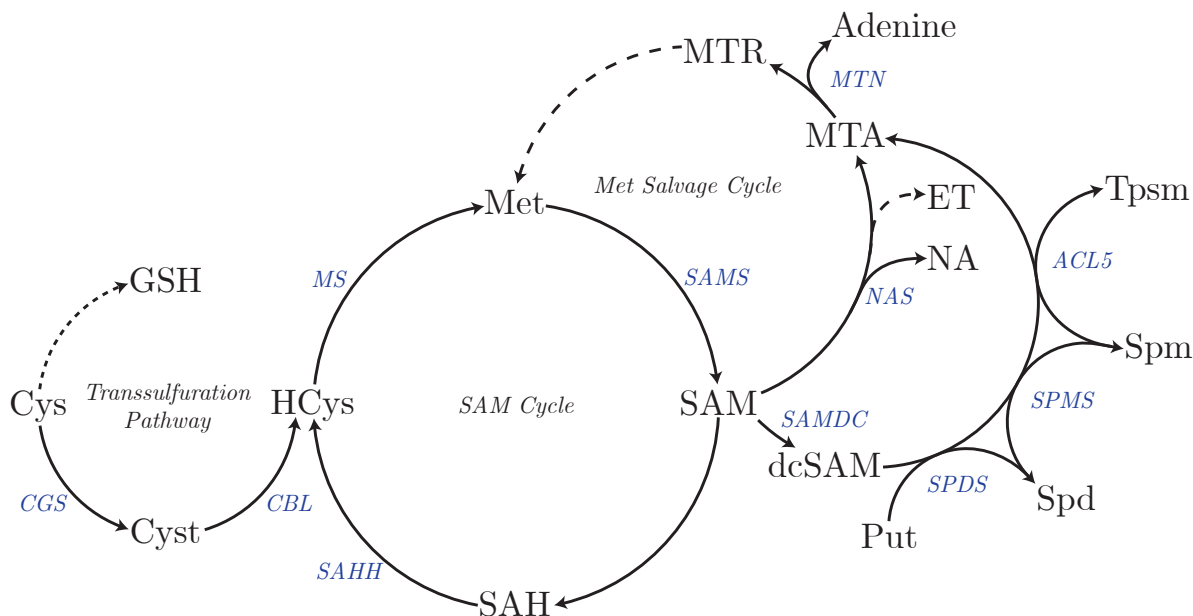
Figure 1.2: Overview of methionine metabolism and salvage in plants.

From the transsulfuration pathway, Cys is incorporated into GSH or used for the production of Met through Cyst and HCys. SAMS activates Met to form SAM, which serves as a primary methyl donor and produces NA and the ET precursor. Reactions that utilize SAM and dcSAM to produce polyamines, Spd, Spm, and Tpsm also produce MTA as a by-product. MTN breaks down MTA to produce MTR and adenine and initiates the Met salvage cycle. Enzymes are in red, while dashed lines depict summarized pathways. *ACL5, ACAULIS 5; CBL, cystathionine β-lyase; CGS, cystathionine γ-synthase; Cys, cysteine; dcSAM, decarboxylated S-adenosylmethionine; ET, ethylene; GSH, glutathione; HCys, homocysteine; Met, methionine; MS, methionine synthase; MTA, 5'-methylthioadenosine; MTN, MTA nucleosidase; NA, nicotianamine; NAS, nicotianamine synthase; SAH, S-adenosylhomocysteine; SAHH, SAH hydrolase; SAM, S-adenosylmethionine; SAMS, SAM synthetase; SAMDC, SAM decarboxylase; Spd, spermidine; SPDS, Spd synthase; Spm, spermine; SPMS; Spm synthase; Tspm, thermospermine.*

1.1.3 Methionine salvage

While the reactions that utilize SAM produce MTA as byproduct, the Met salvage cycle or Yang cycle metabolizes MTA in a series of reactions to recycle the reduced sulfur group (Waduwara-Jayabahu et al., 2012). Met salvage is a vital link between sulfur assimilation and the regeneration of Met and SAM (Sauter et al., 2013). Due to the limited nature of sulfur in the environment and the metabolic cost of SAM synthesis, the ability to salvage Met provides plants with an accessible Met pool (Ravanel et al., 1998; Sekowska et al., 2019). The determining step in the regeneration of Met is the breakdown of MTA.

1.1.4 MTA metabolism

In plants, MTA nucleosidase (MTN; EC 3.2.2.9) catalyzes the breakdown of MTA into 5′-methylthioribose (MTR) and adenine. The series of biochemical reactions comprising the Met salvage cycle transfer the methylthio group of MTR back into Met (Figure 1.2). As a result, MTA levels are drastically lower than SAM and SAM-derived polyamines, highlighting the importance of metabolizing MTA (Bürstenbinder et al., 2010; Waduwara-Jayabahu et al., 2012). The *Arabidopsis thaliana* (Arabidopsis) genome encodes two isoforms of *MTN*, *MTN1* (AT4G38800) and *MTN2* (AT4G34840), responsible for 80% and 20% of MTN activity, respectively, in the unopened buds (Waduwara-Jayabahu et al., 2012). Yang cycle genes are expressed primarily in the leaf vasculature, and metabolic analysis has shown that intermediates, SAM, MTA, and Met, are strongly enriched in vascular tissue (Pommerrenig et al., 2011; Sauter et al., 2013). Specifically, *MTN1* is preferentially expressed in phloem companion and guard cells, while *MTN2* is expressed in epidermal cells in addition to phloem companion cells (retrieved from ePlant Arabidopsis eFP Browser May 25, 2021). *MTN1* transcripts are ten times the abundance of that arising from *MTN2* across different organs, with the highest expression in the anthers of flowers, followed by roots and stems (Oh et al., 2008). On the other hand, *MTN2* has low expression across different organs, with the highest abundance in pollen grains (Ok et al., 2015).

1.2 Previous work on MTN mutants

1.2.1 Past characterizations of MTN-deficient mutants

Understanding the effects of MTN deficiency in plants is of interest due to its critical role in sulfur utilization and plant physiology. Any changes in the levels of Met or Cys due to disruptions in MTA metabolism could well have adverse growth effects. The initial approach to evaluate the impact of MTN deficiency involved characterizing mutants with T-DNA insertions in *MTN* genes. Under sulfur sufficient conditions, single T-DNA insertions in either *MTN* gene (i.e., *mtn1-1* and *mtn2-1*) maintain adequate Met and SAM levels, despite having only a fraction of the WT MTN activity; these mutants are absent of any abnormal phenotypes (Bürstenbinder et al., 2010). However, the growth of *mtn1-1* mutants on media in which MTA is the sole sulfur source leads to decreased primary root growth, increased lateral root development, and impaired vegetative growth (Bürstenbinder et al., 2010). *mtn2-1* mutants have no visible phenotypic changes when grown on this MTA media.

The double mutant, *mtn1-1mtn2-1*, has many developmental defects and phenotypic abnormalities when grown in sulfur-sufficient conditions. The double mutant unopened floral buds accumulate approximately ten times more MTA compared to WT, resulting in an MTA pressure and correlating with its mutant phenotypes (Waduwara-Jayabahu et al., 2012; Tremblay, 2019). The first discernable phenotype occurs soon after germination. The first true leaves of *mtn1-1mtn2-1* are developmentally delayed compared to WT seedlings and exhibit interveinal chlorosis. A condition where the tissue between leaf veins becomes yellow while the vein remains green (Waduwara-Jayabahu et al., 2012). This phenotype is most notable when *mtn1-1mtn2-1* seedlings are grown on half-strength Murashige and Skoog medium (1/2MS; Murashige and Skoog, 1962), but the chlorosis often subsides upon leaf maturation or transfer of the plants to soil.

As *mtn1-1mtn2-1* mutants mature, additional abnormal phenotypes become pronounced. In addition to having an increase in venation, rosette leaves of the double mutant also have thicker midveins (Waduwara-Jayabahu et al., 2012). These vascular phenotypes are similar to a Tspm synthase mutant, thick vein (*tkv*; Clay and Nelson, 2005), an allelic variant of *ACL5* (AT5G19530). Like *tkv*, polar auxin transport is significantly reduced by 50% in *mtn1-1mtn2-1*, associated with the over-proliferation of xylem vessels in inflorescence stems (Waduwara-Jayabahu et al., 2012; Clay and Nelson, 2005). Furthermore, the vascular bundles in *mtn1-1mtn2-1* inflorescence stems are asymmetrically arranged and increased in number. Reproductively, *mtn1-1mtn2-1* siliques produce very few viable seeds as they developmentally arrest after stage 16 (based on the developmental milestones described by Smyth et al., 1990). Developmental defects in both pollen and ovule development resulted in substantially decreased fertility. The anthers of *mtn1-1mtn2-1* do not dehisce and contain aborted pollen encased in callose (Traa, 2019) while carpel and ovule development is impaired; only a fraction of pollen and ovules become fully developed (Waduwara-Jayabahu et al., 2012).

Previous transcriptomic and metabolomic studies characterizing the impact of MTN-deficiency focused on unopened flower buds as the tissue of choice as MTN activity is the highest (Tremblay, 2019). Thus, MTA accumulation is significant, and the physiological effect on development is considerable.

1.2.2 Metabolomic and transcriptomic characterization of MTA accumulation

Early research into the metabolic pathways that produce MTA as a byproduct also implicated MTA in feedback inhibition of those pathways. ACC and NAS are both sensitive to inhibition by MTA (Hyodo and Tanaka, 1986; Dreyfus et al., 2009), while in silico analysis is consistent with MTA inhibiting SPDS and ACL5 activity (Waduwara-Jayabahu et al., 2012). Given that there is some evidence of MTA inhibiting these enzyme activities, the feedback inhibition of MTA-producing processes was proposed to be the basis for the mutant phenotypes of *mtn1-1mtn2-1* plants (Waduwara-Jayabahu et al., 2012). Unfortunately, direct evidence to

support this model is lacking. While there were no changes to the abundance of polyamines, NA content substantially decreased (Waduwara-Jayabahu et al., 2012; Tremblay, 2019), which suggests that not all MTA-producing processes are sensitive to MTA inhibition. The significant decrease in NA in *mtn1-1mtn2-1* supports the diminished iron content and interveinal chlorosis documented in these plants (Waduwara-Jayabahu et al., 2012). The accumulation of MTA and the decrease in NA accumulation also validates that NAS activity is sensitive to feedback inhibition by MTA (Tremblay, 2019).

A large protein-metabolite interaction study revealed that MTA acts as a cofactor in enzymatic reactions found in the Met salvage cycle, demonstrating the potential of MTA interacting directly with a broad range of proteins (Veyel et al., 2018). Furthermore, the NA biosynthetic pathway regulation also illustrates the ability of MTA to affect metabolic processes, which supports the possibility of MTA affecting unknown regulatory pathways resulting in the abnormal phenotypes of *mtn1-1mtn2-1*.

Metabolomic analysis of *mtn1-1mtn2-1* floral buds revealed a significant decrease in sulfur metabolites, Cys, Met, SAM, and SAM-derived metabolites. The considerable depletion of these sulfur metabolites suggests these plants experience sulfur deprivation in the presence of high MTA content, which may contribute to their developmental defects (Tremblay, 2019). RNA-seq analysis indicated that the depletion of these metabolites was not due to a change in transcript abundance of their respective biosynthesis genes (Tremblay, 2019). It is more likely that MTA triggers inhibition of a sulfur assimilation enzyme activity acting upstream of Cys biosynthesis, leading to the depletion of Cys, Met, and SAM in MTN-deficient plants. The enzymatic step(s) affected in the sulfur assimilation pathway remains unknown.

The metabolic profile of *mtn1-1mtn2-1* buds only partially explains the phenotypic abnormalities of MTA accumulation. Certain phenotypic defects of the *mtn1-1mtn2-1* mutant, like delayed bolting, reduced plant growth, and impaired fertility, require an in-depth analysis of these processes to discern the effect of MTA accumulation.

However, the transcriptome profile of the double mutant hinted at a few fundamental regulatory pathways involved in key developmental processes. Genes involved in cell cycle progression, cell growth, and flower development were down-regulated (Tremblay, 2019).

The apparent disruption of these pathways suggests an underlying basis for the phenotypic defects of *mtn1-1mtn2-1*, though a more comprehensive analysis is required to decipher MTA toxicity in these respective pathways. Due to the extensive effect MTA toxicity has on plant development, choosing any particular developmental pathway to focus on is difficult. Therefore, to identify novel targets of MTA toxicity, a genetic screen was implemented (Tremblay, 2019).

1.2.3 Isolation of 5′-*METHYLTHIOADENOSINE RESISTANT* mutants

A genetic screen is a powerful approach to identify affected pathways in a mutant background based on the screen implemented (Li and Zhang, 2016). Given the convoluted evidence associated with MTA accumulation, a forward genetics approach was carried out to understand the molecular basis of this complex phenotype (Tremblay, 2019). The basis of this genetic screen was to identify gene changes that suppress the *mtn1-1* short root phenotype when grown on media with MTA as the sole sulfur source. *mtn1-1* seeds were mutagenized with ethyl methanesulfonate (EMS) to produce single nucleotide polymorphisms (SNP; Tremblay, 2019). M2 seeds were then grown on MTA media for seven days and seedlings that grew long roots were identified. This suppressor screen yielded five distinct *MTA RESISTANT* (*MTAR*) mutants. Of the five *mtar* mutants, *mtn1-1mtar11* was the only dominant suppressor mutant, and *mtn1-1mtar2* was the first *mtar* sequenced, being the first successful suppressor mutant recovered, and thus the first to be analyzed (Tremblay, 2019).

The mutation in *mtn1-1mtar2* causes an amino acid change within the gene encoding nitrile-specifier protein, NSP1 (AT3G16400; Tremblay, 2019). NSP1 catalyzes indole-3-acetonitrile (IAN) synthesis from indole-3-glucosinolate and ultimately leading to the synthesis of, indole-3-acetic acid (IAA; Vik et al., 2018; Figure 1.1). Tremblay (2019) proposed that MTA accumulation changes the flux of sulfur away from Cys biosynthesis towards increased production of GLS and IAA via PAPS. The increase in glucosinolate content and IAA accumulation leads to detrimental effects on root growth (Vik et al., 2018). Therefore, the

mtar2 SNP in NSP1 suggests that IAA production is restricted in this background, resulting in the suppression of the short root phenotype (Tremblay, 2019). More work is needed to validate this explanation of *mtar2*'s effect on root growth and its impact on IAA biosynthesis.

1.3 The role of TOR and phytohormones in plant development

1.3.1 TOR kinase regulation of plant growth

A plant's ability to grow and develop is reliant upon available nutrients and numerous stimuli, including hormones, environmental, and energy status. As sessile organisms, plants must integrate this information to maximize their energy reserves and regulate their growth. The ability to sense and respond to external and internal signals feeds into a central hub in which the target of rapamycin (TOR; AT1G50030) tightly coordinates multicellular growth (Burkart and Brandizzi, 2021; Figure 1.3). TOR is a highly conserved serine/threonine kinase that functions in a complex found in all eukaryotes.

The downstream phosphorylation targets of the TOR complex (TORC) are variable across different species (Menand et al., 2002). However, the core components of the complex, regulatory-associated protein of TOR (RAPTOR) and lethal with SEC13 protein 8 (LST8), are highly conserved (Menand et al., 2002). Two complexes make up the mammalian and yeast TOR regulatory units but only TORC1 is found in plants, made up of LST8 and RAPTOR. Arabidopsis has two isoforms of RAPTOR with *RAPTOR1* (AT3G08850) being highly expressed throughout development (Deprost et al., 2005). There are also two isoforms of LST8; *LST8-1* (AT3G18140) and *LST8-2* (AT2G22040) are expressed throughout plant development (Moreau et al., 2012). One common downstream phosphorylation target of TOR is the PROTEIN-SERINE KINASE 6 (S6K), controlling both translation and ribosome biogenesis (Shi et al., 2018). S6K phosphorylation is commonly used to evaluate TOR activity (Dong et al., 2017). Therefore, each of these regulatory pathways contributes a different role in plant development (Figure 1.3; Burkart and Brandizzi, 2021)

The TOR regulatory pathway surveils the levels of carbon, phosphorus, nitrogen, and sulfur, essential elements needed to generate key macromolecules (Burkart and Brandizzi, 2021). The underlying mechanism for how these elements are monitored remains to be determined. However, there is strong evidence that they affect TOR's activity through a direct or intermediate pathway (Burkart and Brandizzi, 2021). For example, TOR reduces plant growth during sulfur deprivation by monitoring the sulfur precursors for cysteine biosynthesis (Dong et al., 2017). The depletion of sulfide in the SIR mutant, *sir1-1*, inhibits TOR activity, resulting in decreased protein translation, meristematic activity, and plant growth (Dong et al., 2017). In this case, the downregulation of glucose metabolism was connected with the disruption of sulfur assimilation and decreased TOR activity (Dong et al., 2017). Introgression of *cad2-1*, a GSH synthesis mutation, into *sir1-1*, depleted GSH synthesis leading to increases in both TOR activity and plant growth compared to *sir1-1* (Speiser et al., 2018). The addition of the *cad2-1* mutation in the *sir1-1* background promoted the sulfur flux into cysteine biosynthesis, and the activation of TOR was the trigger for this reallocation of sulfur (Speiser et al., 2018). This intricate coordination of nutrient availability and plant growth by TOR is only one example of its role in plant development.

1.3.2   Amino acid homeostasis by TOR signaling

Of the numerous stimuli, amino acid availability is the greatest effector of TOR activity (O'Leary et al., 2020). In mature leaves of Arabidopsis, the accumulation of amino acids activates the TOR signaling network and reduces amino acid catabolism and respiration (O'Leary et al., 2020). At the same time, anabolic pathways are activated via TOR phosphorylation, leading to an increase in plant growth (O'Leary et al., 2020). Unfortunately, an intricate mechanism for sensing and maintaining amino acid homeostasis like the one found in mammals and yeast has been elusive in plants (Wu et al., 2019). In MTN-deficient mutants, the increased MTA content in unopened floral buds of *mtn1-1mtn2-1* limited the production of Cys and Met (Tremblay, 2019). It is possible that in the double mutant, MTA is inhibiting a step of sulfur assimilation upstream Cys biosynthesis, similar to the *sir1-1* mutant.
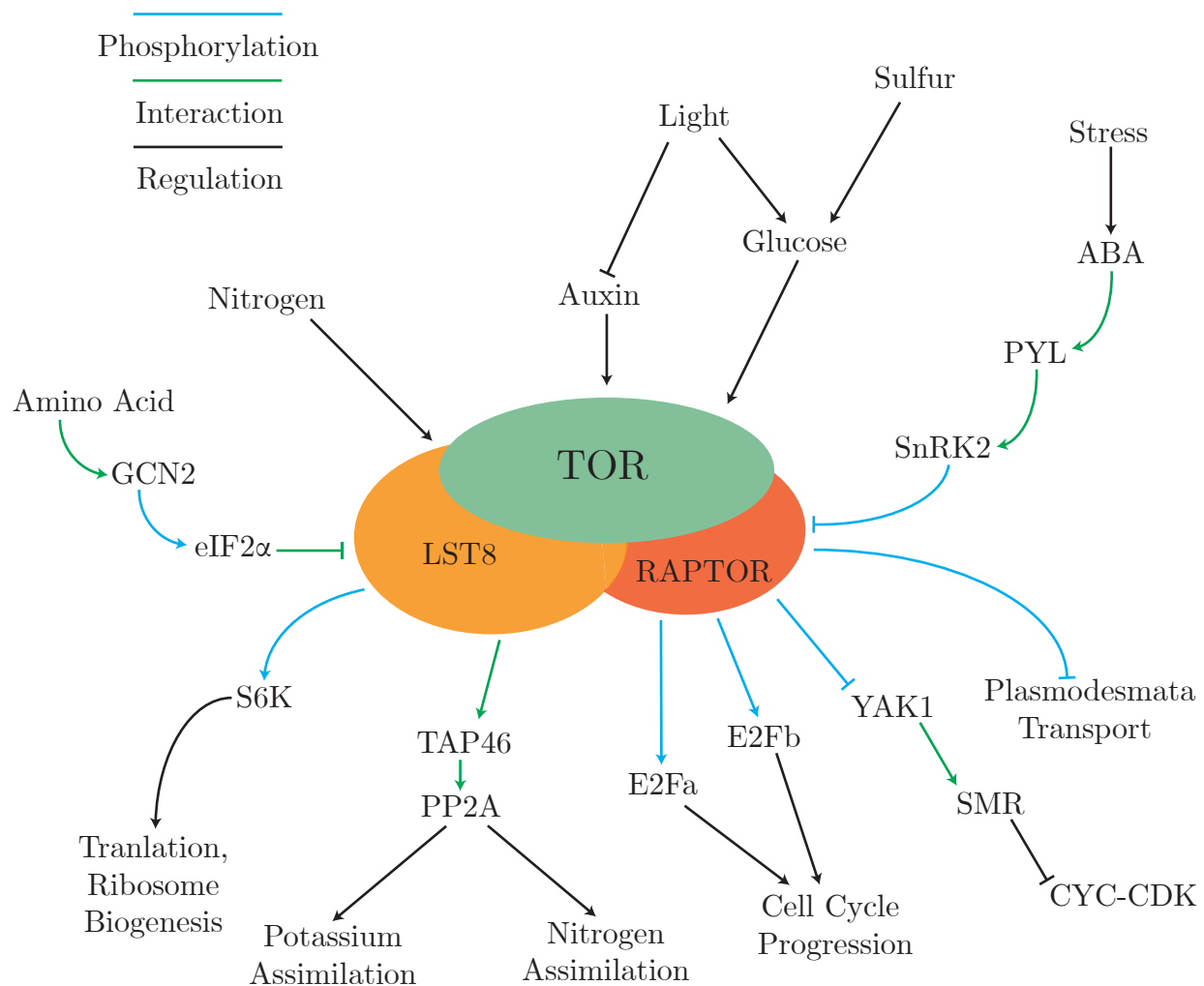
Figure 1.3: Overview of the TOR signaling network in Arabidopsis.

Upstream activators of the TOR signaling network are nutrients like nitrogen, sulfur, glucose, and amino acids. Stress signals negatively regulate TOR's activity via accumulation of ABA and activation of SnRK2. Downstream targets of TOR signaling are associated pathways involved translation, ribosome biogenesis, nitrogen and potassium assimilation, cell-cell communication via plasmodesmata transport, and cell proliferation. *ABA, abscisic acid; CYC-CDK, cyclin-cyclin dependent kinase; eIF2α, eukaryotic initiation factor 2; GCN2, general control non-repressible 2; LST8, lethal with SEC13 protein 8; PP2A, PROTEIN PHOSPHATASE 2A; PYL, PYR1/PYL/RCAR; SMR, SIAMESE-RELATED; SnRK2, SUC NON-FERMENTING 1-RELATED KINASE 2; S6K, PROTEIN-SERINE KINASE 6; TOR, target of rapamycin; YAK1, yet another kinase 1.*

The mammalian and yeast TOR signaling pathway is the most characterized system of amino acid sensing (Kim and Guan, 2011). A general control non-repressible 2 (GCN2) kinase is an essential component in the monitoring of amino acid levels in these organisms. Under amino acid starvation, uncharged tRNA levels increase, and these bind to the conserved C-terminus of GCN2 (Yuan et al., 2017). Once bound by an uncharged tRNA molecule, GCN2 phosphorylates the α subunit of the eukaryotic initiation factor 2 (eIF2α), leading to repression in protein synthesis (Yuan et al., 2017). In *Saccharomyces cerevisiae*, GCN2 directly phosphorylates a component of the TORC1 complex resulting in the loss of TOR activity during amino acid starvation (Yuan et al., 2017; Figure 1.3). GCN2 (AT3G59410) in Arabidopsis is implicated in a wide range of stress and hormone responses (Lageix et al., 2008; Liu et al., 2019) as well as amino acid deprivation (Figure 1.3). There has been no evidence of GCN2 directly phosphorylating a TOR component in Arabidopsis, but a recent study showed that eIF2α interacts with LST8-1 (Van Leene et al., 2019). GCN2 is also sensitive to the precursors of amino acids, indicating that the amino acid starvation may also be due to carbon/nitrogen assimilation limitations, another possible target of MTA inhibition (Dong et al., 2017).

The mechanism by which the TOR signaling network senses sulfur and amino acid deprivation remains uncharacterized in plants. Thus, elucidating this mechanism is vital to understanding TOR's effect on individual developmental stages (Figure 1.3).

1.3.3   Meristem development

The presence of stem cells in strategic locations gives plants the ability to produce new organs throughout their life cycles. These stem cell populations are located in the shoot and root apical meristems, allowing for the continuous generation of organs - a process called organogenesis (Figure 1.4). Both these meristems are established during embryogenesis at the shoot and root apexes (Mayer et al., 1998). In dicots, such as Arabidopsis, the shoot apical meristem is located between two cotyledons and is responsible for generating above-ground tissue during post-embryonic development. Once the plant transitions into reproductive growth, the shoot apical meristem transitions to the inflorescence meristem,

generating both the floral meristem and floral organs (Endrizzi et al., 1996). The root apical meristem is responsible for generating the underground root architecture. The shoot and root meristems share similar molecular machinery, but each responds to their respective environments differently (Li et al., 2017).

Shoot apical meristem

The shoot meristem comprises a central zone where the stem-cell niche is located and contains a pool of cells that slowly divide. The boundaries of the central zone are easily distinguishable from the surrounding peripheral zone, where cells are rapidly dividing, and organ initiation occurs (Steeves and Sussex, 1989). Three germ layers make up the shoot apical meristem, with the outermost layer defined as L1, giving rise to the epidermis, while the L2 and L3 layers form internal tissues (Steeves and Sussex, 1989; Shi and Vernoux, 2019).

In Arabidopsis, the CLAVATA/WUSCHEL negative feedback loop is the central mechanism regulating stem cell proliferation and differentiation (Figure 1.4a). Throughout development, the homeodomain transcription factor, WUSCHEL (WUS; AT2G17950), plays a central role in regulating stem cell fate. In line with this, *WUS* is located in the central zone where a lack of its expression results in the loss of stem cell identity, leading to the failure of the shoot meristem maintenance (Mayer et al., 1998). CLAVATA 3 (CLV3; AT2G27250), along with its signaling cascade partners, CLV1 (AT1G75820), CLV2 (AT1G65380), promote the progression of stem cells towards differentiation and organ initiation (Brand et al., 2000; Nimchuk et al., 2011). *clv* mutants have an enlarged central zone and an increased number of leaves and floral organs (Clark et al., 1997; Nimchuk et al., 2011). The balance between repetitive organ formation and cell proliferation is precisely coordinated further by CLV and SHOOT MERISTEMLESS (STM; AT1G62360; Clark et al., 1996). A member of the *KNOTTED-1* family, STM is an antagonist of CLV1 receptor kinase. While CLV1 promotes organogenesis by suppressing *WUS* expression (Clark et al., 1997), the interaction between STM and CLV1 prevents cells' entry into organogenesis, thereby promoting meristem maintenance (Figure 1.4; Clark et al., 1997). It is noteworthy that STM mutants have normal root

apical meristems (Clark et al., 1996), indicating that not all developmental signals are shared across the root and shoot meristems.

Both light and sugar metabolism modulate shoot apical meristem development as *WUS* expression is repressed in the dark, keeping the meristem dormant (Figure 1.4*a*; Pfeiffer et al., 2016). However, increased photosynthesis or exogenous feeding of sugar drives *WUS* expression via TOR activation (Pfeiffer et al., 2016). Temperature also strongly influences the transition of the shoot apical meristem to a flowering meristem by affecting TOR and meristem activity (Wang et al., 2017b). The temperature sensing mechanism is not well characterized, but PHYTOCHROME B is also a thermo-sensor and perceives light (Legris et al., 2016). Therefore, the perception of these two entities may involve a simple mechanism integrated with TOR's activity and meristem maintenance.

The plant hormones auxin and cytokinin play essential roles in regulating shoot apical meristem development, from the control of meristem formation during embryogenesis and the continuous maintenance of cell proliferation and organogenesis (Zhao et al., 2010; Luo et al., 2018). Auxin response factor 5 (ARF5; AT1G19850) mediates auxin signaling in the stem cells by directly repressing the transcription of *enhancer of shoot regeneration 1* (*ESR1*; AT1G12980). ESR1 promotes *CLV3* expression, but when auxin is high in the shoot meristem, ARF5 repression of *ESR1* decreases *CLV3* expression leading to the development of an enlarged the central zone size similar to that found in *clv* mutants (Ma et al., 2019; Figure 1.4*a*). The naturally low auxin signaling in the shoot apical meristem protects the central zone and stem cells from the differentiation effects of high auxin (Ma et al., 2019). In fact, the auxin minima in the central zone is driven by WUS, and its expression is sufficient in reducing auxin signaling by a system-wide transcriptional control (Figure 1.4). Primarily due to the repression of auxin transport, perception, signal transduction, and transcriptional response (Ma et al., 2019). While WUS protects auxin-mediated differentiation of stem cells, it is also concurrently enhancing cytokinin biosynthesis (Wang et al., 2017a; Figure 1.4). Cytokinin positively regulates *WUS* expression, and therefore, this positive feedback loop helps sustain *WUS* expression in the meristem.

Root apical meristem

The root apex is comprised of three regions, the meristematic zone, the elongation zone, and the differentiation zone. The meristematic zone is located at the root tip and contains a stem cell niche (Figure 1.4*b*). The stem cell niche encompasses three to four slow dividing cells that make up the quiescent center (QC) and the adjacent stem cells (van den Berg et al., 1997). The daughter cells produced by the QC undergo further cell divisions as they shift further away from their origin until they reach the elongation zone, where they begin to differentiate. The position of the original stem cell defines the cell fates of each root cell, though the position remains the same throughout development. Therefore, cell lineages develop a spatiotemporal developmental gradient (Dolan et al., 1993). These cell lineages represent the different cell layers of the roots, each with specialized roles (see reviews: Benfey and Scheres, 2000; Augstein and Carlsbecker, 2018). The root has similar molecular players as the shoot apical meristem, but their mechanisms are slightly varied.

Light-mediated plant development still plays a critical role in root meristem activity. In the absence of light, seedlings enter an arrested developmental state once the embryonic glucose reserves are depleted (Xiong et al., 2013). At this point, shoot photosynthetic-derived glucose drives TOR signaling and root meristem activity (Figure 1.4*b*). Although TOR is found in the QC, it does not regulate the maintenance of these stem cells due to the absence of essential partners, targets, and inputs (McCready et al., 2020). Instead, TOR controls cell proliferation and expansion of root cells outside the QC via Yet another kinase 1 (YAK1: AT5G35980). During periods of low TOR activity, YAK1 represses CYCLIN DEPENDENT KINASE (CDK) activity by inducing *SIAMESE-RELATED* (*SMR*) expression (Figure 1.4*b*) which negatively regulates cell cycle progression (Barrada et al., 2019; Forzani et al., 2019).
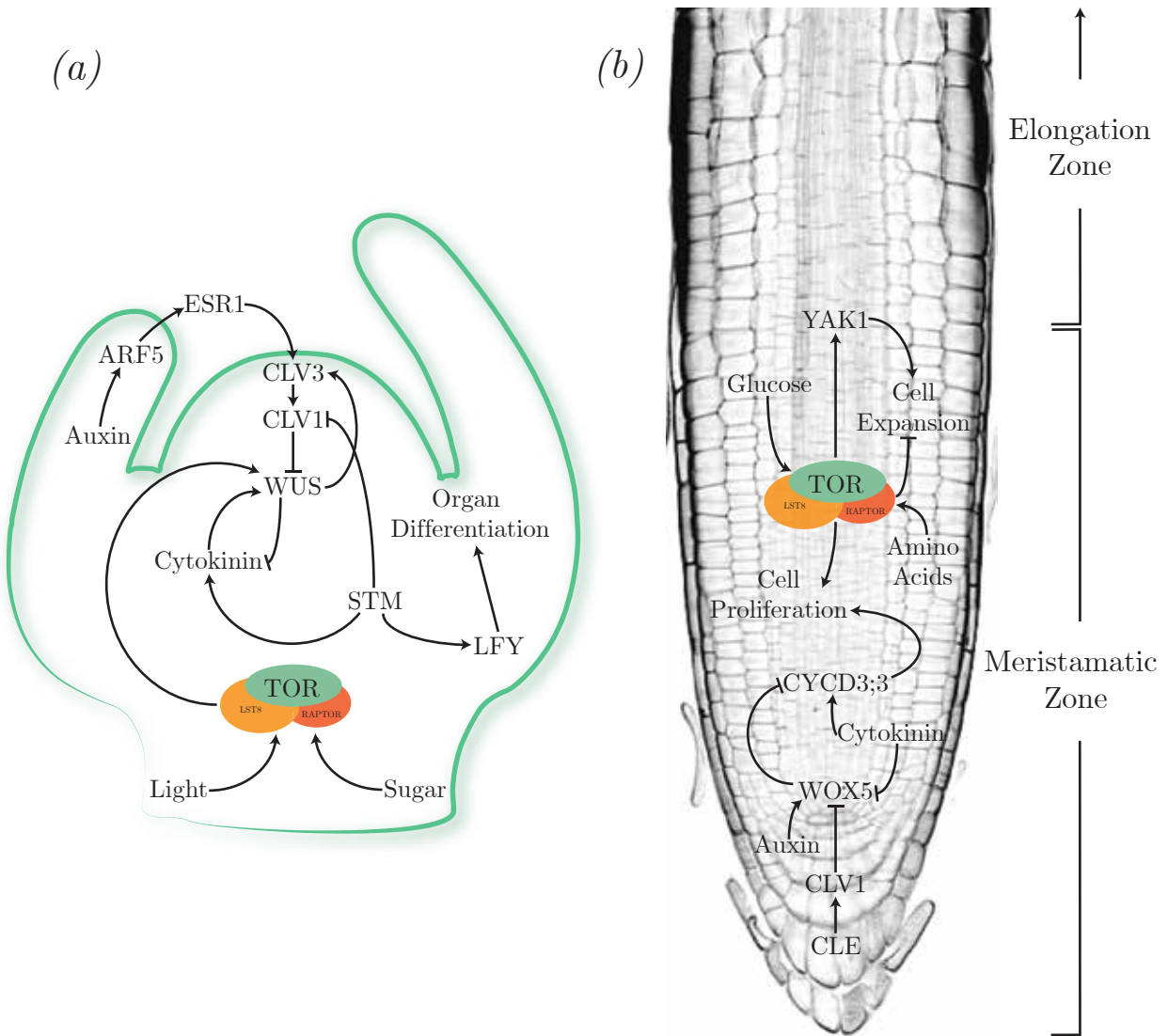
Figure 1.4: Apical meristem development.

Regulatory models depict the complex relationship between light, sugar, phytohormones, and the central WUSCHEL/CLAVATA genetic mechanism that coordinates stem cell proliferation and differentiation in (a) the shoot and (b) root apical meristem. *ARF5, auxin response factor 5; CLE, CLAVATA3/ESR; CLV1, CLAVATA 1; CLV3, CLAVATA 3; CYCD3;3, cyclin D3;3; ESR1, enhancer of shoot regeneration 1; LST8, lethal with SEC13 protein 8; LFY, LEAFY; STM, SHOOT MERISTEMLESS; TOR, target of rapamycin; WOX5, WUSCHEL RELATED HOMEOBOX 5; WUS, WUSCHEL; YAK1, yet another kinase 1.*

The interplay between phytohormones and TOR signaling is evident in meristem development, and any disruption in the interaction between these is detrimental to plant growth. The presence of an auxin maximum at the QC is vital for proper root development. High auxin levels promote the expression of cyclins (CYC) and CDKs in Arabidopsis seedlings (Barrada et al., 2015). The biosynthesis and accumulation of auxin at the root tip indicate that auxin has a significant role in maintaining and initiating mitotic activity in the meristem (Barrada et al., 2015). Auxin promotes the expression of *WUSCHEL RELATED HOMEOBOX 5* (*WOX5*; AT3G11260) in the QC (Petersson et al., 2009). Furthermore, cytokinin biosynthesis is negatively regulated by WOX5, thereby modulating auxin flux in the root and promoting cell division (Zhang et al., 2013). Auxin and cytokinin biosynthesis are also reliant upon amino acid and nucleotide metabolism, and therefore, the availability of these nutrients influences the mechanisms these phytohormones regulate (Ubeda-Tomás et al., 2012).

1.3.4 Vegetative growth

The regulation of plant size and productivity balances environmental stress signals and the availability of nutrients. The TOR signaling network strongly influences plant growth by monitoring these two entities. Mutations in either TOR complex genes or the downregulation of TOR itself result in a detrimental loss in plant biomass and productivity (Deprost et al., 2005; Anderson et al., 2005). As such, the main proponents of plant productivity and TOR activation are available nutrients. Exogenous feeding of glucose activates TOR signaling and reprograms several transcriptional networks increasing sulfur and nitrogen assimilation, promoting cell cycle, and upregulating carbon and energy metabolism (Xiong et al., 2013).

Any disruption in the TOR signaling network leads to a global reduction in translation, decreased polyribosome accumulation, and in turn, a depletion in plant biomass (Forzani and Meyer, 2019). The overexpression of TOR or its protein partners increases both plant size and leaf surface area (Deprost et al., 2005). In order to increase plant biomass, TOR positively regulates cell proliferation and increases cell size by upregulating cell expansion genes. The increase in ribosome biosynthesis and mRNA translation additionally increases plant growth (Dong et al., 2015).

Plants thrive under conditions that positively contribute to growth, but environmental fluctuations that induce stress will limit plant growth. In Arabidopsis, abiotic stresses, including heat, cold, and drought, reduce plant productivity even if the duration of the stress is short-lived (Wu et al., 2019). Phytohormones play a role in the signal transduction of these stresses, with abscisic acid (ABA) signaling being the critical proponent of growth inhibition as it reduces TOR's activity (Dong et al., 2015). As ABA accumulates, it binds to PYR1/PYL/RCAR (PYL) receptors, triggering the activation of SUC NON-FERMENTING 1-RELATED KINASE 2 (SnRK2; Park et al., 2009). The SnRK2 family of kinases phosphorylates RAPTOR1, thereby inhibiting TOR complex signaling and promoting stress-induced growth inhibition (Wang et al., 2018). Under normal conditions, TOR phosphorylates PYLs permitting healthy growth conditions as this phosphorylation activity prevents ABA from binding to PYLs (Wang et al., 2018). Increased ABA signaling during stress leads to the repression of TOR activity, delays flowering, and triggers developmental defects in flower organogenesis, leading to impaired fertility (Wang et al., 2018).

1.3.5 Reproductive development

Given that plant reproduction is strongly influenced by MTN deficiency (Waduwara-Jayabahu et al., 2012), understanding the fundamental mechanisms that influence reproductive development is critical in understanding the effect MTA accumulation has on this developmental stage. This stage begins with the transition from vegetative growth to reproductive, marking a substantial change in the plant's physiology. This transition occurs under suitable environmental conditions, enabling plants to maximize seed production in favorable conditions. Three fundamental genetic pathways regulate the transition to flowering in Arabidopsis. These pathways define the roles of inductive photoperiods, gibberellic acid (GA; Kinoshita and Richter, 2020), and vernalization (Koornneef et al., 1991).

The coordinated response of a few genes common among these pathways accelerates the transition to the reproductive phase. The three essential genes responsible are *FLOWERING LOCUS T* (*FT*; AT1G65480; Kardailsky et al., 1999), *SUPPRESSOR OF OVEREXPRESSION OF CONSTANS1* (*SOC1*; AT2G45660; Kobayashi et al., 1999), and *LEAFY* (*LFY*;

AT5G61850; Blázquez and Weigel, 2000). In the rosette leaves of Arabidopsis, a long-day photoperiod promotes flowering by activating a signal cascade converging on FT in the phloem companion cells (An et al., 2004). FT, along with TWIN SISTER OF FT (TSF; AT4G20370), are transported to the shoot apical meristem via the phloem upon which a change in shoot identity occurs through transcriptional regulation of tissue identity factors (An et al., 2004; Abe et al., 2019).

One of the more discernible abnormal phenotypes of the severe MTN double mutant, *mtn1-1mtn2-1*, is a significant delay in flowering. The altered vasculature of this mutant may also hinder the transport of FT and TSF; a decrease in these factors in the shoot apex would prevent the transition to the floral meristem, thereby delaying the reproductive phase.

Much of plant seed production is reliant upon proper floral organogenesis. In the *mtn1-1mtn2-1* mutant, one suspected cause of the impaired fertility is abnormal floral development. It is not clear why the decreased MTA metabolism disrupts floral organogenesis (Waduwara-Jayabahu et al., 2012). Fortunately, flower development is well characterized with detailed insights into many cellular and developmental processes that control the formation of flowers. Much of the research in this area has been guided by the ABC model of floral organ identity (see review: Thomson et al., 2017). The model simply states that the combinations of specific floral organ identity genes lead to the formation of sepals, petals, stamens, and carpels (Coen and Meyerowitz, 1991). For plant fertilization to occur, proper formation of the male and female gametophytes is needed. Both DNA methylation and phytohormones are key factors that regulate the development of these structures.

The female gametophyte of angiosperms develops within the maternal sporophytic tissue of the ovule (Yadegari and Drews, 2004). Any disruption of auxin signaling, transport, or synthesis leads to abnormal female gametophyte development, resulting in the loss of ovules in the carpels (Cheng et al., 2006; Okada et al., 1991; Cucinotta et al., 2020). In recent years, emerging evidence implicates cytokinins playing a vital role in ovule patterning and development (Terceros et al., 2020). Fewer ovule primordia arise from the floral meristem when cytokinin synthesis or perception is compromised (Higuchi et al., 2004; Bencivenga et al., 2012).

The male gametophyte develops within stamens, which are composed of a filament and anther. Within anthers, a specialized tissue layer called the tapetum surrounds sporogenous cells and hosts successive developmental phases, microsporogenesis and microgametogenesis, leading to the production of the mature pollen grain. However, both cytokinin and auxin signaling disruptions result in abnormal anthers that do not dehisce and contain few viable pollen (Kinoshita-Tsujimura and Kakimoto, 2011; Cardarelli and Cecchetti, 2014).

1.4   The plant cell cycle

Plant cells have evolved a complex pathway to regulate cell proliferation, but the plant cell cycle generally follows the basic strategy found in other eukaryotes (Figure 1.5). Cell proliferation is highly concentrated in meristems where pools of undifferentiated cells undergo many rounds of cell division. The tightly regulated cell cycle gives rise to two daughter cells, and for this to occur successfully, both the genome and organelles must duplicate before the physical division of the cells, cytokinesis, can occur. The balance between cell proliferation and cell growth drives plant growth, and since cell proliferation is energetically intensive, the TOR signaling pathway strongly influences the cell cycle (Figure 1.5a).

In addition to cell proliferation, proper organogenesis depends on the differentiation of cells into several cell types. The differentiation of various cell types occurs as they enter the endoreduplication cycle, whereby cells duplicate their genome without undergoing mitosis (Figure 1.5b). In Arabidopsis, a large complex family of CYC genes regulates cell cycle progression. These CYCs are grouped into four different types, A, B, D, and H, with their respective CDK binding partners. Each group of CYCs is involved in either the G_1/S phase transition, S phase progression, G_2/M transition, and mitosis (Inzé and De Veylder, 2006; Ahmad et al., 2019).

1.4.1 G_1/S

The cell cycle nominally begins at the transition from G_1 to S phase. The commitment to enter the cell cycle relies upon the inactivation of the nuclear G_1/S repressor, RETINOBLASTOMA-RELATED (RBR; AT3G12280; Figure 1.5a) protein. Three E2F proteins, E2Fa, E2Fb, and E2Fc, control the expression of genes required for this transition and S-phase progression. These proteins form a heterodimeric complex with DIMERISATION PARTNER (DP), a DNA binding protein. While E2Fa-DP, E2Fb-DP complexes are transcriptional activators whose activities are inhibited by RBR, E2Fc-DP is an inhibitor of the cell cycle that is degraded upon initiation of cell division (Li et al., 2017; del Pozo et al., 2006). As the cells transition from G_1 to S phase, CYCD proteins bind to CDKA;1 forming a complex which phosphorylates RBR, resulting in the release of E2Fa-DP and E2Fb-DP (Van Leene et al., 2010; Desvoyes et al., 2006). The activation of these transcription factors triggers the expression of genes involved in DNA replication, chromatin dynamics, and other cell cycle genes.

Phytohormones, sucrose, and stress are important factors that strongly influence cell division by regulating the expression or activity of cell cycle genes implicated in initiating the cycle. Auxin signaling upregulates *CDKA* expression while cytokinin, brassinosteroids, and sucrose upregulate *CYCD* expression (Richard et al., 2002; Li et al., 2017; Yang et al., 2021). The maximal abundance of each of these factors are found in meristematic regions (Barrada et al., 2015). The resulting accumulation of CDKA and CYCD initiates the cell cycle by their phosphorylation of E2F complexes which commences a signal cascade. The TOR signaling pathway also directly phosphorylates E2Fa and E2Fb, making this an alternative entry point into the cell cycle, independent of the CDK-CYC-RBR route (Li et al., 2017).

1.4.2 G_2/M

The progression of the G_2/M transition follows a similar cascade of events, with CDKA and CDKB being the main drivers when associating with CYCDs and CYCBs, respectively (Boudolf et al., 2004). Similar to the E2F transcription factor complexes, the G_2 CDKA/B-
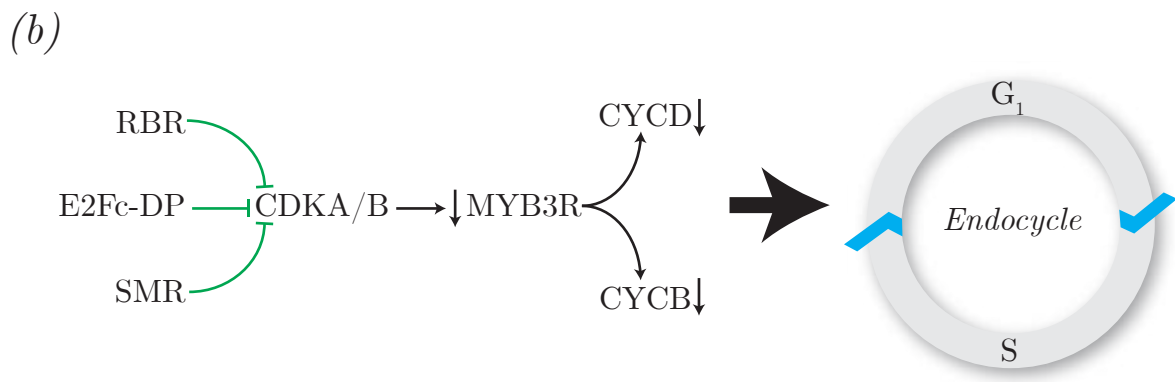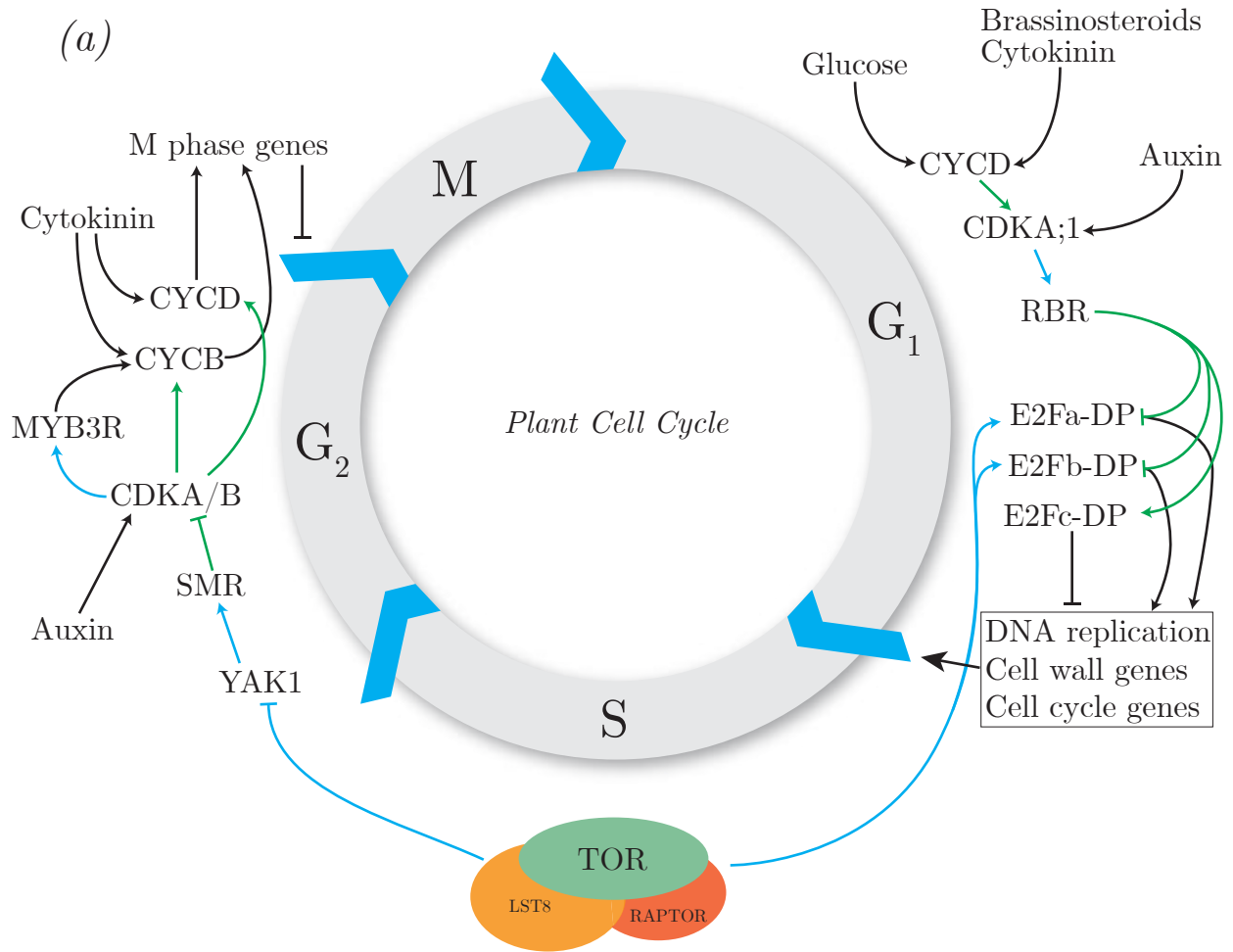
Figure 1.5: The plant cell cycle and the induction of endoreduplication.

Figure 1.5 *(previous page)*: **The plant cell cycle and the induction of endoreduplication.**

A schematic representation of the (a) mitotic plant cell cycle and (b) endocycle with the regulatory effects of the TOR signaling pathway and phytohormones. During the G1 phase, CYCD accumulates early and associates with CDKA;1, becoming active. The active CYCD-CDKA complex phosphorylates RBR, which causes the release of RBR from E2Fa/b-DP and induces S phase genes associated with DNA replication, cell wall expansion, and other cell cycle markers. At the G2/M transition, CYCA and CYCB accumulate early on and induce the transition into mitosis and cell division. The repression of either CYCs or CDKA/B at the G2/M transition prevents the cell cycle from proceeding and induces endoreduplication (b). *CDKA/B CYCLIN DEPENDENT KINASE A/B; CYCB, cyclin B; CYD, cyclin D; LST8, LST8 lethal with SEC13 protein 8; MYB3R, MYB DOMAIN PROTEIN 3R; RBR, RETINOBLASTOMA-RELATED; SMR, SIAMESE-RELATED; TOR, target of rapamycin; YAK1, yet another kinase 1.*

CYC complexes phosphorylate several G_2-specific transcription factors accumulating the necessary genes for the M phase (Araki et al., 2004; Figure 1.5a). Both cytokinin and auxin have similar roles in this transitional phase, with cytokinin strongly inducing *CYCB1* expression and auxin inducing *CDKA* expression. TOR also regulates cell cycle progression through SMR proteins which may act on both G_1/S and G_2/M transitions. Under TOR control, YAK1 negatively regulates the cell cycle by initiating the accumulation of several SMR proteins (Barrada et al., 2019). SMRs 4, 5, and 7 (AT5G02220; AT1G07500; AT3G27630) each act negatively on both CDKA;1 and CDKB1;1 (Van Leene et al., 2010). During TOR deficiency, YAK1 inhibits cell proliferation in favor of differentiation. When TOR is active, TOR-mediated inhibition of YAK1 results in cells switching in favor of proliferation (Barrada et al., 2019; Forzani et al., 2019).

1.4.3   Endoreduplication

The process of endoreduplication is the doubling of chromosomal DNA and expanding cell size in the absence of cell division (Massonnet et al., 2011). Arabidopsis mutants with an impaired cell cycle are more likely to enter the endocycle and induce endoreduplication (Noir et al., 2015), leading to the increase in genome ploidy. In situations of stress, plants may shut down cell division in favor of endoreduplication as cell proliferation becomes too energetically expensive (Ahmad et al., 2019).

The endocycle comprises two steps, the exit from the cell cycle and the continued rounds of DNA replication. The requirement of establishing an endocycle is maintaining the activity of CDKs below the level that triggers mitosis (Figure 1.5b). Thus, transcriptional downregulation of M-phase-specific CDKs by SMRs, RBR, and E2Fc-DP is one likely route for a cell to enter the endocycle (Boudolf et al., 2004; del Pozo et al., 2006). Furthermore, any repression of CDK/CYC complexes decreases the activity of MYB3Rs (Figure 1.5b), which control transcription of G$_2$/M phase expressed genes, including CYCBs (Araki et al., 2004). Therefore, a lack of MYB3R phosphorylation through initial repression of pre-mitotic CDK activity may represent a way of arresting the expression of all downstream M-phase genes (Ito et al., 2001), inhibiting the G$_2$/M phase transition and inducing entry into the endocycle.

1.5 Research Objectives

Preliminary observations of the phenotypes associated with MTN deficiency have implicated a wide range of plant physiological pathways altered by the toxic effects of MTA accumulation, including changes to sulfur metabolism, impairment of growth, and fertility (Waduwara-Jayabahu et al., 2012; Tremblay, 2019). These investigations have only characterized the effects of MTA on sulfur metabolism and described abnormalities but have yet to implicate the underlying pathways affected by MTA. The abnormalities including, delayed bolting, reduced growth, and sterility, are likely a result of MTA affecting meristem maintenance, reproductive development, cell proliferation, and the TOR signaling network. Thus, this research focuses on deciphering the molecular basis of the abnormal phenotypes associated with MTA accumulation and improving our understanding of its impact in these pathways.

The pursuit of this overarching goal is aided by the identification and characterization of the *mtar11* suppressor mutant. The suppressor screen implemented by Tremblay (2019) produced five mutants that suppressed the short root phenotype of *mtn1-1* on media containing MTA as a sole sulfur source. Therefore, the suppression mechanism of *mtar11* would implicate processes affected by MTA and how the plant overcomes the MTA pressure.

Hence, the first objective is to identify the *mtar11* mutation and characterize the pathway that contributes to the abnormal phenotypes of MTA accumulation. Furthermore, the *mtn1-1mtar11* plant is considerably larger and more fertile than WT. These phenotypes are consistent with domesticated plants. Thus, *mtar11*'s association with domesticated plants will be assessed to determine its involvement in their domestication. Chapter 2 documents the investigation of these goals.

The final objective will determine the pathways affected by MTA accumulation by characterizing its effect on root development, cell proliferation, plant architecture, and TOR activity. These investigations will be aided by attempting to suppress abnormal phenotypes of the *mtn1-1mtn2-1* mutant with *mtar11*. How much this mutant recovers the vegetative and reproductive phenotypes will help implicate the pathways impacted by MTA. Chapter 3 documents the investigation of these goals.

Chapter 2

Amino acid change in *bZIP29* confers resistance to MTA toxicity and is associated with domesticated plants

2.1 Introduction

Met is an essential sulfur-containing amino acid that plays a central role in protein synthesis as well as a regulatory role in the active form of SAM (Bürstenbinder et al., 2010). SAM functions as a primary methyl donor and as a precursor for the biosynthesis of ethylene and the polyamines Spd, Spm, and Tspm (Bhagavan and Ha, 2015). The reactions that form these compounds produce MTA as a by-product while consuming SAM. In microorganisms and plants, MTA is recycled back via the Met salvage cycle (Miyazaki and Yang, 1987). Under sulfur limiting conditions, salvage of Met is crucial. Thus, the synthesis, accumulation and consumption of Met in plants is assumed to be under stringent control (Hesse and Hoefgen, 2003).

In Arabidopsis, the initiation of the Met salvage cycle begins with the breakdown of MTA into MTR and adenine by MTN. MTA toxicity was first noted by Bürstenbinder et al. (2007) when WT seedlings were grown on sulfur-free growth media supplemented with 500 μM of MTA. This treatment resulted in reduced root and shoot growth as well as a substantial decrease in fresh weight. T-DNA insertions in *mtn1-1* and *mtn2-1* further increased this growth reduction on MTA but do not display any apparent phenotypic abnormalities under sulfur-sufficient conditions. In contrast, the *mtn1-1mtn2-1* double mutant shows an array of abnormalities under sulfur-sufficient conditions, including delayed bolting and impaired fertility (Waduwara-Jayabahu et al., 2012). However, this double mutant does not survive on media with MTA as the sole sulfur source. The complex phenotype of this severe MTN mutant can be traced back to the effects of MTA accumulation.

Despite the previous work involving metabolite, transcriptomic, and careful physiological assessments, the mechanisms of MTA toxicity in MTN-deficient plants are still not well understood (Waduwara-Jayabahu et al., 2012; Tremblay, 2019). This provided an opportunity to implement a forward genetic approach in an attempt to identify mutants that suppress the mutant phenotypes of MTA toxicity and pinpoint the direct effects of MTA. By introducing SNPs into the *mtn1-1* background using EMS mutagenesis, mutants that resist MTA pressure when grown on media with MTA as the sole sulfur source and resemble WT seedlings could

be identified. From this approach, five suppressor mutants were isolated and named MTARs. At the start of this research, only the causative SNP of *mtar2* was identified out of the five *mtars*. The *mtar2* mutation lies within *NSP1*, a GLS-related gene (Tremblay, 2019).

The significance of this SNP suggested that MTA accumulation has a role in changing GLS metabolism by shifting the sulfur flux towards glucosinolates and auxin biosynthesis in the MTN-deficient mutants (Tremblay, 2019). GLS are primarily precursors for the synthesis of defense compounds used by the plant upon herbivory (Bednarek et al., 2009). GLS are also used to form ITC, thiocyanates, and simple nitriles produced by NSP1 (Bednarek et al., 2009; Sugiyama et al., 2021). While the majority of GLS in seedlings are converted into simple nitriles, a recent study suggests that sulfur is reallocated back to Cys production via ITCs in a retrograde pathway under sulfur deprivation (Sugiyama et al., 2021). It is unknown how the *mtar2* mutation affects its retrograde flux of sulfur back to Cys or whether it accumulates simple nitriles. The accumulation of GLS directly correlates to increased auxin in the form of IAA from the simple nitrile biosynthesis pathway in seedlings (Urbancsok et al., 2017). The suppressor mutant may prevent elevated IAA biosynthesis, thus suppressing the short root when MTA is the sole sulfur source.

Of the five *mtn1-1mtars* recovered from the suppressor screen, only *mtn1-1mtar11* was a dominant mutant (Tremblay, 2019). Thus, the focus of this study is to identify and confirm the causative mutation in *mtn1-1mtar11*. Preliminary phenotypic assessments of the *mtar11* plant indicated that this mutation positively affected the plant's growth as both the silique size and plant height were larger than the parent *mtn1-1* and WT plants.

Humans have domesticated certain plant species for traits, including increased fruit size, rapid generation times, and increased seed yield. The positive growth effects of the *mtar11* mutation coincide with domesticated characteristics. This observation initiated the investigation of whether specific amino acid changes are more associated with domesticated species. The characterization of mutations that lead to domestication provides a clue about the function of the genes involved in the domestication process. Determining whether *mtar11* is associated with domesticated species will assist in characterizing the effect of the mutation and the function of the gene in plant physiology.

2.2   Materials and Methods

2.2.1   Plant material and growth conditions

Seedling growth

Arabidopsis seeds were surface sterilized using chlorine gas generated by mixing 100 mL of household bleach with 4 mL of concentrated hydrochloric acid in a designated glass sterilization chamber. Tubes containing seeds were left in the sterilization chamber for an hour and a half (Lindsey et al., 2017). Sterilized seeds were then sown on solid 1/2MS media with 0.8% (w/v) agar and 1% (w/v) sucrose (Murashige and Skoog, 1962). These plates were left to stratify for two days, in the dark at 4°C. Plates were then placed in a growth chamber with continuous light from fluorescent bulbs set to 100 μE m^{-2} s^{-1} and the temperature set at 20°C for 14 days (TC7, Conviron, Winnipeg, Canada).

MTA and MgSO$_4$ media were prepared as described by (Bürstenbinder et al., 2010). Extra care was taken to avoid sulfur contamination and reduce concentrations of sulfur in the modified 1/2MS sulfur-deficient media. The 1/2MS media was modified by substituting sulfur-containing ingredients with their respective sulfur-free alternatives. MTA growth experiments were performed using sulfur-deficient medium supplemented with 500 μM MgSO$_4$ or 650 μM MTA (Abcam, Lot: GR3319559).

Adult plant growth

Seedlings were transplanted from solid growth media into individual 2.5 inch pots containing Sunshine SS LC1 (SunGro Horticulture Inc., Washington, USA). Plants were grown in growth chambers with a 16 h daily light cycle from fluorescent bulbs with light levels set at approximately 160 μE m^{-2} s^{-1} and the temperature set at 20°C. They were watered every two or three days and fertilized once every week using 1.5 gL^{-1} of a 20:20:20 (N:P:K)

fertilizer mix (Plant Products Co. Ltd., Brampton, Canada). The plant height was measured from the soil level to the top of the primary inflorescence stem when the apical bud cluster failed to produce new flowers.

Plant lines

Arabidopsis mutant plants, including WT control plants, were in the Columbia (Col-0) ecotype. The mutant line containing a T-DNA insertion in *MTN1* (*mtn1-1*; SALK_085385) was obtained from the Arabidopsis Biological Resource Center (Ohio State University, USA). The suppressor mutant *mtar11* was generated in the *mtn1-1* background by Tremblay (2019) using EMS mutagenesis. Transgenic plant lines with T-DNA insertions were genotyped with a PCR condition as follows: 94°C for 5 min, 34 cycles with 94°C for 1 minute, 53°C for 30 seconds and 72°C for 1 minute and 30 seconds and a final extension step at 72°C for 10 min (Waduwara-Jayabahu et al., 2012). The *mtar11* SNP was genotyped as described by Hirotsu et al. (2010), using the primers listed in Table 2.1. The PCR condition for genotyping the *mtar11* SNP is similar to genotyping the T-DNA insertions with the exception of a 65°C annealing temperature and a 40 second extension time per cycle.

2.2.2   Genomic DNA extraction

Genomic DNA was extracted from approximately 1 g of frozen vegetative tissue from four-week-old *mtar11* plants and ground into a fine powder using liquid nitrogen, a mortar, and a pestle. The fine powder was directly added to 10 mL of cetyltrimethyl ammonium bromide (CTAB) extraction buffer (100 mM Tris-HCl pH 8.0, 20 mM EDTA pH 8.0, 1.4 M NaCl, 2% CTAB, 1% polyvinylpyrrolidone (PVP) 40 000), thoroughly mixed, and incubated at 65°C for 10 min with gently inversion every 2 min. Chloroform:isoamyl alcohol (24:1) was added after incubation and mixed by inversion for 5 min. The solution was then centrifuged for 10 min at 4°C and max speed using a bench-top centrifuge (model 5415R; Eppendorf, Hamburg, Germany). After centrifugation, the aqueous phase was mixed with one volume of

isopropanol and incubated for 20 min at -20°C. This solution was centrifuged for 20 min at max speed at 4°C. The supernatant was discarded after centrifugation, and the DNA pellet was washed with 75% ethanol and then centrifuged once again for 5 min at max speed. The supernatant was removed and the pellet was left to dry. The DNA was resuspended in 50 μL TE buffer (pH 8.0). RNA contamination was removed by adding RNase A to the solution at a concentration of 10 μg mL^{-1} and incubated for one hour at 37°C and then stored at 4°C. The final DNA solution was cleaned using a DNeasy Plant Mini Kit (Qiagen Inc., Toronto, ON, Canada).

2.2.3   Whole-genome sequencing and SNP mapping

Whole-genome sequencing and library preparation was performed by Novogene Corporation (Sacramento, CA, USA). A 350 bp insert DNA library was prepared and sequenced using Illumina Novaseq 6000 (Illumina Inc., San Diego, CA, USA) with a 150 bp paired-end sequencing strategy and 40x coverage.

The raw reads generated from sequencing were trimmed and their qualities were assessed with Trim Galore! (v0.6.1; Krueger, 2012). Quality reads were then assembled and mapped on to TAIR10 Arabidopsis reference genome with BWA (v0.7.17; Li and Durbin, 2009) while duplicate reads were removed using Picard (v2.19.0; Broad Institute, 2019). Read recalibration and SNP mapping were done with GenomeAnalysisTK (v4.1.4.0; McKenna et al., 2010). SnpSift (v4.3; Cingolani et al., 2012) was then used to mark and annotate SNPs. The raw list of SNPs was further analyzed and filtered to produce a list of intragenic homozygous SNPs using a Python (v3.8.9) script.

Table 2.1: PCR primers used for genotyping.

Allele	Primer Name	Sequence
MTN1	*mtn1-1F*	TGACGGAGACCAACTCCATAC
	mtn1-1R	GAGGCTCTTCCTTTGGTCAAC
mtn1-1	LBb1.3	ATTTTGCCGATTTCGGAAC
	mtn1-1R	GAGGCTCTTCCTTTGGTCAAC
MTN2	*mtn2-1F*	CCTTGCTTACGTGGCATAAAC
	mtn2-1R	AGGAAAGGGCAAAAATATATGG
mtn2-1	LBb1.3	ATTTTGCCGATTTCGGAAC
	mtn2-1R	AGGAAAGGGCAAAAATATATGG
MTN2-5	*mtn2-5F*	ACTGTGCCAACACTCTCAACC
	mtn2-5R	AAGATTTCCGCTTCCTGAAAG
mtn2-5	LBb1.3	ATTTTGCCGATTTCGGAAC
	*mtn2-5*R	AAGATTTCCGCTTCCTGAAAG
MTAR11	p11g_noSNP_F	GAGCAGCAGAGCAAGCGGTAC
	pDKML_R	GCACCCGAGTTCCCATCAAC
mtar11	p11g_SNP_F	GAGCAGCAGAGCAAGCGGTAT
	pDKML_R	GCACCCGAGTTCCCATCAAC

2.2.4 Dataset curation, alignment, and annotation of bZIP29 homologs

Sequences were gathered from PSI-BLAST by searching the NCBI non-redundant database while specifying the Plantae kingdom and using *bZIP29*'s amino acid sequence as the query. The initial search was followed by three iterative PSI-BLAST searches. After the removal of poorly aligned sequences, a total of 461 bZIP29 homologs were retrieved. These sequences were aligned using the G-INS-i algorithm from the MAFFT package (v7.475; Katoh and Standley, 2013). The multiple sequence alignment was further pruned, conserved regions were selected for phylogenetic and residue analysis using a strict trimAl algorithm (v1.4.rev22; Capella-Gutiérrez et al., 2009). The plant species in the curated sequence database was manually categorized as either wild or domesticated after a thorough literature search for each plant species (Table A1). Of the 173 plant species assessed, 85 species were wild, and 88 were domesticated.

2.2.5 Evolutionary analysis of bZIP29 protein

The number of sequences was further reduced to a set of 155 non-redundant sequences by clustering using USEARCH (v11.0.667) at 90% identity (Edgar, 2010). A maximum-likelihood tree was created from the pruned sequence alignment using RAxML (v8.2.11) with PROTGAMMALG4M model selection, automatic bootstrapping, and an ML search (Stamatakis, 2014). A species tree consisting of the plant species found in the bZIP29 curated data was constructed using NCBI Taxonomy and manual placement of organisms with undefined lineages (Schoch et al., 2020). The phylogenetic trees was visualized with iTOL (v5.0; Letunic and Bork, 2021).

2.2.6 Residue analysis

The residue analysis algorithm was constructed in Python (v3.8.9). Probability scores were generated from the curated multiple sequence alignment for each amino acid residue

using Jensen-Shannon divergence and the BLOSUM62 matrix from the Protein Residue Conservation Prediction tool (Capra and Singh, 2007). This algorithm also generates a consensus sequence from the sequence alignment. It compares each residue in that consensus sequence with the corresponding residue in the multiple sequence alignment as long as it meets the probability threshold of greater than 0.6. The conserved residues with an amino acid change were then grouped as belonging to a plant species classified as wild or domesticated. Residues that did not have an amino acid change in the sequence alignment were not analyzed. From here, a heatmap was constructed with the individual squares of the plot representing the fold change from the expected number of amino acid changes associated with domesticated species at each residue using the hypergeometric statistical distribution (Berkopec, 2007).

After constructing the heatmap, amino acid changes were scored using the BLOSUM62 matrix, and conserved changes were removed from this residue analysis (Trivedi and Nagarajaram, 2019). After which, non-conserved amino acid changes at every site of the multiple sequence alignment were binned as to whether they belonged to a wild or domesticated species. The significance of these residues and their association to domesticated species were tested using a hypergeometric test (Evangelou et al., 2012). The test parameters were the following: the total number of entities in this analysis were 173 species, 88 domesticated species are classified as a successful outcome, the number of observations and successes in a sample varied based on the residue analyzed in the multiple sequence alignment.

2.2.7   Data analysis

All statistical analyses in this chapter were performed within the R environment. One-way ANOVA, Tukey's honest significant difference (HSD) and the expected fold change for the heatmap and the hypergeometric test was done using the base stats package in R (R Core Team, 2020).

2.3 Results

2.3.1 Whole-genome sequencing and identification of *mtar11* SNPs

Early characterization of the *mtn1-1mtar11* mutant revealed that the causative SNP resulted in over 75% of a segregating progeny population having increased root length when MTA was fed as the sole sulfur source (Tremblay, 2019). This segregation pattern indicates the *mtar11* SNP is a dominant mutation as a single mutant allele was sufficient to confer MTA resistance. The difficulty of isolating homozygous *mtn1-1mtar11* mutants by screening on MTA required a unique approach in identifying the causal SNP by whole-genome sequencing (WGS). A single backcross to the parent *mtn1-1* plant was performed to remove approximately 50% of the extraneous SNPs produced as a by-product of EMS mutagenesis. The F_2 progeny of this cross were screened on MTA medium, and resistant and non-resistant plants were selected. Homozygous lines were then identified by screening F_3 progenies from the resistant plants and assessing their segregation on MTA. After homozygous lines were isolated, four resistant, four MTA-sensitive, and two homozygous plants were used for WGS.

A map-by-sequence approach for SNP mapping generated a pool of putative causative *mtn1-1mtar11* SNPs (James et al., 2013). Background SNPs found in the *mtn1-1* parent background were pruned from this data set in addition to the SNPs found in the MTA-sensitive *mtn1-1mtar11* F_2 progenies plants. The cross-referencing of non-synonymous and intragenic SNPs found in the homozygous and resistant plants produced a list of six putative causative SNPs (Table 2.2).

Of the six putative SNPs, only SNP3 was found in all resistant and homozygous plants, which results in a threonine (T) to isoleucine (I) change at residue 269 in Arabidopsis. Nevertheless, another SNP other than or in addition to SNP3 may be the causative change in *mtn1-1mtar11*. The importance of these mutations was contextualized by examining the conservation of these sites, beginning with the different Arabidopsis ecotypes. After a thorough local database search of the 1001 genome database, none of these SNPs were found

Table 2.2: List of candidate *mtar11* mutations.

Homozygous *mtar11* mutations retrieved from WGS of *mtn1-1mtar11* plants. SNP6 was located in a 3′-untranslated region and has no amino acid associated with it.

SNP	Chromosome	Location	Gene	Gene symbol	DNA change	AA change
1	3	6222469	AT3G18160	*PEX3-1*	C → T	S → F
2	3	6256676	AT3G18240	-	C → T	D → N
3	4	18140715	AT4G38900	*bZIP29*	C → T	T → I
4	5	2139078	AT5G06905	*CYP712A2*	C → T	A → V
5	5	3774399	AT5G11710	*EPSIN1*	C → T	D → N
6	5	4568574	AT5G14170	*CHC1*	C → T	-

in any Arabidopsis ecotype. In fact, there are no variants found at each of these sites in all of the Arabidopsis ecotypes (retrieved from Bar:Variant Viewer June 25, 2021). This analysis was broadened beyond just Arabidopsis by conducting a protein BLAST search in the Plantae kingdom using the amino acid sequences of each gene (Table 2.2) associated with the SNP. The retrieved homologs of each gene were aligned using MAFFAT (Katoh and Standley, 2013) and pruned with trimAL (Capella-Gutiérrez et al., 2009), at which point the amino acid changes found in *mtn1-1mtar11*, alternative amino acids, and gaps were counted (Table 2.3).

This survey did not detect any amino acid changes identified in *mtn1-1mtar11* when looking at approximately 94 close homologs of each gene (Table 2.3). Even though all these amino acid substitutions are novel, only the conservation probabilities for SNP2 and 3 were larger, indicating a highly conserved residue, with SNP2 slightly edging out SNP3 (Table 2.3). There were no alternative amino acid changes for SNP2 and SNP3 among the 94 and 95 homologs. In addition, SNP2 and SNP3 are located within highly conserved regions (Figure 2.1). For comparison, the regions where SNP1, 4, and 5 are located are not conserved, suggesting that changes in these regions have little impact on protein function, making SNP2 and 3 the primary focus.

While SNP2 is highly conserved in this survey, there is no function documented for the gene it resides in, AT3G18240. Computational modeling predicts this gene encodes a ribosomal protein, highly enriched in the mitochondria and the roots of one-day-old seedlings (retrieved from ePlant Arabidopsis eFP Browser June 25, 2021).

SNP3, on the other hand, is found in a *basic-Leucine Zipper 29* transcription factor (*bZIP29*) that is implicated in regulating plant growth and has a known interaction with the TOR signaling complex (Van Leene et al., 2019). Furthermore, bZIP29 regulates several cell cycle-related genes, including *CYCB1;2* and *SMR4*. Since the amino acid conservation survey did not discount either of these SNPs, further validation was required to determine the causal SNP of *mtn1-1mtar11*. Since SNP2 does not have a known function associated with it and was not identified in all *mtn1-1mtar11* resistant plants, SNP3 in bZIP29 became the primary focus going forward.

Table 2.3: Amino acid changes at putative _mtar11_ sites.

The amino acid sequences of the putative _mtar11_ genes listed in Table 2.2 were queries for BLAST search. The retrieved homologs were then aligned with MAFFATT (Katoh and Standley, 2013) and pruned using trimAL (Capella-Gutiérrez et al., 2009). The amino acid changes at the putative _mtar11_ mutation sites for each gene were counted. SNP1, serine (S) to phenylalanine (F). SNP2, aspartic acid (D) to asparagine (N). SNP3, threonine (T) to isoleucine. SNP4, alanine (A) to valine (V). SNP5, aspartic acid (D) to asparagine (N). The Jensen-Shannon divergence scored the conservation of each SNP.

SNP	AA Change	Sequences	Original AA	New AA	Other	Gap	Conservation score
1	**S**275**F**	91	77	0	8	6	0.636
2	**D**215**N**	94	94	0	0	0	0.814
3	**T**269**I**	95	95	0	0	0	0.809
4	**A**309**V**	95	86	0	9	0	0.665
5	**D**198**N**	96	87	0	4	5	0.694
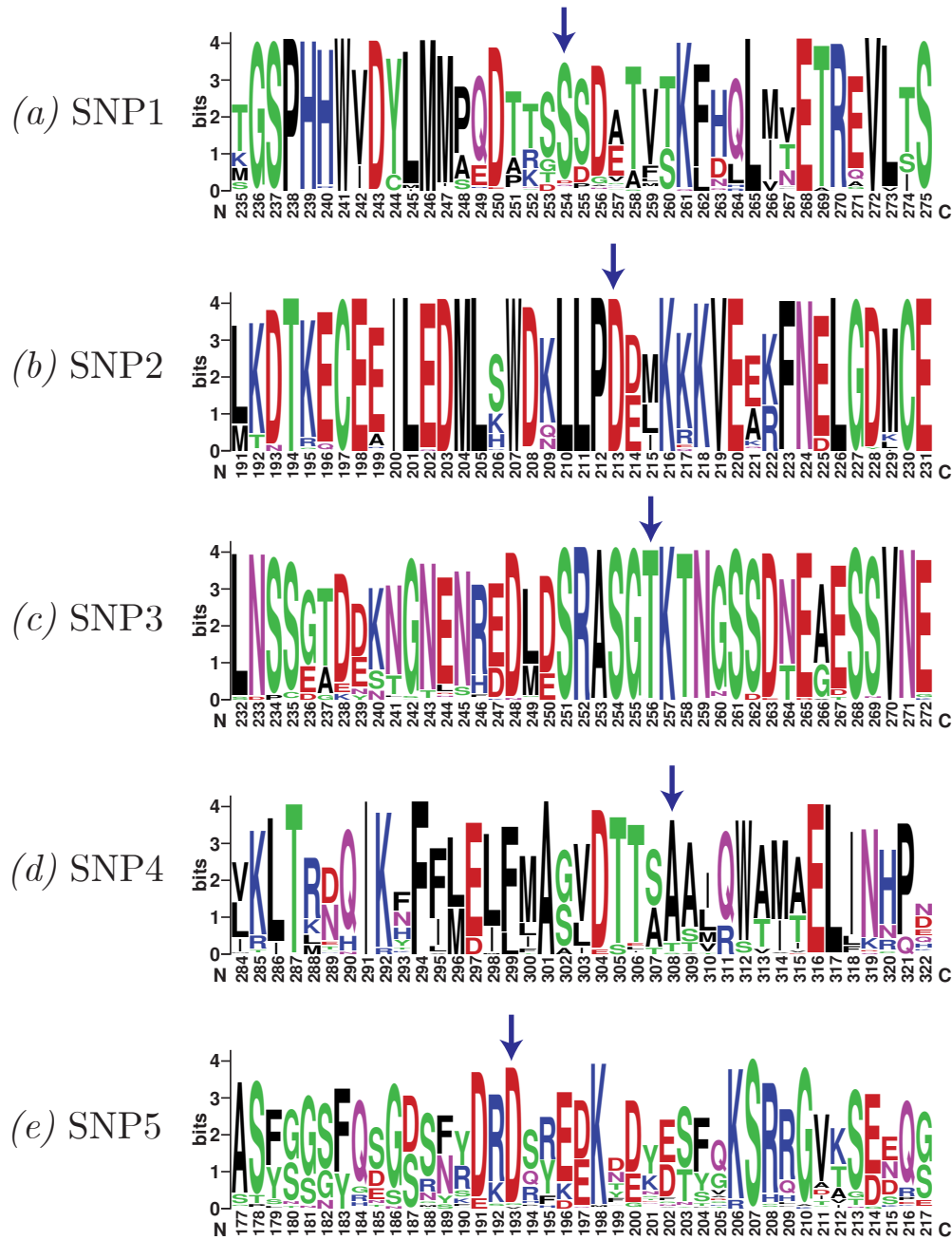
Figure 2.1: Residue conservation of putative *mtar11* amino acid substitutions.

The homologs of each gene for which a putative *mtar11* SNP lies in from Table 2.2 were aligned and pruned. The resulting multiple sequence alignment was converted into sequence logos using WebLogo (Crooks et al., 2004). The location of the amino acid substitution identified in *mtar11* was used to center these logos. At these locations, the following changes found are marked by a blue arrow: *(a)* for SNP1, serine (S) to phenylalanine (F), *(b)* SNP2, aspartic acid (D) to asparagine (N), *(c)* SNP3, threonine (T) to isoleucine, *(d)* SNP4, alanine (A) to valine (V), *(e)* SNP5, aspartic acid (D) to asparagine (N).

2.3.2 Segregation analysis of *bZIP29* as the candidate *mtn1-1mtar11* SNP

A common approach to confirm the location of a causal SNP produced by forward-genetics is to introduce a known T-DNA insertion into the respective gene and assess if a similar mutant phenotype is produced. For *mtn1-1mtar11*, a T-DNA insertion would be introduced into *bZIP29* in the *mtn1-1* background to assess if this mutation results in MTA resistance. Unfortunately, *bZIP29* is close in proximity to the *MTN1* gene, being only approximately 29 kb upstream of *MTN1* on chromosome 4, making these two genes genetically linked. Therefore, the inability to introgress a characterized T-DNA insertion into the *mtn1-1* background for the *bZIP29* locus made confirming this SNP difficult and required an alternative method.

In this case, a homozygous *mtn1-1mtar11* plant was backcrossed for a second time to the parent *mtn1-1* plant, and the F_2 plants were screened on MTA medium as previously done in preparation for WGS of *mtn1-1mtar11*. A range of 24 resistant and sensitive seedlings selected off MTA was genotyped for SNP3. Since the *mtn1-1mtar11* mutation is dominant, a single allele would confer resistance against MTA. From this assay, all resistant seedlings were either heterozygous or homozygous for SNP3, while sensitive seedlings selected off MTA did not have that mutation (Table 2.4). A select few of these resistant seedlings were progressed to the next generation and screened on MTA (Table 2.4). Resistant plants which were homozygous for SNP3 all had long roots with no segregation. In contrast, heterozygous plants only had a 70% MTA-resistant seedlings ratio, consistent with the segregation of a dominant mutation (Table 2.4). The progeny from sensitive plants showed no resistance to MTA in the F_3 generation.

SNP2, which was also highly conserved, is located on chromosome 3 instead of chromosome 4, where *bZIP29* is found. Thus, it is unlikely that the two SNPs segregate together, which further validates this segregation analysis of SNP3 and gives confidence to SNP3 in *bZIP29* as the causative SNP in *mtn1-1mtar11*.

Table 2.4: Segregation analysis of SNP3 in F$_3$ progenies on MTA.

Homozygous *mtn1-1mtar11* plants were backcrossed for a second time to *mtn1-1*. The F$_2$ progeny from this cross were screened on MTA and resistant and non-resistant seedlings were selected. MTA resistant *mtn1-1mtar11* seedlings had root lengths that were approximately twice the length of *mtn1-1* after 7 days after stratification (DAS) and closely resemble WT root growth. The F$_2$ plants were genotyped by PCR for SNP3 and followed another generation. The F$_3$ progeny from a select few genotyped plants was then screened on MTA. (+) represents the WT allele and (-) the mutant allele with SNP3.

mtn1-1 mtar11 plant	Genotype	MTA Resistant seedlings	Total seedlings	Ratio (%)
R5	*mtar11*$^{-/-}$	41	42	97.6
R7	*mtar11*$^{-/-}$	29	30	96.7
R8	*mtar11*$^{+/-}$	31	40	77.5
R9	*mtar11*$^{+/-}$	26	34	76.5
R11	*mtar11*$^{-/-}$	22	22	100.0
R12	*mtar11*$^{+/-}$	27	38	71.1
R13	*mtar11*$^{+/-}$	20	23	87.0
S15	*mtar11*$^{+/+}$	0	25	0.0
S16	*mtar11*$^{+/+}$	0	20	0.0
S22	*mtar11*$^{+/+}$	0	28	0.0
S23	*mtar11*$^{+/+}$	0	29	0.0
S24	*mtar11*$^{+/+}$	0	35	0.0

2.3.3 Phenotypic characterization of the causal *mtn1-1mtar11* mutation

Preliminary phenotypic observations of the *mtn1-1mtar11* plant agree with a previously characterized T-DNA insertion mutant located within *bZIP29* (Lozano-Sotomayor et al., 2016) as both plants are taller and produce longer siliques than Col-0 plants. However, the T-DNA insertion in *bZIP29*, named *drink me-like* (*dkml*; Lozano-Sotomayor et al., 2016), is a knock-out mutant, and since the effect of the *mtn1-1mtar11* T26I amino acid change on the protein's function is unknown, careful phenotypic characterization of the causal *mtn1-1mtar11* mutation was required. This phenotypic characterization began with assessing root growth.

mtn1-1mtar11 seedlings grew a slightly longer root on $MgSO_4$ media than WT and *mtn1-1*, with no size differences in the shoot system 10 days after stratification (DAS; Figure 2.2). However, when grown on MTA, *mtn1-1mtar11* seedlings were resistant to the MTA pressure and grew longer roots than *mtn1-1*, with lateral root growth suppressed and a substantially larger shoot system (Figure 2.2). Similarly, the causal *mtn1-1mtar11* SNP results in a considerably taller plant than WT and *mtn1-1*, with longer siliques and a greater seed yield per plant (Figure 2.3). Though the increase in silique length of *mtn1-1mtar11* is minimal compared to *mtn1-1*, it is much longer than the silique length of *dkml* and resulting in a much greater seed yield (Lozano-Sotomayor et al., 2016).

2.3.4 Functionally significant amino acid changes at the causal *mtar11* mutation are associated with domesticated plants

Changes to *bZIP29*'s amino acid sequence results in impactful physiological alterations, leading to increased plant productivity, as shown by the *dkml* mutant and the *mtn1-1mtar11* causal SNP. In addition, the causal *mtn1-1mtar11* SNP lies within a highly conserved region of the protein (Figure 2.1) and affects a predicted phosphorylation site (retrieved from NetPhos3.1; Blom et al., 1999). Given that alterations to this site results in advantageous phenotypes for the plant, an opportunity arose to assess if changes to amino acid 269 are associated with
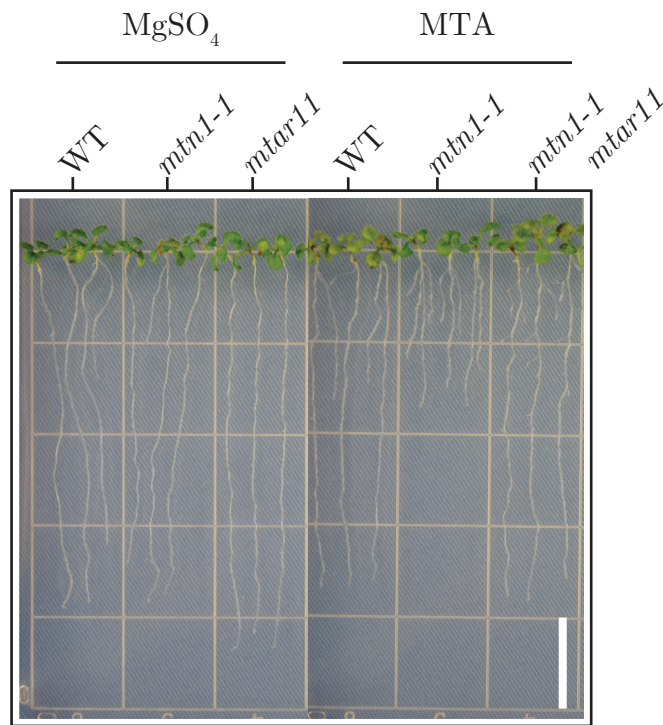
Figure 2.2: Increased root growth of *mtn1-1mtar11* seedlings on MTA.

These representative seedlings were sown on sulfur-free media supplemented with either 500 μM MgSO$_4$ or 650 μM MTA and grown vertically for 10 DAS. Scale bar represents = 1 cm. *mtar11*, *mtn1-1mtar11*.
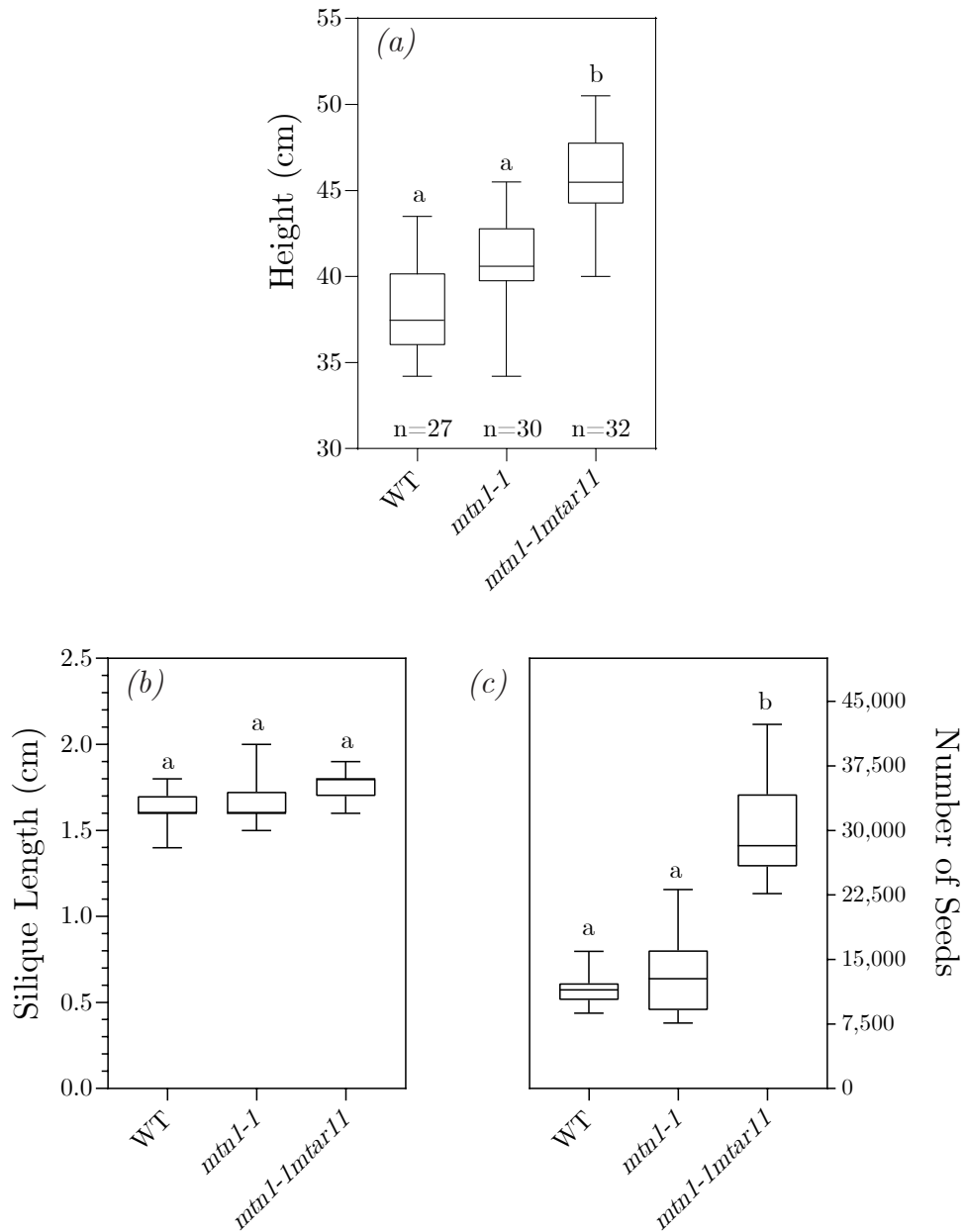
Figure 2.3: Early phenotypic effects of *mtar11* mutation on plant growth and reproductivity of *mtn1-1*.

Once WT, *mtn1-1*, and *mtn1-1mtar11* plants reached their maximum height which was marked by the lack of production of new floral buds and inflorescence stem elongation, the plant height was measured from the base of the primary inflorescence stem to the highest point *(a)*. As plants began to senescence, the average length of the siliques were measured *(b)* and seeds were harvested and counted by weighing the seeds after the plants were completely dry *(c)*. The number of replicates of each genotype is indicated in *(a)* and the letters represent statistical significance from Tukey's HSD post hoc test after a one-way ANOVA ($p < 0.05$).

47

domesticated plants. Unfortunately, the initial protein BLAST search to evaluate the conservation of the *mtn1-1mtar11* site was not sufficient to evaluate the broad phylogenetic inheritance of bZIP29 and its homologs. Therefore, after three iterations of PSI-BLAST and the removal of poorly aligned sequences, a database was constructed comprising a total of 461 bZIP29 homologs. A thorough literature survey classified each plant species in this curated database as wild or domesticated (Table A1).

In this database, the *mtn1-1mtar11* residue (106) is still highly conserved, but interestingly, amino acid changes at this residue are more commonly associated with domesticated species (Figure 2.4*b*). The site of the *mtn1-1mtar11* amino acid substitution tolerates a threonine to serine change though, domesticated species significantly alter this residue by substituting threonine to amino acids alanine, asparagine, or isoleucine (Figure 2.4*c*). However, the amino acid change of threonine to isoleucine found in *mtn1-1mtar11* was only identified in two domesticated plants (Table 2.5). In addition, these two species primarily use two different modes of reproduction, with *T. cacao* and *C. esculenta* relying on sexual and asexual reproduction, respectively (Chaïr et al., 2016; Bekele and Phillips-Mora, 2019).

2.3.5 Detailed residue analysis of bZIP29

Considering that the amino acid change at the *mtn1-1mtar11* mutation site is associated with domesticated species and bZIP29 is involved in regulating plant growth, a detailed residue analysis explored the possibility that other residues of bZIP29 are associated with domesticated species. Thus, a thorough residue analysis was conducted at other conserved sites to assess if non-conserved amino acid changes are found in domesticated species. The residue analysis algorithm generates a consensus sequence. It then compares each residue with the corresponding residue in the sequence alignment as long as it meets the probability threshold of greater than 0.6. By setting a high probability value, poorly conserved residues were not carried over in subsequent analysis. The conserved residues with an amino acid change were then grouped as belonging to a plant species classified as either wild or domesticated. Residues that do not have an amino acid change in the sequence alignment were not analyzed.
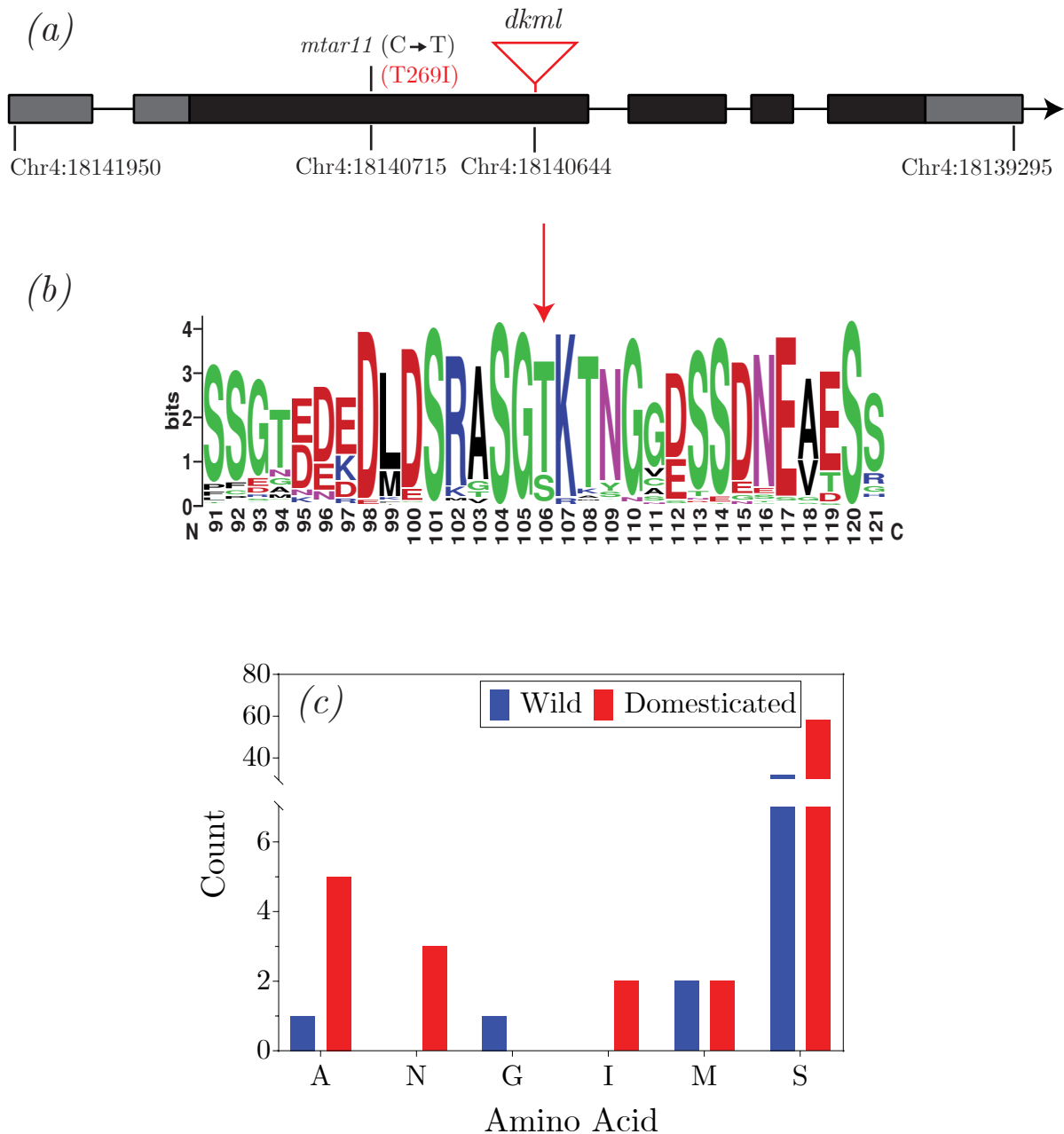
Figure 2.4: *mtar11* mutation in bZIP29 is more associated with domesticated species.

Schematic representation of *bZIP29 (a)*. Exons and untranslated regions are represented by black and grey boxes, respectively. The location of *mtar11* SNP and *dkml* T-DNA insertion is shown as well as the threonine (T) to isoleucine (I) amino change in *mtar11*. A redundancy-removed, pruned alignment of bZIP29 homologs after 3 iterations of PSI-BLAST were converted to sequence logos using WebLogo *(b)*. The location of the *mtar11* mutation is pointed to with a red arrow. The amino acid changes found at the site of the *mtar11* mutation and their species classification *(c)*. Isoleucine at this position was seen in only domesticated species.

Table 2.5: Plant species that have an amino acid change at the *mtar11* residue.

Each plant species in the curated database of *bZIP29* homologs was manually classified as either wild or domesticated after a thorough literature search (Table A1). The *mtar11* residue tolerates a threonine (T) to serine change so only non-conserved amino acid changes are listed here. *A, Alanine*; *N, Asparagine*; *I, Isoleucine*; *W, Wild*; *D, Domesticated.*

Organism	Common Name	Order	Change	Classification
Arachis hypogaea	Peanut	Fabales	T → A	D
Gossypium harknessii	San Marcos Hibiscus	Malvales	T → A	W
Elaeis guineensis	Afican Oil Palm	Arecales	T → A	D
Glycine max	Soybean	Fabales	T → A	D
Phaseolus vulgaris	Common Bean	Fabales	T → A	D
Vigna radiata var. radiata	Mung Bean	Fabales	T → A	D
Camelina sativa	False Flax	Brassicales	T → N	D
Citrus sinensis	Sweet Orange	Sapindales	T → N	D
Brassica rapa	Field Mustard	Brassicales	T → N	D
Theobroma cacao	Cacao Tree	Malvales	T → I	D
Colocasia esculenta	Taro	Alismatales	T → I	D

Several amino acids are highly conserved throughout the alignment, especially in the predicated bZIP domain (210-255; Figure 2.5). Before assessing whether substitutions at these conserved sites are associated with domesticated species, amino acid changes that were functionally significant at each residue were considered. Each site may tolerate a specific substitution, as illustrated by the *mtn1-1mtar11* mutation site (Figure 2.4). Therefore, a heatmap was constructed based on observed amino acid substitutions at each residue (Figure 2.6). The individual squares represent the fold change from the expected number of amino acid changes associated with domesticated species using the hypergeometric statistical distribution (Evangelou et al., 2012). This distribution analysis allowed for assessing both substitution biases and noteworthy trends associated with wild or domesticated species.

What is striking about this heatmap is the enrichment of gaps found at most residues associated with domesticated species. After carefully pruning the multiple sequence alignment used for this analysis, each gap represents an insertion or deletion. Given that insertion/deletions are associated with substantial effects on protein structure (Zia and Moses, 2011), the enrichment of this element at each residue appears to correlate with that residue's association with domesticated or wild species (Figure 2.6). For example, residues 1 to 11, 187 to 212, and 254 to 277 are more associated with domesticated species, while residues 75 to 97 and 140 to 154 are associated with wild species. These series of gaps also represent sizable insertions and deletions between homologs and likely represent functionally important changes to bZIP29 homologs (Figure 2.6).

For the most part, the bZIP domain between residues 210 and 255 is conserved, but interestingly, there are a few residues within this domain associated with domesticated plants. Overall, several residues are associated with domesticated plants (Figure 2.6), and many are highly represented in conserved regions (Figure 2.5).

When assessing the distribution of amino acid substitutions found in bZIP29 homologs, countless cases illustrate substitution bias of conserved amino acids. For example, at residue 43, phenylalanine (F) is highly conserved in the multiple sequence alignment but there is an enrichment of tyrosine (Y) substitutions in domesticated species. Based on the BLO-SUM62 matrix, which is used to assess the biological probability of a substitution (Eddy, 2004),
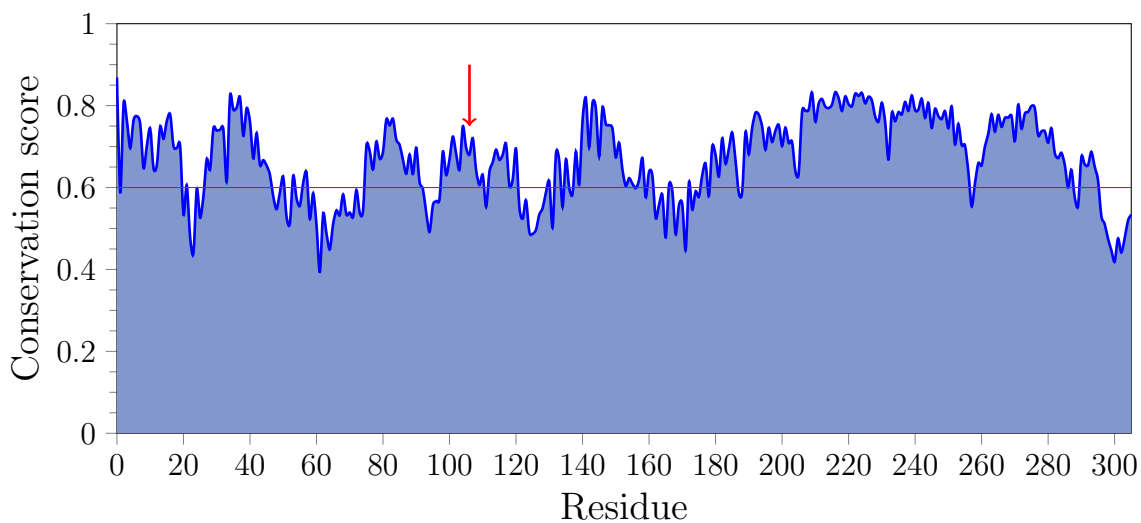
Figure 2.5: Amino acid conservation scores for residues in bZIP29 and its homologs.

The Jensen-Shannon divergence score was calculated for each residue in the multiple sequence alignment of bZIP29 homologs following 3 iterations of PSI-BLAST and alignment pruning using trimAL (Capella-Gutiérrez et al., 2009). This score measures the conservation of residues between multiple sequences (Capra and Singh, 2007). The first residue in the multiple sequence alignment was considered residue 0 rather than 1. The red arrow indicates the position of the *mtar11* mutation and the red horizontal line at 0.6 is the cut-off score used for follow-up residue analyses.
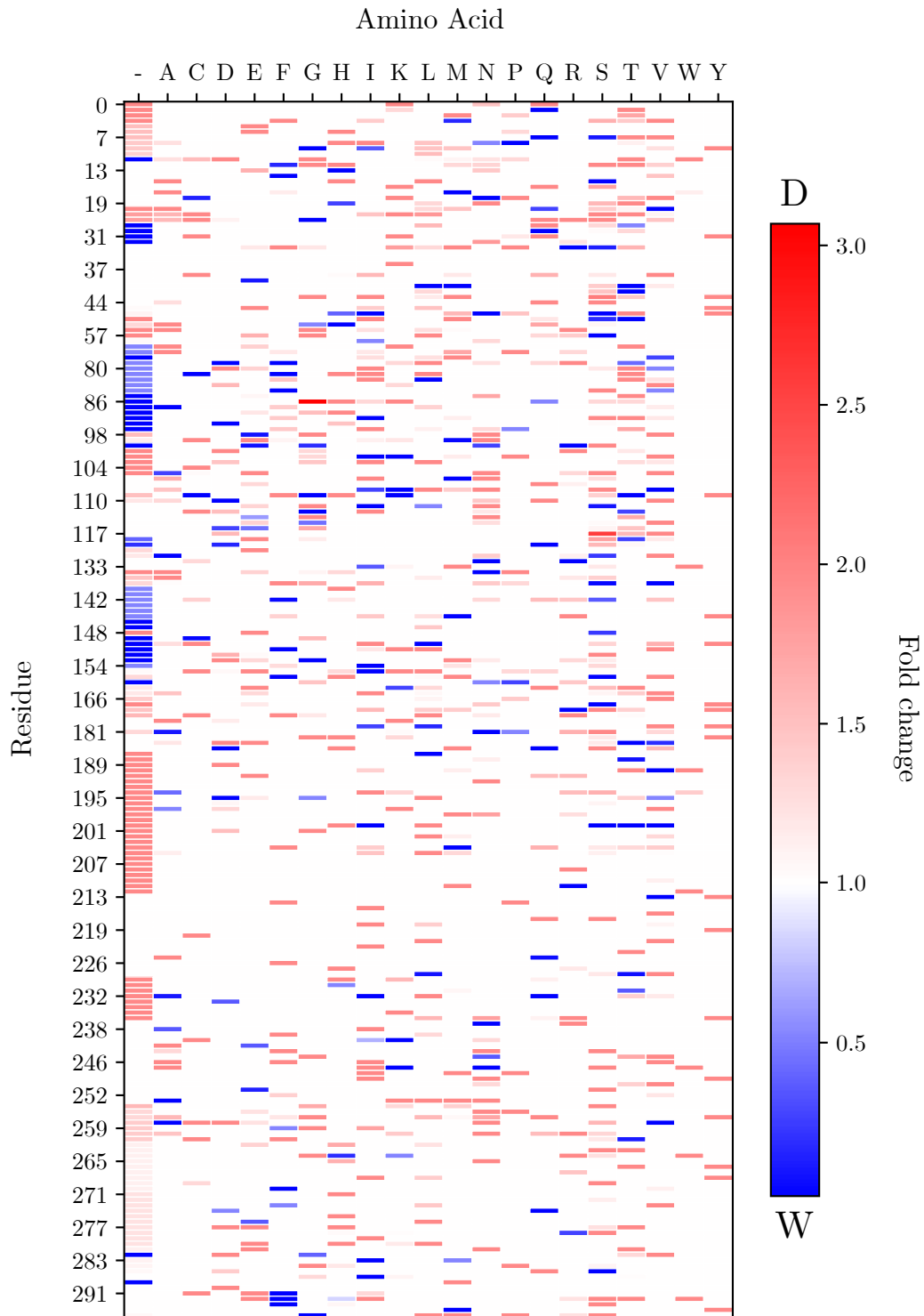
Figure 2.6: Distribution of amino acid changes for each conserved residue of bZIP29 homologs.

From the curated database of bZIP29 homologs, a heatmap was constructed based on the observed amino acid changes at each residue that met the conservation score threshold of 0.6.

Figure 2.6 *(previous page)*: Distribution of amino acid changes for each conserved residue of bZIP29 homologs.
The individual squares in this plot represent the fold change from the expected number of amino acid changes at each residue associated with domesticated species using hypergeometric statistical distribution (Berkopec, 2007). Amino acid changes that were more likely to be found in domesticated (D) species are illustrated in red while blue labels amino acid changes found in wild (W) plant species. The first residue in the multiple sequence alignment was considered residue 0 rather than 1. *(-), gap; A, Alanine; C, Cysteine; D, Aspartic acid; E, Glutamic acid; F, Phenylalanine; G, Glycine; H, Histidine; I, Isoleucine; K, Lysine; M, Methionine; N, Asparagine; P, Proline; Q, Glutamine; R, Arginine; S, Serine; T, Threonine; V, Valine; W, Tryptophan; Y, Tyrosine.*

this amino acid change is functionally conserved (Figure 2.6). In contrast, glutamine (G) isoleucine (I) Met (M), Ser (S), are non-conserved substitutions at this residue and are enriched in domesticated species. There are also many cases of conserved amino acid substitutions enriched in wild plant species. At residue 154, the amino acid change of leucine (L) to isoleucine (I) is highly enriched in wild species (Figure 2.6). These instances of conserved amino acids present in this database would skew statistical analysis of amino acids associated with domesticated species.

By assessing substitution bias at every conserved residue using the BLOSUM62 matrix, concentrating on non-conserved substitutions, and assessing the association of each residue with domesticated species using a hypergeometric statistical test, several novel residues of bZIP29 are associated with domesticated species (Figure 2.7). This analysis also confirms that the changes at the *mtar11* mutation site (residue 106) are associated with domesticated species (Figure 2.7). In accordance with the distribution of amino acid changes, groups of residues that are close in proximity are also found in domesticated species. These distinct clusters are located in the middle and towards the C-terminus of the protein (Figure 2.7). Interestingly, many were correctly associated with domesticated species because of the cluster of residues in which gaps were identified, like 254 to 277 (Figure 2.6). This correlation validates the association of insertions and deletions significantly altering bZIP29's protein function in domesticated species.
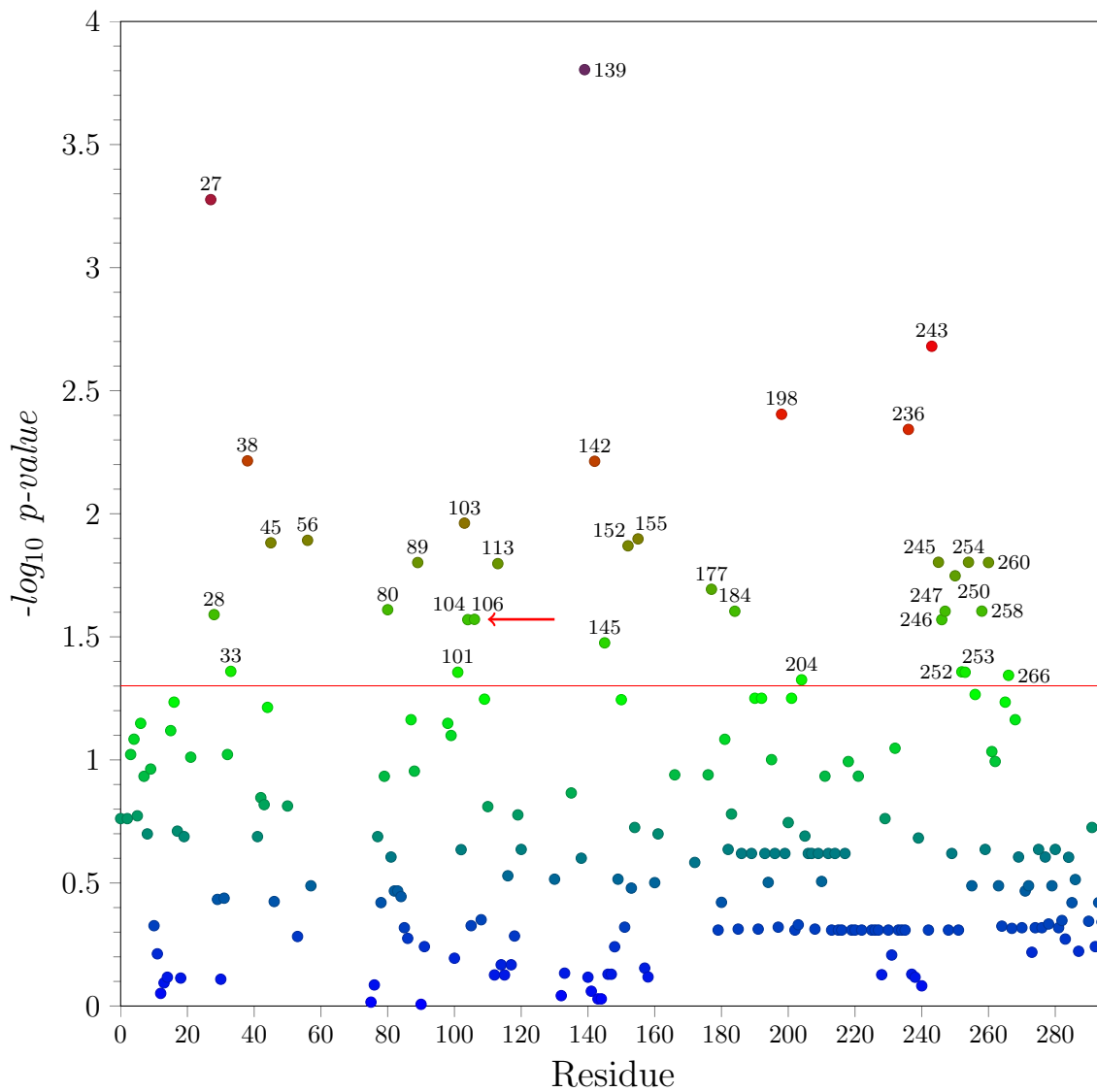
Figure 2.7: Several novel bZIP29 residues are associated with domesticated species.

Conserved amino acid changes were pruned from this residue analysis using the BLOSUM62 matrix. The significance of these residues and their association to domesticated species were tested using a hypergeometric test (Evangelou et al., 2012). Only residues that are statistically significant are labeled. The first residue in the multiple sequence alignment was considered residue 0 rather than 1. The *mtar11* mutation residue (106) is indicated with a red arrow while the red horizontal line marks statistical significance at p < 0.05.

2.3.6 Phylogenetic analysis of amino acid changes in bZIP29 found in domesticated species

A phylogenetic analysis was conducted to determine if amino acid substitutions associated with domesticated plants have been independently selected when comparing the evolution of the 173 plant species within this curated database (Table A1). The evidence for this test would be the presence of an amino acid at a particular site found in members of two distantly related monophyletic groups. This analysis further validates that changes at conserved residues have been naturally selected in domesticated plants rather than passed on from a common ancestor. Any instances of independent evolution would indicate that changing the function of a bZIP29 homolog is at least involved in the domestication process of a plant. Two approaches were taken to infer the phylogenetic significance of residue changes in bZIP29. The first was to assess the phylogenetic distribution of the *mtar11* mutation across the phylogeny of the 173 plant species. The second was to evaluate congruence between the phylogeny of bZIP29 and the plant species (Leigh et al., 2011).

The non-conserved amino acid substitutions at the *mtar11* residue are consistently found in domesticated species across the phylogeny of the plant species in this database (Figure 2.8). This distribution is consistent with the previous result associating the *mtar11* mutation with domesticated species. There are several instances of independent amino acid substitutions found across the species tree, which supports that changes to bZIP29 may have contributed to the domestication of certain plants (Figure 2.8). For example, when assessing plant species within the Brassicales order (indicated with the number 5), there are two occurrences of non-conserved amino acid substitutions. The first is a threonine to asparagine substitution in *Camelina sativa*, a domesticated species (Figure 2.8). Of the five other species apart of the same monophyletic group, only *C. sativa* has this amino acid substitution. In contrast, the other close relatives, other than *Raphanus sativus*, are wild species that do not significantly alter the *mtar11* residue.
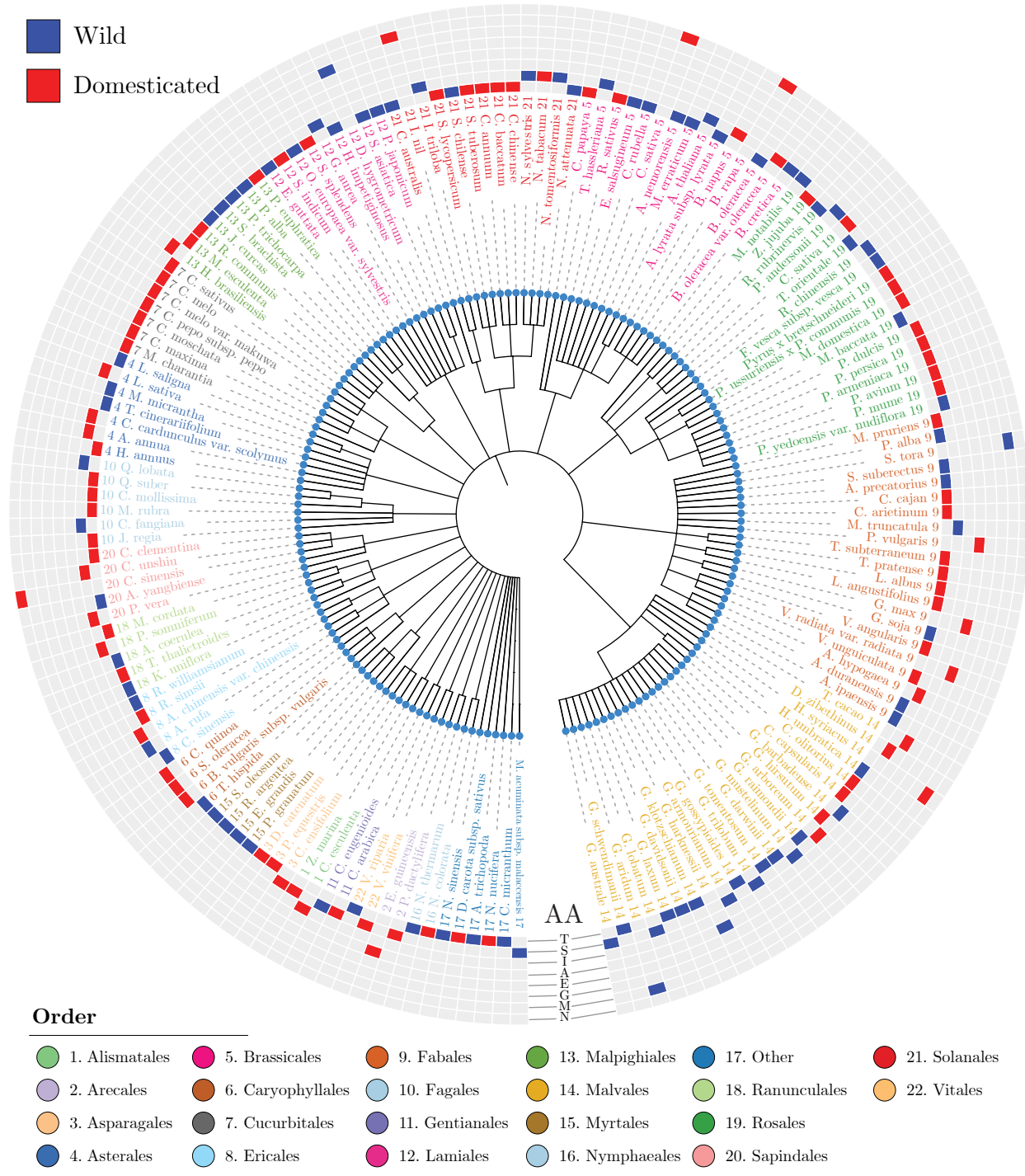
Figure 2.8: Phylogenetic variation at the *mtar11* residue across a species phylogeny.

The NCBI taxonomy browser mapped 173 plant species from the curated bZIP29 homolog database onto a species tree. The plant species within this tree and their domestication status are listed in the appendix (Table A1), while the taxonomic order each plant species belongs to is colored and numbered. Visualization of amino acid variation at the *mtar11* residue was plotted as a heatmap and aligned to this tree.

Furthermore, *Ipomoea nil* and its closely related wild relative, *Ipomoea triloba*, differ in the amino acid found at the *mtar11* residue. Within the Solanales clade (21), the domesticated plant, *I. nil*, has a threonine to Met amino acid substitution, while the wild plant species, *I. triloba*, contains a substitution to serine (Figure 2.8). Thus, the non-conserved amino acid substitution at this site may have influenced the domestication of *Ipomoea sp.* Finally, the only plants with the same amino acid substitution as *mtar11* (threonine to isoleucine) were in *Colocasia esculenta* and *Theobroma cacao*. These two are an additional example of the parallel evolution of bZIP29 as *C. esculenta* is a part of the Alismatales (1) order while *T. cacao* is a part of the Malvales order (14; Figure 2.8).

A maximum-likelihood gene tree was constructed using the 461 homologs of bZIP29 to evaluate if the bZIP29 gene tree is congruent with the species tree. It is clear that these two trees are incongruent as many individuals within a single phylogenetic order are scattered across the bZIP29 phylogeny (Figure 2.9). There are only a few rare cases where a monophyletic clade is formed, indicating several lateral gene transfers occurred within this phylogeny. One occurrence of this is within the Malvales (14) order. A cluster of bZIP29 homologs belonging to individual plant species of the Fagales (10) are more related to clusters of Malvales (14) than other members of Fagales (10; Figure 2.9). Another cluster of homologs belonging to the Fagales are more related to Cucurbitales (7) individuals. Furthermore, the considerable evolutionary distance between different occurrences of these divergent clusters indicates the varying rates of evolution of bZIP29 homologs (Figure 2.9).

58
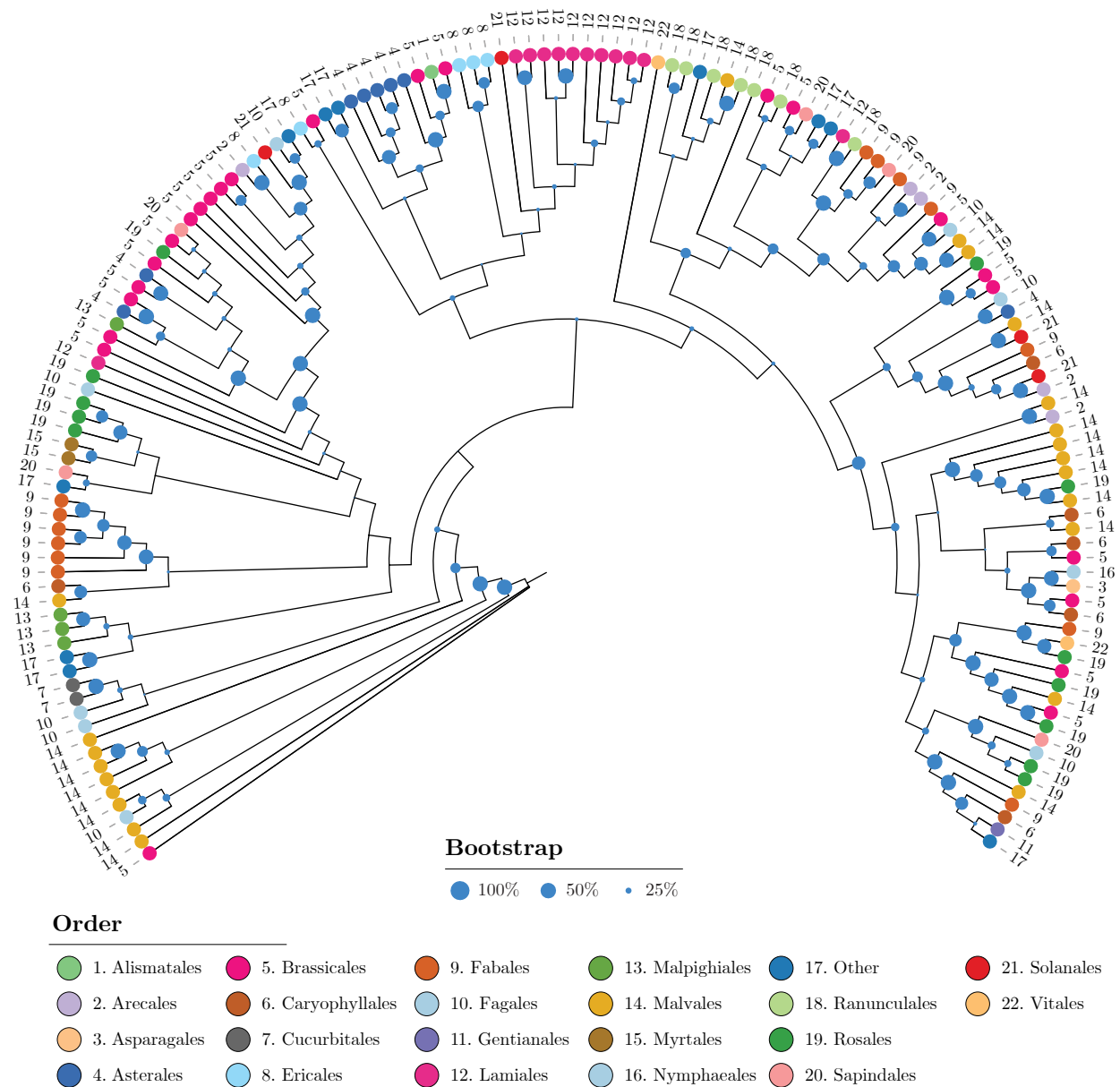
Figure 2.9: Evolutionary diversification of bZIP29 by parallel evolution and later gene transfers.

The pruned alignment of bZIP29 homologs was clustered into representative sequences using USEARCH (v11.0.667; Edgar, 2010). These 155 clusters representing the 461 bZIP29 homologs were then used to generate a maximum likelihood phylogeny of bZIP29. Each tip represents a sequence cluster, colored and numbered according to their taxonomic order. A different size of circle represents the range of bootstrap values for each node. This tree was visualized with iTOL (Letunic and Bork, 2021).

2.4 Discussion

2.4.1 *bZIP29* and proposed mechanism of suppression of the short root phenotype by *mtar11*

Previous investigations into MTN deficiency in Arabidopsis have implicated the adverse effects of MTA accumulation on numerous physiological pathways, all of which stem from the misregulation of sulfur metabolism upon MTA accumulation (Tremblay, 2019; Waduwara-Jayabahu et al., 2012). The exact mechanism of toxicity is unknown, but with a forward genetics approach, this can be further elucidated. By conducting a suppressor screen experiment, Tremblay (2019) was able to identify several unique mutants that suppressed the short root phenotype of *mtn1-1* caused by MTA. Of all the candidate *mtar11* SNPs, the likely causative SNP lies within a *bZIP29* transcription factor. The segregation analysis and the highly conserved site give confidence in identifying this as the causal SNP.

The implications of the *mtar11* mutation are noteworthy as bZIP29 is specifically expressed in proliferative tissues, with the highest expression in the QC (Van Leene et al., 2016). This suggests a concentrated role in both cell proliferation and growth. As such, previous studies have characterized bZIP29's interaction with several core cell cycle genes and cell wall genes responsible for expanding cell size. Of the various promoters bound by bZIP29, *CYCB1;2* was identified as the most commonly bound gene (Van Leene et al., 2016). Furthermore, additional cell cycle regulators like *SMR4* were targeted by bZIP29 as well as several cell wall proteins like xyloglucan endotransglucosylase (XTH9; AT4G03210), which are involved in cell wall organization (Van Leene et al., 2016; Hyodo et al., 2003). In addition to bZIP29's involvement in cell cycle regulation, this transcription factor may also have a pleiotropic role in plant development given its broad range of downstream targets and transcriptional control (Van Leene et al., 2016).

The pleiotropic effect of bZIP29 is most likely due to its various protein interactions and complexes with many other bZIPs. A comprehensive interactome showed that bZIP29 forms heterodimers with multiple group I members (Van Leene et al., 2016) consisting of

13 bZIPs primarily involved in vascular development (Torres-Schumann et al., 1996), with the most studied being VirE2-interacting protein 1 (VIP1; AT1G43700; Li et al., 2005). VIP1 is involved in vascular development and cell proliferation, oxidative stress, osmosensory, and low-sulfur responses (Wu et al., 2010). Additionally, dimerization is also influenced by phosphorylation in bZIP members, including bZIP29 (Mair et al., 2015; Van Leene et al., 2016). Thus, the unique formation of bZIP complexes with each other and other proteins will result in unique DNA-binding preferences as well as unique functions. The ability to tailor its interactions implicates bZIP29 in a broad range of effects, from low-sulfur response in the case of *mtar11* to increased stress response due to MTA toxicity.

The mechanism by which bZIP29 induces certain phenotypes of MTA toxicity requires further investigation. It is certainly clear that a mutation in this gene positively affects plant growth as the *dkml* mutation led to more productive growth than WT plants (Lozano-Sotomayor et al., 2016). Furthermore, the *mtar11* mutation not only confers resistance to MTA's effect on root growth but increases seed yield and plant growth as compared to *mtn1-1* (Figure 2.2). Given that bZIP29 controls cell number both in the leaves and the root meristem and overexpression of this transcription factor results in adverse growth effects (Van Leene et al., 2016), bZIP29 is likely involved in negatively regulating growth, especially during stress conditions like the one experienced by MTN-deficient mutants.

One possible mechanism for bZIP29's regulation of growth is via its phosphorylation by both CDKB-CYCB complexes (Van Leene et al., 2010) and Mitogen-Activated Protein Kinase (MPK3; AT3G45640; Pitzschke et al., 2009). Both of which may influence how bZIP29 interacts and functions with other bZIPs. During stress responses, VIP1 is activated by MPK3, leading to a negative effect on plant growth. Recent investigations into the TOR phosphoproteome also implicated an interaction with bZIP29 to the TOR signaling network (Van Leene et al., 2019). This striking result supports bZIP29's role in regulating growth.

2.4.2 Several novel amino acid changes in bZIP29 are highly associated with domesticated species

Since introducing a mutation into *bZIP29* correlates with positive plant productivity, an opportunity arose to assess how changes to this protein are associated with domesticated plants. Domesticated plants have been either naturally or artificially selected for increased productivity, measured by increased seed yields, large fruits, and rapid life cycles. Considering the relationship between effecting bZIP29's function and the positive effect on growth, the *mtar11* SNP increases seed yield and produces larger siliques (Figure 2.3), similar to a domesticated plant.

A thorough assessment of bZIP29 homologs, which were classified as belonging to either wild or domesticated species, led to the conclusion that the *mtar11* mutation is associated with domesticated species (Figure 2.4c). Furthermore, non-conserved amino acid changes were only identified in domesticated species, suggesting that significant alterations to this site may result in positive growth effects. The amino acid substitution identified in *mtar11* was seen in only two domesticated species in this database, *Theobroma cacao* (Cacao Tree) and *Colocasia esculenta* (Taro). Phylogenetic inheritance of these changes was also assessed, which indicated these substitutions occurred independently (Figure 2.7, Table 2.5). Furthermore, there are many examples of lateral gene transfers and independent evolution with the bZIP29 phylogeny which exemplify the evolutionary pressure behind this transcription factor (Figure 2.8, 2.9).

Though amino acid changes in bZIP29 and its homologs are associated with domesticated species, it is possible that the number of genes analyzed in this database was insufficient and may have introduced bias. This is unlikely the case as the initial curation of the bZIP29 homologs was performed looking for distant homologs using three iterations of PSI-BLAST. This curated database provided an excellent source to investigate the association of amino acid changes to domesticated species.

Aside from the *mtar11* site, several other residues are significantly associated with domesticated species (Figure 2.7). In fact, these residues appear in clusters along the protein

sequence (Figure 2.7), suggesting that conserved regions are indirect targets of selection via a top-down approach of domestication exemplified by the selection of obvious advantageous phenotypes resulting in genetic changes (Kantar et al., 2017). Thus, changes to these important evolutionary motifs are associated with domesticated species. Remarkably, of the changes observed in bZIP29's homologs, an amino acid deletion or insertion proved to be an impactful alteration to the protein and dictated whether or not a residue is associated with domesticated species (Figure 2.6). This investigation not only found an association between amino acid changes and domestication but further confirms the impact of genetics on domestication. An additional avenue to provide significance to these findings would be assessing the impact of amino acid changes on bZIP29's protein structure. Unfortunately, crystal structures of this transcription factor and the various homologs of bZIP29 do not exist.

It is then plausible to suggest that this investigation should be extended beyond just one locus and look at domestication's impact across plant genomes. A multiple genome-wide association study may provide a genetic explanation as to why certain plants are selected for domestication. There are pitfalls to selective breeding, including deceased genetic diversity, especially in self-pollinating crops resulting in a genetic drift of deleterious mutations. Nevertheless, haplotypes in certain plant genomes are likely associated with wild and domestic varieties of a selected plant species.

The *mtar11* mutation resulting in increased plant growth and its association with domesticated species points to significant implications as to the mechanism of conferring resistance to MTA toxicity. Since MTA accumulation results in numerous growth defects, investigations into the effect of the *mtar11* mutation on MTA toxicity will be informative. Particularly, the impact of *mtar11* on balance between growth and stress response in an *mtn1-1mtn2-1* background with impaired sulfur metabolism.

Chapter 3

MTN deficiency in Arabidopsis negatively affects growth by disrupting TOR signaling and cell cycle progression

3.1 Introduction

Plants continuously monitor their nutrient status and environmental conditions to balance their growth and stress responses. Their inability to migrate from stressful environments further complicates this back-and-forth. An example of this balancing act occurs within sulfur metabolism. Plants fine-tune the flux of sulfur towards various sulfur-containing compounds to coordinate growth and nutrient limitations with Cys biosynthesis at the center of this flux regulation (Takahashi et al., 2011; Watanabe et al., 2021). This central metabolite constitutes a flux of not only sulfur but carbon and nitrogen precursors (Takahashi et al., 2011). Depending on the abundance of these precursors, Cys utilization may shift sulfur flux towards GSH or Met biosynthesis (Speiser et al., 2018). Furthermore, GLS biosynthesis may feedback to Cys in periods of sulfur deprivation (Sugiyama et al., 2021). Thus, many studies have focused on this Cys biosynthesis to elucidate how sulfur metabolism interconnects with the remobilization of nutrients to coordinate growth during nutrient limitation.

The *de novo* biosynthesis of Met in the transsulfuration pathway uses Cys as a precursor (Figure 1.2). Met is converted into SAM and serves as a primary methyl donor for methylation reactions. The by-product of these reactions, SAH, is recycled back to HCys, and eventually to Met completing the SAM cycle. (Ravanel et al., 1998). One type of reaction uses SAM to produce ACC and NA (Figure 1.2) while another converts SAM into dcSAM to produce the polyamines, Spd, Spm, and Tspm (Figure 1.2). Both these sets of reactions produce MTA as a byproduct (Bürstenbinder et al., 2010).

MTA is metabolized into MTR and adenine by MTN (Bürstenbinder et al., 2007). The sulfur group in MTR is subsequently recycled back into Met in a series of reactions in the Met salvage cycle (Sauter et al., 2013). Under sulfur sufficient conditions, the salvage of Met is not reliant upon to maintain adequate sulfur levels. In contrast, the recovery of the sulfur group in MTA during periods of sulfur starvation is crucial for sustaining the Met pool (Bürstenbinder et al., 2007). By introducing T-DNA insertions into the MTN genes, MTN-deficient plants cannot effectively initiate the Met salvage cycle, and accumulate MTA during sulfur starvation conditions. This disruption of MTN activity has been shown to be

toxic to plant physiology (Bürstenbinder et al., 2010; Waduwara-Jayabahu et al., 2012).

The specific mechanism underlying MTA toxicity is unknown, but the accumulation of this sulfur-containing metabolite in specific cell types alters sulfur assimilation by shifting its flux away from Cys and Met metabolism (Tremblay, 2019). As such, the abundance of both Cys and Met is substantially reduced in unopened floral buds of *mtn1-1mtn2-1* plants (Tremblay, 2019). The transcriptional changes and metabolic abnormalities due to MTA accumulation are associated with numerous phenotypic effects including reduced root length, delayed bolting, altered phyllotaxy and infertility. The pleotropic phenotype of MTN-deficient mutants has made pinpointing the exact mechanism of disruption by MTA quite difficult. Previous studies have suggested that feedback inhibition by MTA on SAM utilizing reactions is the direct target (Waduwara-Jayabahu et al., 2012). It is also possible that MTA may inhibit a biochemical reaction along the sulfur assimilation pathway prior to Cys biosynthesis, thus, limiting both Cys and Met production.

The reduction in sulfur containing amino acids found in the *mtn1-1mtn2-1* mutant has likely negatively affected TOR activity as amino acid availability is the greatest effector of TOR activity (O'Leary et al., 2020). Given the wide-ranging phenotypes of MTA toxicity, it is possible that MTA's impact on amino acid abundance has affected this regulatory hub of growth. A similar but more significant disruption of sulfur assimilation by the *sir1-1* mutant dramatically affects TOR activity and plant growth due to lack of sulfide (Dong et al., 2017). There are many compelling links to the disruption of TOR activity by MTA toxicity. For example, the decrease in meristematic activity is seen in MTN-deficient mutants, delaying bolting in *mtn1-1mtn2-1* plants and reducing root lengths of *mtn1-1* seedlings in the presence of exogenous MTA (Waduwara-Jayabahu, 2012; Tremblay, 2019). TOR also regulates responses to stress via ABA, activating many stress response genes (Shi et al., 2018). Many of these genes are upregulated in the unopened buds of *mtn1-1mtn2-1* due to the considerable MTA pressue in this tissue (Tremblay, 2019).

The mutation found in *bZIP29* in *mtn1-1mtar11* links phenotypes of MTA accumulaiton to decreased TOR activity (Van Leene et al., 2010, 2016, 2019). A recent study by Van Leene et al. (2019) found a direct interaction of *bZIP29* with the TOR complex in Arabidopsis.

Furthermore, bZIP29 is a transcriptional regulator of genes involved in cell proliferation like *CYCB1;2*, *SMR4*, and cell expansion genes such as *XTH9* (Van Leene et al., 2019). bZIP29 is also involved in many other facets of plant development based on its interactions with other proteins and bZIPs (Van Leene et al., 2016). The evidence behind bZIP29's function suggests that it negatively regulates growth, particularly during stress responses. Therefore, it is likely that this mutation in bZIP29 counteracts the adverse growth effects caused by the physiological stress associated with MTA accumulation.

Thus, this study aims to reveal the underlying cause of MTN deficiency phenotypes by characterizing its effect on the TOR signaling network, elucidate the effect of MTA on cell proliferation and the loss of meristem homeostasis. Since the *mtar11* mutation in *bZIP29* may implicate MTA in limiting growth, *mtn1-1mtar11* will be used to help understand MTA's toxic effect on plant growth and nutrient availability.

3.2 Materials and Methods

3.2.1 Plant material and growth conditions

Plants were germinated and maintained as described in Chapter 2. Sulfur-deficient, $MgSO_4$, and MTA solid growth media were prepared as described in Chapter 2.

Plant lines

The plant lines used in this study are listed in Chapter 2 with the addition of SALK_071127 (*mtn2-1*) and SALK_022510 (*mtn2-5*). From those lines, the double mutants *mtn1-1mtn2-1* and *mtn1-1mtn2-5* were generated (Waduwara-Jayabahu et al., 2012). *pCYCD3;1::GUS* and *pCYCD3;3::GUS* reporters were provided by Jim Murray (Collins et al., 2015). *CYCB1;2::CYC-GUS* was provided by Karel Říha (Bulankova et al., 2013), and Lieven De Veylder (Yi et al., 2014) provided *SMR4::nlsGFP-GUS*. *DR5::n3GFP* reporter was provided by Liao et al. (2015).

3.2.2 Root meristematic zone measurements

Arabidopsis seedlings were harvested off growth media and rinsed in a pool of deionized Milli-Q water on a microscope slide. The water was wicked away with a Kimwipe and replaced with the SR staining solution (Musielak et al., 2015). This staining solution contains 0.1% (v/v) SR2200 (Renaissance Chemicals; stock solution of the supplier was considered as 100%), 1% (v/v) DMSO, 0.05% (v/v) Triton-X100, 5% (w/v) glycerol and 4% (w/v) paraformaldehyde in PBS buffer (pH 8.0). SR staining solution was stored in aliquots at -20°C prior to use. The seedlings were vacuum infiltrated with staining solution for 2 min at room temperature for better tissue penetration. The staining solution was then replaced with water to wash off excess stain, and samples were mounted in 20% glycerol.

Stained seedlings were imaged using confocal microscopy. The meristematic zone was measured as the distance from the isodiametric cells of the QC to the first cortex cell that was approximately double in size compared to the previous cell. The meristematic zone was measured in ImageJ (Schneider et al., 2012). Primary root lengths were measured by taking pictures of the growth plate every day, and root lengths were quantified in ImageJ (Schneider et al., 2012).

3.2.3   Microscopy

Confocal images were obtained using a Zeiss 700 confocal microscope (Carl Zeiss Inc., Toronto, Canada) with a plan-apochromat 20x/0.80 objective. For the SR staining solution, SR2200 was excited with a 405 nm solid-state laser, and the emission was recorded between 415 and 476 nm. GFP was excited with a 488 nm solid-state laser, and emissions were recorded between 505 to 540 nm. All Zeiss ZEN files were processed using ImageJ (Schneider et al., 2012).

Light microscope images of GUS-stained seedlings were obtained using a Nikon ECLIPSE Ni (Nikon Canada, Mississauga, Canada) light microscope with a Nikon DS-Ri2 colored camera. A Nikon Plan Fluor 20x/0.50 objective was used to imaging seedlings mounted in chloral hydrate. *CYCD3;1* and *CYCD3;3* GUS stained seedlings were imaged using a Zeiss Axio Observer 5 light microscope with a QImaging colored camera and a 10x/0.50 objective.

3.2.4   GUS histochemical staining

GUS staining solution contained 1 mM potassium ferrocyanide, 1 mM potassium ferricyanide, 50 mM sodium phosphate buffer (pH 7.0), 0.1% (v/v) Triton X-100, 10 mM EDTA (pH 8.0) and 1 mM X-Gluc (5-Bromo-4-chloro-3-indolyl-β-D-glucuronide, BioShop, Burlington, Canada). Seedlings were harvested from media and chemically fixed using cold 90% acetone for 30 min under a soft vacuum. Seedlings were washed with 50 mM sodium phosphate buffer (pH 7.0) for 10 min under soft vacuum. The wash buffer was replaced with the GUS staining solution and vacuum infiltrated for 30 min before incubating the samples overnight at 37°C,

in the dark. The staining solution was replaced the next day with 70% ethanol and stored at 4°C until samples are ready to mount. Seedlings were mounted in a chloral hydrate solution (25 g chloral hydrate, 15 mL water, and 15 mL glycerol) before imaging.

3.2.5   YAK1 and TOR drug inhibition

Seedlings were grown on solid media containing the YAK1 inhibitor, proINDY (Glixx Lab, Hopkinton, USA), and the TOR inhibitor, AZD-8055 (Cayman Chemical, Burlington, Canada), for 14 days. Stock solutions of these drugs were made with DMSO and filter-sterilized with a 0.2 μm sterile filter. The final concentrations of proINDY, AZD-8055, and DMSO used in the growth media were 20 μM, 1 μM, 0.1% (v/v), respectively.

3.2.6   TOR activity assay

Developmentally matched rosette leaves five and six of 21-day old plants were harvested and flash-frozen. Immunological detection of S6K and S6K-P was performed by a collaborator, Dr. Yihan Dong (IBMP, Strasbourg, France) as outlined in Dong et al. (2017).

3.2.7   Flow cytometry

In order to determine the representative whole-plant ploidy level, developmentally matched rosette leaves five and six were harvested from approximately 21-day old plants. Approximately 20 mg of leaf tissue was chopped finely using a new double-sided razor blade on a pre-chilled watch glass with 600 μL of freshly made ice-cold Aru buffer (Yang et al., 2019; 9.65 mL MgSO4 buffer, 1 mM DTT, and 0.1% (v/v) Triton X-100). The extract was transferred to a 3 mL syringe with a homemade adapter, for a a 40 μm Nitex nylon mesh filter, and collected into a polystyrene 5 mL tube. The suspended nuclei were treated with RNase (50 μg/mL; BioShop, Toronto, Canada) for 10 min and stained with propidium iodide (50 μg/mL). Samples were run on an Accuri C6 flow cytometer, and the 2C peak was identified and used to set up gates for analysis of cell ploidy.

The endoreduplication index was determined by multiplying the fraction of events at each ploidy level by the value of the ploidy level (i.e., 2C, 4C, 8C, 16C, 32C, or 64C) and then summing all these values. $EI = \frac{4C + (2 \times 8C) + (3 \times 16C) + (4 \times 32C) + (5 \times 64C)}{100}$.

3.2.8   Plant developmental monitoring

The transition from vegetative to flowering was marked by the visual emergence of the apical floral buds. The bolting time was measured from seed germination to this milestone. At bolting, the number of rosette leaves was counted by taking pictures of the plants and using ImageJ (Schneider et al., 2012). The plant height was measured from the soil level to the top of the primary inflorescence stem when the apical bud cluster failed to produce new flower buds. Internode lengths were measured between the siliques of the primary inflorescence stem; only the first ten internodes were measured.

3.2.9   Quantification of phytohormones

Developmentally matched rosette leaves five and six of 21-day old plants and unopened buds were harvested and flash-frozen. The extraction and quantification of IAA, different types of cytokinins, and ABA was performed by a collaborator, Dr. Anna Kisiała in the lab of Dr. Neil Emery (Trent University, Peterborough, Canada). Šimura et al. (2018) described the extraction, purification, and quantification of these phytohormones.

3.2.10   Data analysis

All statistical analyses in this chapter were performed within the R environment. One and two-way ANVOA, Tukey's honest significant difference (HSD) tests and principle component analysis (PCA) was done using the base stats package in R (R Core Team, 2020).

3.3 Results

3.3.1 Investigating root meristematic development on MTA

Exogenous feeding of MTA has detrimental effects on the root development of MTN-deficient seedlings. For instance, when grown on media containing MTA, concentrations higher than 100 μM hinders the viability of *mtn1-1mtn2-1* seedlings (Tremblay, 2019). On the other hand, *mtn1-1* seedlings remain viable when grown on concentrations higher than 100 μM, though their root lengths become considerably reduced compared to WT. In order to understand the effects of MTA accumulation on root development, WT, *mtn1-1*, and *mtn1-1mtar11* seedlings were grown vertically on sulfur-free media supplemented with $MgSO_4$ or MTA and analyzed over 14 days.

The goal of this investigation was three-fold: 1), investigate meristematic development of the root by assessing the effect of MTA on the length of the meristem region; 2), evaluate the impact of MTA on cell proliferation in roots, and 3), monitor the development of the root apical meristem under high MTA pressure.

Root meristem size

The development of the meristematic zone was documented by measuring the length from the isodiametric cells of the QC to the first cortical cell that doubles in size (Petricka et al., 2012; Figure 3.1). On $MgSO_4$, there are very subtle differences in the size of the meristematic zone between 4 and 7 days after stratification (DAS) when comparing the three genotypes (Figure 3.2). Consistent growth in meristem size is maintained in each genotype, peaking at 7 DAS. Both *mtn1-1* and *mtn1-1mtar11* exhibit a significant reduction in meristem size 9 DAS, only to recover a day later (Figure 3.2).
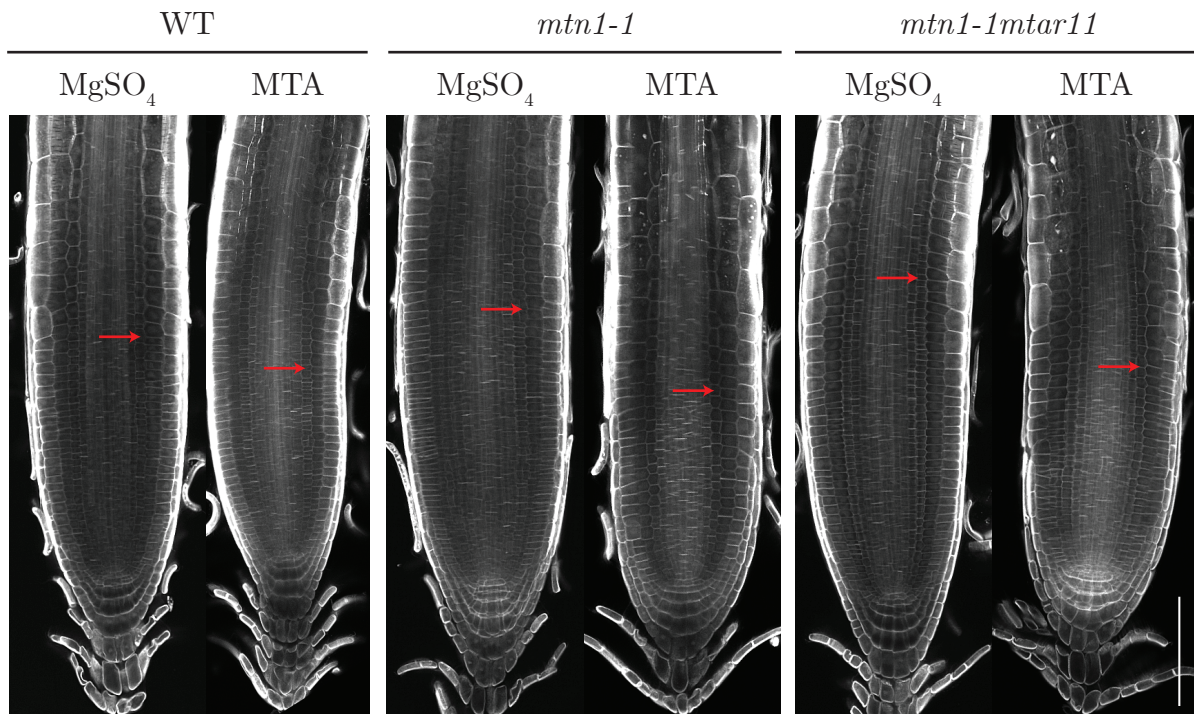
Figure 3.1: SR2200 stained seedlings.

Representative images of seedlings 7 DAS illustrate the longitudinal optical sections obtained using confocal imaging and a cell wall stain, SR2200. The red arrows indicate the end of the meristematic zone along the cortical cell layer. Scale bar = 100 μm, n = 10 per genotype per day.
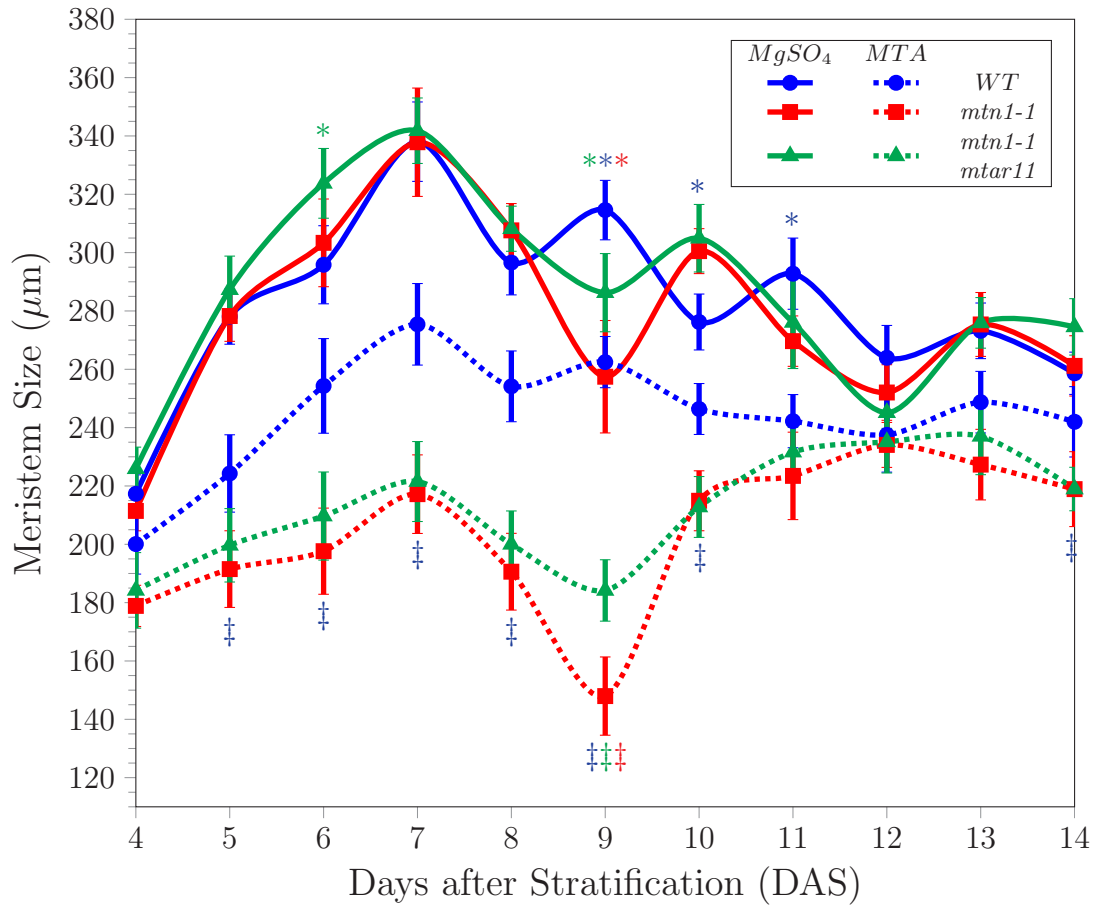
Figure 3.2: Temporal effects of exogenous MTA on root meristem size.

The changes of meristem size were observed for WT, *mtn1-1*, *mtn1-1mtar11* over 14 DAS on sulfur-free media supplemented with either 500 μM $MgSO_4$ or 650 μM MTA. The meristematic zone was measured from the isodiametric cells of the QC to the first cell that doubles in length (μm) in the cortex cell layer. These measurements were compiled per day to depict the temporal changes in meristem size after 4 DAS when seedlings become established after germination. (*) and (‡) represents a statistical significance for seedlings on $MgSO_4$ and MTA, respectively. A Tukey's HSD post hoc test after a two-way ANOVA was conducted for each media type ($p < 0.0001$), n = 10 per genotype per day. The color of (*) and (‡) represent significantly different genotypes.

A remarkable periodicity appears on $MgSO_4$ in the days following a peak in meristem growth at 7 DAS (Figure 3.2). This growth pattern in the root meristem marks periods of cell proliferation by the increasing meristem size leading to a peak while the decrease in meristem size precedes a trough, marking the end of cell elongation as the dominant process in the root. It is important to note that WT has a cyclic period of two days between growth peaks while both *mtn1-1* and *mtn1-1mtar11* have a cyclic period of three days (Figure 3.2).

The periodicity in the change in meristem size is attenuated when seedlings are grown on MTA. Similar to the growth on $MgSO_4$, all three genotypes have a consistent increase in meristem size until 7 DAS, followed by a decrease in size (Figure 3.2). This is quite pronounced in *mtn1-1* roots 9 DAS, but remarkably, these seedlings recover meristem size by the following day (Figure 3.2). Thereafter, the meristematic zone steadily increases in size over the remaining days.

Overall, seedlings grown on MTA have a significant reduction in meristem size compared to those grown on $MgSO_4$. In addition, both *mtn1-1* and *mtn1-1mtar11* are more affected by exogenous feeding of MTA than WT due to their reduced in MTN1 activity (Waduwara-Jayabahu et al., 2012). *mtn1-1mtar11* seedlings have a longer root length than WT and *mtn1-1* on $MgSO_4$ (Figure 2.2), although this does not translate to a significant increase in meristem size over the 14 days (Figure 3.2). However, *mtn1-1mtar11* seedlings have considerability longer meristematic zones than *mtn1-1* 9 DAS when grown on both $MgSO_4$ and MTA.

Cell proliferation of the meristematic zone

Cells along a single cell file are similar in length within the meristematic zone before transitioning to the elongation zone (Petricka et al., 2012). Intriguingly, cells within the meristematic zone of the *mtn1-1* root prematurely elongate prior to reaching the transition zone when MTA is the sole sulfur source (Figure 3.3). This abnormal phenotype became noticeable by 7 DAS, and by 9 DAS on MTA, several cells had stalled and began to elongate (Figure 3.3). This pattern was absent in both WT and *mtn1-1mtar11* seedlings and seedlings that were grown on $MgSO_4$. Of the ten biological replicates analyzed for each genotype, eight and nine different seedlings exhibited this pattern at 7 and 9 DAS, respectively.
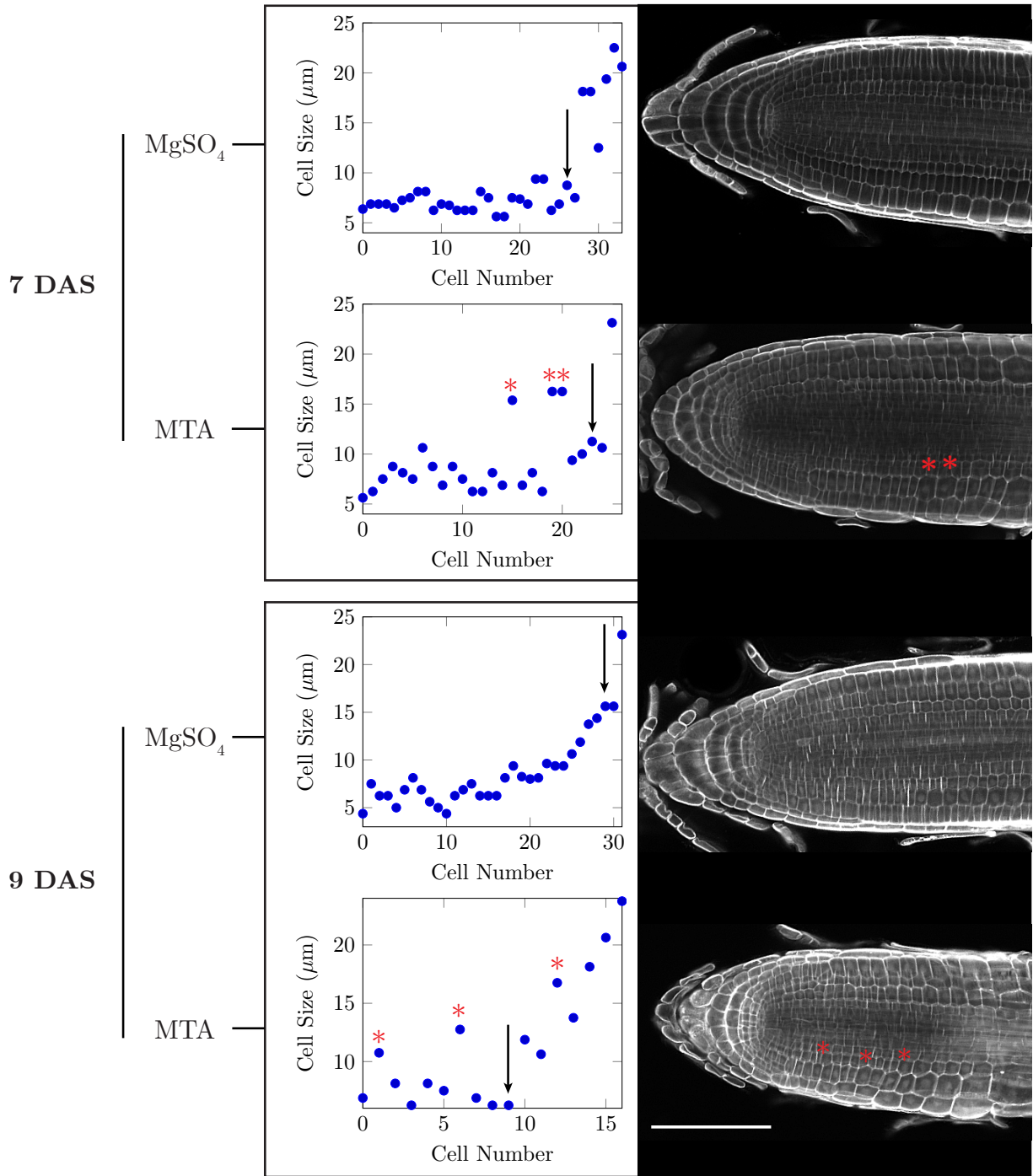
Figure 3.3: Premature elongation of cells within the meristematic zone.

Increased cellular resolution using SR2200 stained *mtn1-1* seedlings revealed meristematic cells elongate within the division zone of the root meristem prior to reaching the transition zone as indicated by the red (*). This was confirmed by measuring each cell in the cortex cell layer of the meristematic zone using Cell-o-Tape tool in ImageJ. Each plot corresponds with the root image on the right. Early elongation of cells was only observed in *mtn1-1* vertically grown seedlings off MTA, 7 (n = 8/10), and 9 (n = 9/10) DAS. Scale bar = 100 μm.

76

In accordance with the loss of meristem size and the premature elongation of meristematic cells due to MTA treatment, cell proliferation of the root meristematic zone was quantified by counting the cells within this region. In order to account for the differences in cell length, the cells of the cortex layer were counted starting from the QC until the transition zone, marked by a cortex cell that doubles in length. The increase in meristem size for the first 7 DAS for both $MgSO_4$ and MTA (Figure 3.2) agrees with a proliferation of meristematic cells for WT, *mtn1-1*, and *mtn1-1mtar11* seedlings (Figure 3.4). Most notably, the number of meristematic cells for MTA-grown seedlings is a fraction of $MgSO_4$ seedlings and reduced further in the *mtn1-1* background. Interestingly, *mtn1-1* seedlings grown on MTA media for 9 DAS have more meristematic cells than they do 4 DAS (Figure 3.4) though, its meristematic length on MTA is significantly shorter (Figure 3.2).

Root apical meristem development

The root apical meristem comprises the QC and the stem cell niche, which maintains a pool of stem cells that rarely divide and provide initials for the various root layers (Augstein and Carlsbecker, 2018). WOX5 regulates the maintenance of these stem cells by suppressing cell proliferation at the QC and establishing a stem cell niche during embryogenesis (Forzani et al., 2014). Any disruption in the maintenance of these stem cells results in the increase in QC cell division and loss of cell proliferation in any of the root layers due to a lack of stem cell initials (Sarkar et al., 2007). In addition to measuring the meristematic zone, a direct approach was used to quantify the disruption of the root apical meristem by MTA accumulation involving the columella cells. Given that columella stem cells are directly derived from the QC (Sarkar et al., 2007; Forzani et al., 2014), counting the number of columella layers and the number of columella cells provides a cursory assessment of any disruption to the root apical meristem maintenance (Sarkar et al., 2007; Forzani et al., 2014).
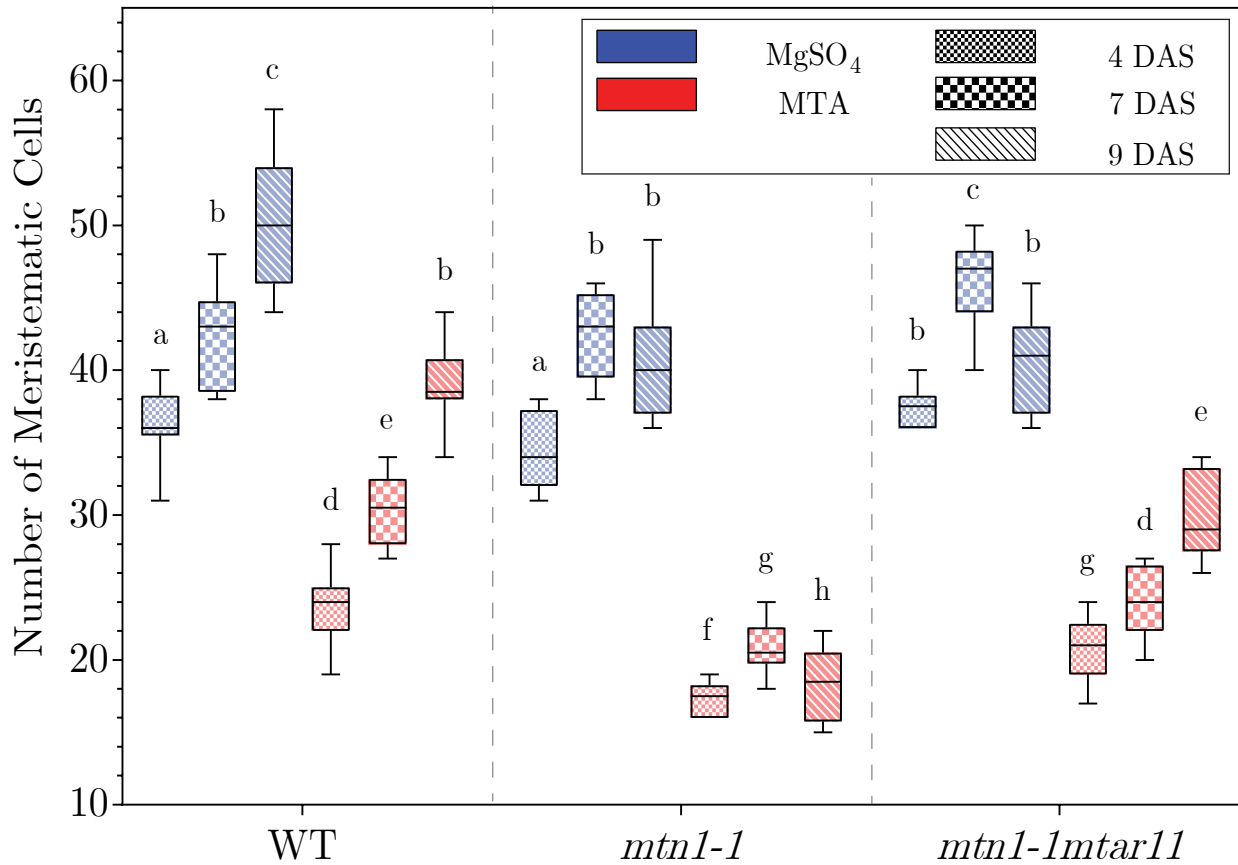
Figure 3.4: Exogenous MTA decreases cell proliferation in the meristematic zone of the root.

WT, *mtn1-1*, and *mtn1-1mtar11* seedlings were vertically grown on sulfur-free media supplemented with either 500 μM MgSO4 or 650 μM MTA. After confocal imaging of SR2200 stained seedlings, meristematic cells were counted within the cortex cell layer beginning at the QC till the beginning of the transition zone for 4, 7, and 9 DAS. Letters represent statistical significance from Tukey's HSD post hoc test after a two-way ANOVA ($p < 0.05$), n = 10 per genotype per day.

Based on this metric, exogenous MTA feeding impairs root apical meristem development. The delayed development is first depicted by the number of cell layers when comparing WT, *mtn1-1*, and *mtn1-1mtar11* when grown on MTA as a sole sulfur source (Figure 3.5). The inability to metabolize the exogenous MTA in the *mtn1-1* background results in a delay in columella development by a single columella layer in the majority of seedlings 4 DAS when compared to WT. It is not until 7 DAS when most *mtn1-1* seedlings catch up to WT seedlings in terms of the number of columella layers in their roots (Figure 3.5). *mtn1-1mtar11*, on the other hand, has slightly restored this delay as most of the *mtn1-1mtar11* seedlings developed one or two more columella layers compared to *mtn1-1* for each day assessed. The reduction in the number of columella cells in *mtn1-1* due to MTA treatment exemplifies the delay in root apical meristem development and reduced cell proliferation (Figure 3.6). Both *mtn1-1* and *mtn1-1mtar11* have a fraction of the number of columella cells compared to WT, and this difference becomes more substantial by 9 DAS (Figure 3.5).

3.3.2   Evaluating the disruption of the cell cycle by MTA

The significant loss of cell proliferation in the root meristematic zone of seedlings due to MTA led to the hypothesis that MTA inhibits the cell cycle progression as a result of altered activity in cell cycle activators or inhibitors. This was evaluated by assessing the expression of key cell cycle genes of seedlings grown on media with MTA as the sole sulfur source. For this analysis, strategic cell cycle reporters were selected based on when and where they are expressed during the cell cycle. Entry into the cell cycle requires on the expression of *CYCD3;3*, which is highly expressed during the G_1 phase, while the expression of *CYCD3;1* marks the G_1/S checkpoint (Masubelele et al., 2005; Collins et al., 2015). At the G_2/M checkpoint, *CYCB1;2* expression marks cells that are dividing (Van Leene et al., 2010). SMR4 is a known inhibitor of these CYCs and their associated CDKs (Yi et al., 2014). Furthermore, bZIP29 transcriptionally regulates several cell growth genes, including *CYCB1;2* and *SMR4*, though the effects of its regulation are unknown (Van Leene et al., 2016). GUS reporters for each these factors were used as an indicator of the effects of MTA on the cell cycle. These were assessed 4, 7 or 9 DAS to coincide with the growth milestones of the meristematic zone (Figure 3.2).
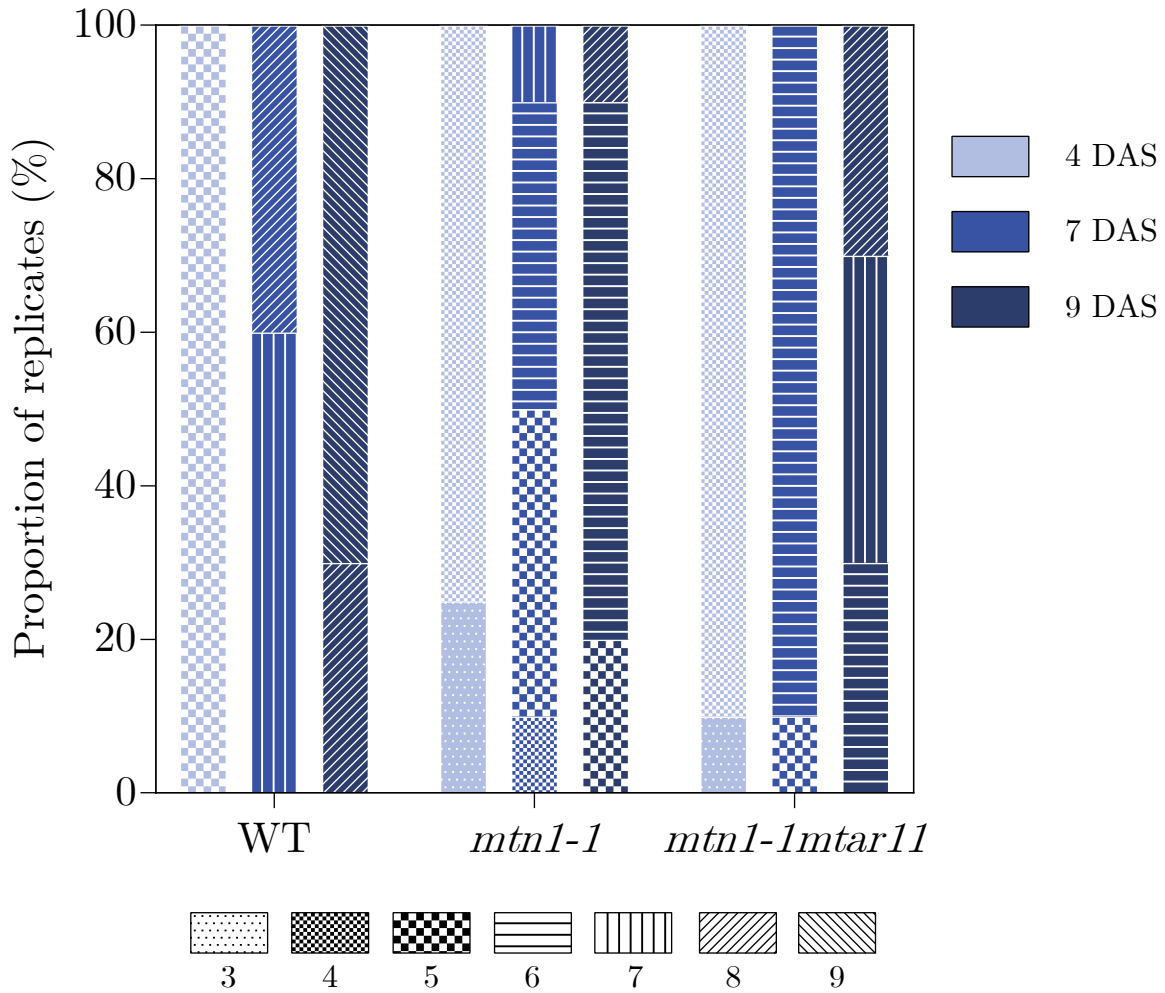
Figure 3.5: Quantification of columella layers of MTA treated seedlings.

WT, *mtn1-1*, and *mtn1-1mtar11* seedlings were vertically grown on sulfur-free media supplemented with either 500 μM MgSO4 or 650 μM MTA. The columella layers were counted using SR2200 seedlings from the columella layer after the columella stem cell layer in the root apical meristem. The columella layers were quantified by grouping the percentage of seedlings that contain the number of columella layers depicted by a different pattern along the bottom. The days analyzed were 4, 7, and 9 DAS represented by a different shade of blue. n = 10 per genotype per day.
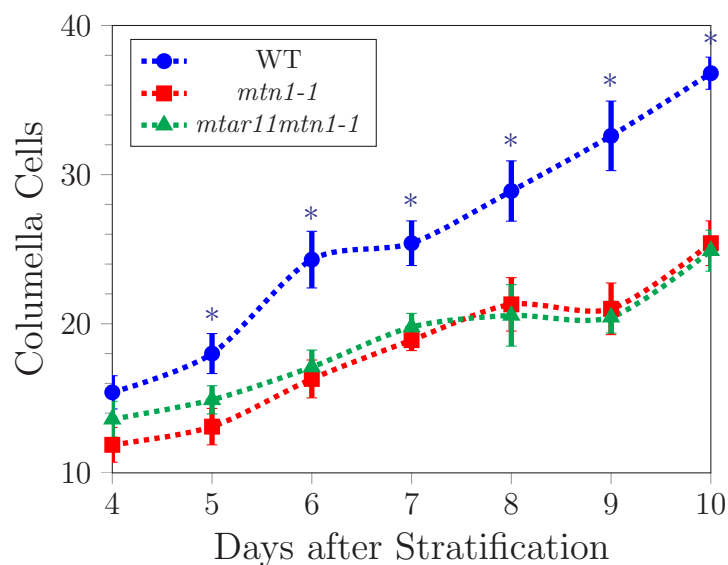
Figure 3.6: Loss of columella transverse cell division due to MTA treatment.

WT, *mtn1-1*, and *mtn1-1mtar11* seedlings grown vertically on MTA supplemented media were stained with SR2200. After confocal imaging, the columella cells within the columella layers were counted. (*) represents a statistical significance for seedlings on MTA from Tukey's HSD post hoc test after a two-way ANOVA ($p < 0.0001$), n = 10 per genotype per day. The color of (*) represents the significantly different genotype.

Beginning with the entry to the cell cycle, *CYCD3;3* expression does not change in seedlings grown on MgSO$_4$ or MTA media for any genotype (Figure 3.7*a*). Nevertheless, *mtn1-1* and *mtn1-1mtar11* have a significantly higher expression of *CYCD3;3* than WT 4 DAS. Interestingly, both *mtn1-1* and *mtn1-1mtar11* express *CYCD3;3* in the QC and the columella layers 4 DAS although this is not observed in WT seedlings (Figure 3.7*a*; Forzani et al., 2014). Similarly, there are also subtle changes in the expression of the G$_1$/S checkpoint reporter, *CYCD3;1* in seedlings grown with or without MTA (Figure 3.7*b*). Seedlings treated with MTA have slightly higher *CYCD3;1* expression, with minimal changes in expression between genotypes or timepoints.

At the G$_2$/M phase checkpoint, *mtn1-1* seedlings supplied with MTA as their sulfur source have a consistent reduction in *CYCB1;2* expression compared to WT seedlings (Figure 3.8). *mtn1-1mtar11* seedlings restored this repression of *CYCB1;2* expression (Figure 3.8). Furthermore, the changes in *CYCB1;2* expression between each time point coincides with the number of meristematic cells within this region (Figure 3.4). The significant decrease in meristem cells 9 DAS in *mtn1-1* seedlings on MTA agrees with the loss of *CYCB1;2* expression (Figure 3.8). SMR4 usually acts on G$_2$/M phase checkpoint by inhibiting the CDKA-CYCB1. Changes in *SMR4* expression are also consistent with changes to both the number of meristematic cells and *CYCB1;2* expression (Figure 3.9). MTA feeding results in an increase in *SMR4* expression in *mtn1-1* seedlings. *SMR4* expression is highest within the transition zone, but in the case of *mtn1-1* on MTA, *SMR4* expression is consistently high throughout the seedling (Figure 3.9). In contrast, *mtn1-1mtar11* reduces the expression of *SMR4* (Figure 3.9) and, in part, the cell cycle repression caused by MTA toxicity.
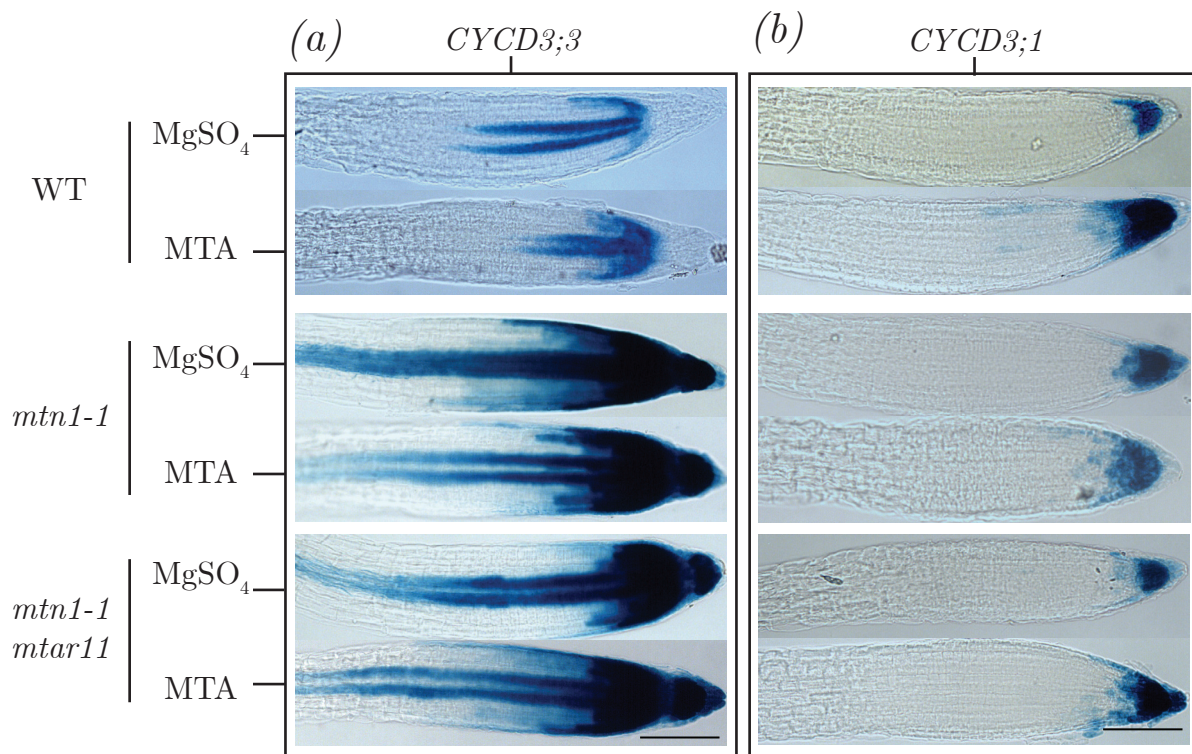
Figure 3.7: The effect of MTA on *CYCD3;3* and *CYCD3;1* G_1/S cell markers.

WT, *mtn1-1*, and *mtn1-1mtar11* seedlings with the *(a) CYCD3;3::GUS* and *(b) CYCD3;1::GUS* reporter were vertically grown on sulfur-free media supplemented with either 500 μM MgSO$_4$ or 650 μM MTA. Seedlings were harvested 4 DAS, stained for GUS, and imaged using a light microscope. n = 5 per genotype per day. Scale bar = 100 μm.
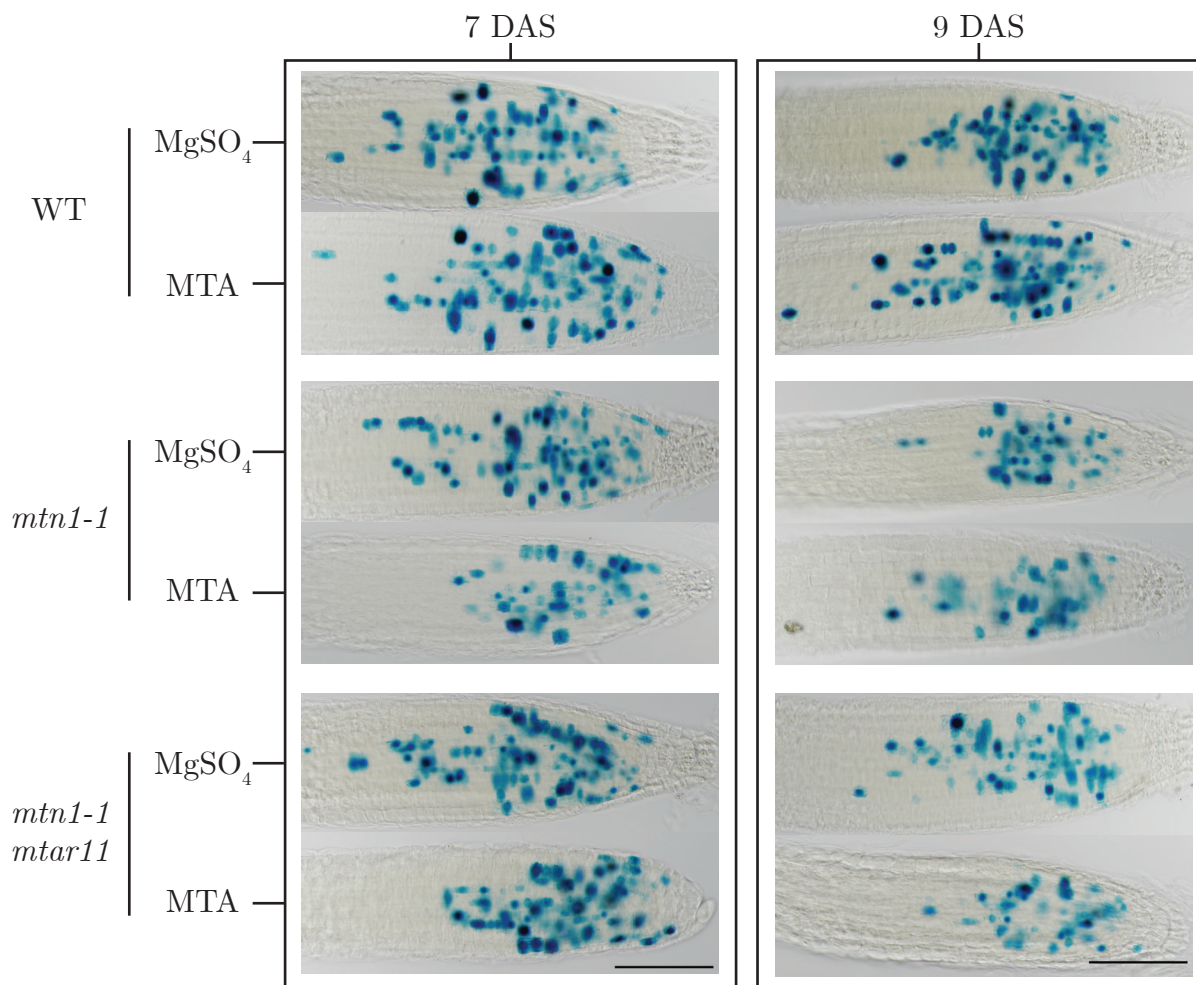
Figure 3.8: Decrease in cell proliferation is marked by loss of *CYCB1;2* expression due to MTA.

WT, *mtn1-1*, and *mtn1-1mtar11* seedlings with the *CYCB1:2::GUS* reporter were vertically grown on sulfur-free media supplemented with either 500 μM MgSO$_4$ or 650 μM MTA. Seedlings were harvested 7 and 9 DAS, stained for GUS, and imaged using a light microscope. n = 10 per genotype per day. Scale bar = 100 μm.
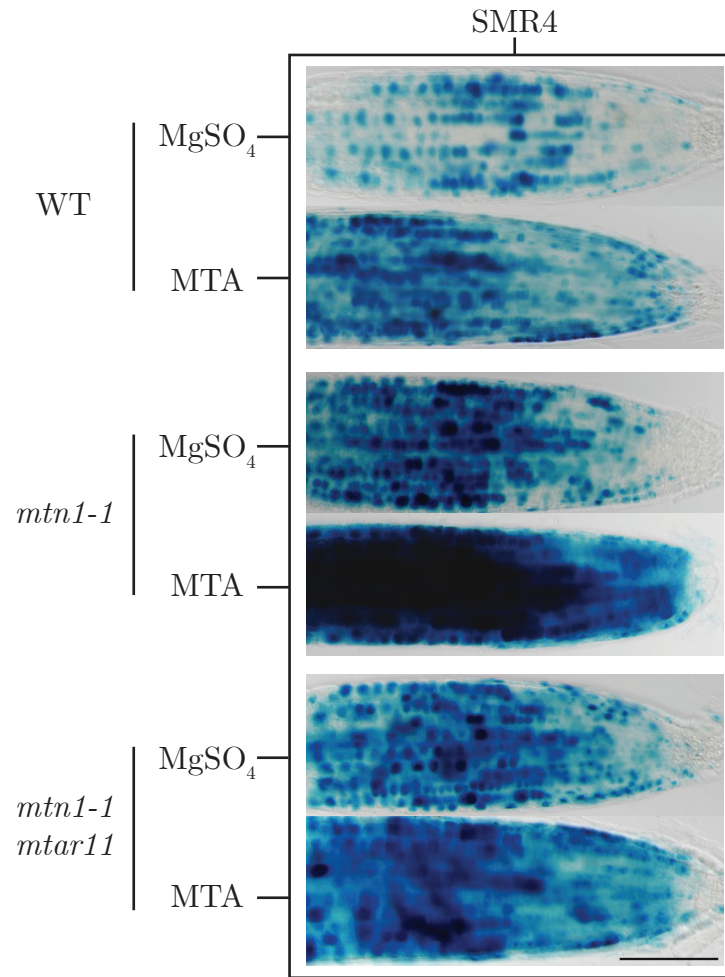
Figure 3.9: Upregulation of *SMR4* expression due to MTA.

WT, *mtn1-1*, and *mtn1-1mtar11* seedlings with the *SMR4::nlsGFP-GUS* reporter were vertically grown on sulfur-free media supplemented with either 500 μM MgSO$_4$ or 650 μM MTA. Seedlings were harvested 7 DAS, stained for GUS, and imaged using a light microscope. n = 10 per genotype per day. Scale bar = 100 μm.

3.3.3 Suppression of *mtn1-1mtn2-1* phenotypic traits by *mtn1-1mtar11*

An *mtn1-1mtar11* plant was crossed to *mtn1-1* $\frac{MTN2}{mtn2-1}$ to introduce the *mtar11* mutation into the double MTN mutant background to assess if the *mtar11* muation could restore a WT phenotype for developmental abnormalities of *mtn1-1mtn2-1*. F_2 seeds were sown on 1/2MS, and *mtn1-1mtn2-1* mutants were identified based on their chlorotic true leaves and later confirmed by PCR genotyping. From the pool of *mtn1-1mtn2-1* plants, homozygous *mtar11* SNPs were identified by PCR genotyping and followed to assess their development. In general, *mtn1-1mtn2-1mtar11* plants were much healthier than *mtn1-1mtn2-1* plants, and the *mtar11* mutation restored the fertility of the *mtn1-1mtn2-1* plants (Figure 3.10). Previous segregation analysis of the *mtn1-1* $\frac{MTN2}{mtn2-1}$ showed that the F_2 progeny did not follow a typical Mendelian inheritance, instead favoring the WT copy of *MTN2* (Waduwara-Jayabahu, 2012). The *mtar11* mutation restored the skewed segregation of *mtn1-1* $\frac{MTN2}{mtn2-1}$, allowing the *mtn1-1* $\frac{MTN2}{mtn2-1}$ background to follow a typical Mendelian inheritance and producing an expected number of *mtn1-1mtn2-1mtar11* mutants (Table 3.1).

3.3.4 Monitoring plant development

Previous work documented several vegetative and reproductive abnormalities of the *mtn1-1mtn2-1* mutant, including increased vascularization of the rosette leaves and stem, reduced auxin transport, and improper ovule and pollen development (Waduwara-Jayabahu, 2012). This monitoring of plant development was also used examine the effects of *mtar11* on plant growth and development as well as the effect on the abnormal developmental phenotypes of *mtn1-1mtn2-1* in the *mtn1-1mtn2-1mtar11* line. An additional comparison was made to the moderate MTN mutant, *mtn1-1mtn2-5*, in order to assess how substantial the phenotypic changes are when *mtar11* is introduced into the *mtn1-1mtn2-1* background. This investigation focused on changes in vegetative growth, flowering time, and fertility.
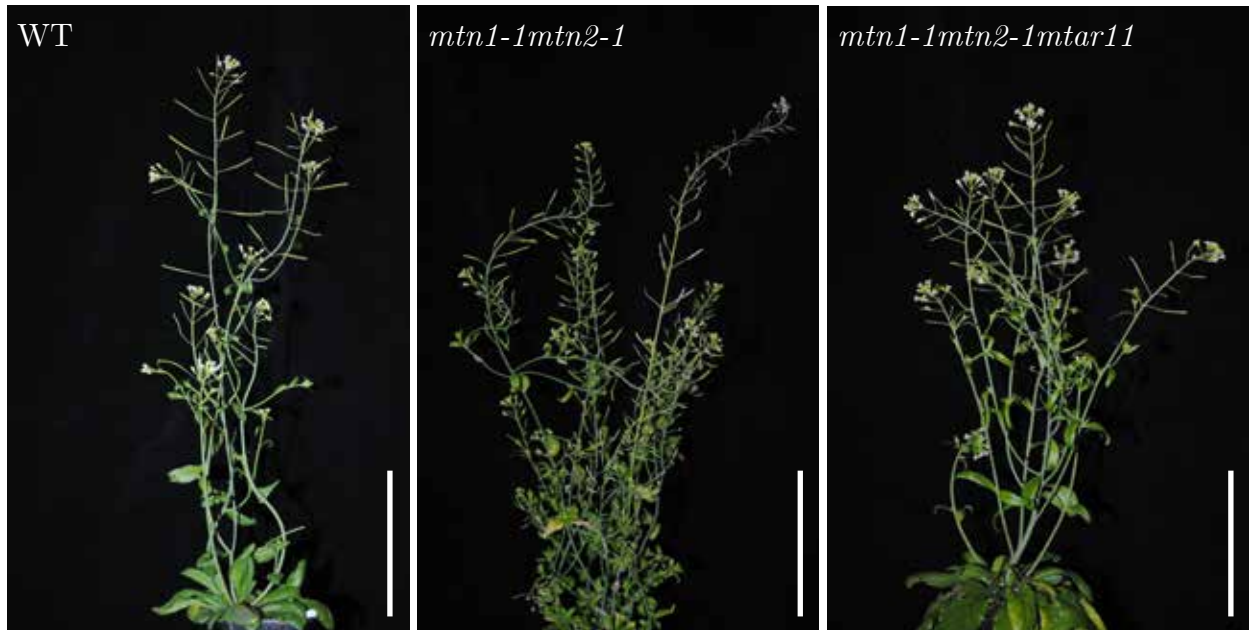
Figure 3.10: *mtn1-1mtn2-1mtar11* restores phenotypes of MTA toxicity.

Representative images of adult WT, *mtn1-1mtn2-1*, and *mtn1-1mtn2-1mtar11* plants approximately 6, 10, and 8 weeks after germination, respectively. Scale bar = 10 cm.

Table 3.1: Segregation analysis of _mtn1-1mtar11_ $\frac{MTN2}{mtn2-1}$ F$_3$ progeny.

mtn1-1mtar11 was crossed to _mtn1-1_ $\frac{MTN2}{mtn2-1}$ plants. After isolating an _mtn1-1mtar11_ $\frac{MTN2}{mtn2-1}$ plant, the F$_3$ progeny was germinated on 1/2MS and genotyped for both the WT _MTN2_ (+) and _mtn2-1_ (-) allele. A χ^2 value was calculated using the observed and expected frequencies in this dataset. A χ^2 distribution critical value of 3.841 was obtained using one degree of freedom (d.f.) and p <0.05. The expected ratio is 1:2:1 (_MTN2_:_MTN2_$^{+/-}$:_mtn2-1_).

Genotype	Observed	Expected	$\frac{(Expected-Observed)^2}{Expected}$	
$MTN2^{+/+}$	10	12	0.33	
$MTN2^{+/-}$	23	24	0.042	
$mtn2\text{-}1^{-/-}$	15	12	0.75	
Total	48	48	1.1	$= \chi^2$
			1	$=$ d.f.

(a)

WT   *mtn1-1mtn2-5*   *mtn1-1mtn2-1*

mtn1-1   *mtn1-1mtar11*   *mtn1-1mtn2-1*
                                          mtar11
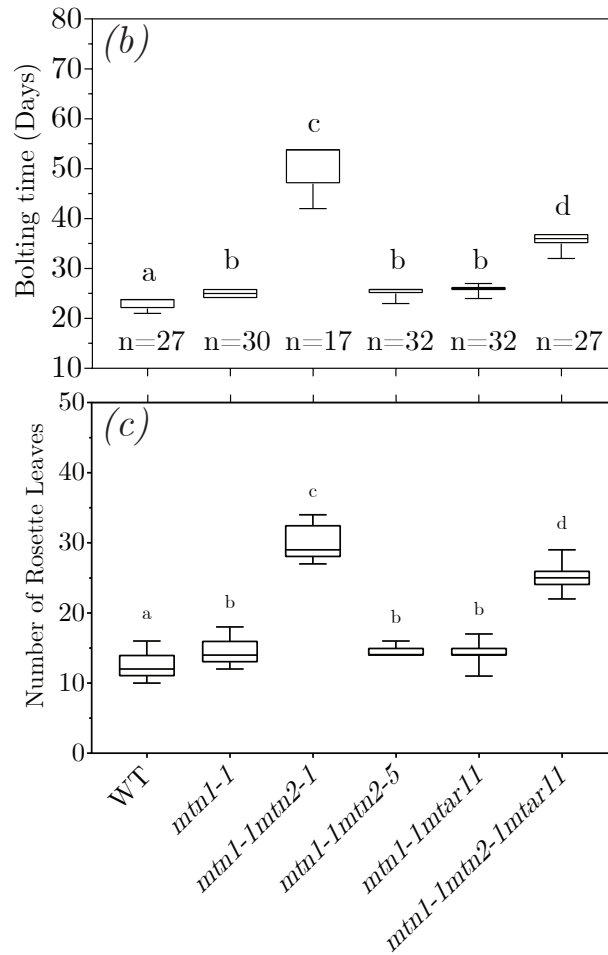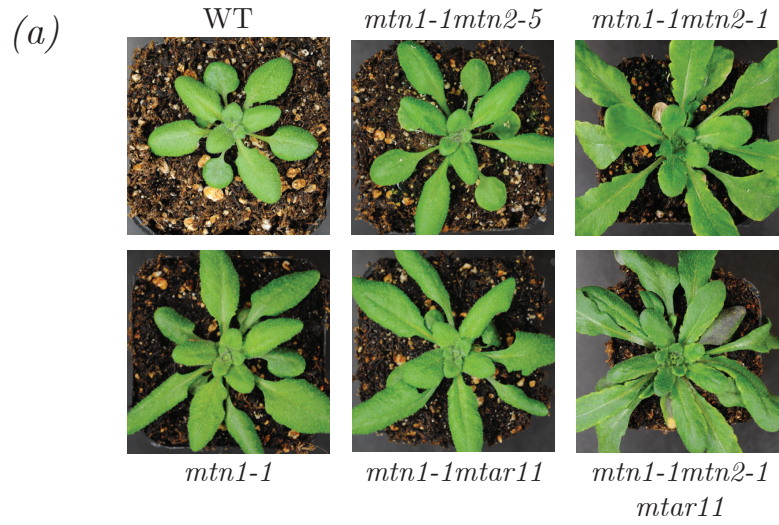
Figure 3.11: The effect of MTA accumulation on vegetative growth of MTN-deficient plants.

Figure 3.11 *(previous page)*: **The effect of MTA accumulation on vegetative growth of MTN-deficient plants.**
Phenotypic monitoring of vegetative growth began after transplanting seedlings off 1/2MS into pots. *(a)* Representative images of WT, *mtn1-1*, *mtn1-1mtar11*, *mtn1-1mtn2-5*, *mtn1-1mtn2-1*, and *mtn1-1mtn2-1mtar11* rosettes at bolting. *(b)* Bolting time was marked from germination to when the appearance of the first apical bud cluster at the center of the rosette. At which point, the number of rosette leaves was counted *(c)*. The number of replicates per genotype is marked under the data points in *(b)* and coincides with the data in *(c)*. After a one-way ANOVA, letters represent statistical significance from Tukey's HSD post hoc test ($p < 0.05$).

Vegetative growth

The vegetative growth of MTN-deficient mutants was assessed at bolting, beginning with the number of rosette leaves produced at this developmental milestone. The number of rosette leaves produced by WT and *mtn1-1mtn2-1* was consistent with the previous results of Waduwara-Jayabahu (2012). *mtn1-1mtn2-1* plants produced twice as many rosette leaves as compared to WT while also taking twice as long to transition to flowering (Figure 3.11*b*). While *mtn1-1mtn2-1mtar11* produced slightly fewer rosette leaves than *mtn1-1mtn2-1* (Figure 3.11*c*), there was a considerable reduction in the time for the transition to flowering (Figure 3.11*b*). Thus, the accumulation of MTA in the *mtn1-1mtn2-1* background produces a much larger rosette in terms of the number of leaves and the size of individual leaves (Figure 3.11*a*). The WT, *mtn1-1*, *mtn1-1mtar11*, and *mtn1-1mtn2-5* rosette leaves are a fraction of the size of *mtn1-1mtn2-1*, with the *mtar11* mutation having minimal effect on this phenotype.

In order to encompass the overall effect of MTN deficiency on vegetative growth, the plant heights were measured upon maturation of the plant's life cycle. There is a substantial increase in plant height with the addition of the *mtar11* mutation (Figure 3.12). *mtn1-1mtar11* plants are much taller than *mtn1-1* plants but not as tall as *mtn1-1mtn2-5* plants. When introduced into the *mtn1-1mtn2-1* background, the positive growth effect of the *mtar11* mutation is limited, still resulting in impairment of vegetative growth relative to *mtn1-1mtar11*. *mtn1-1mtn2-1* and *mtn1-1mtn2-1mtar11* plants are slightly shorter than WT but this difference is not statistically significant (Figure 3.12).
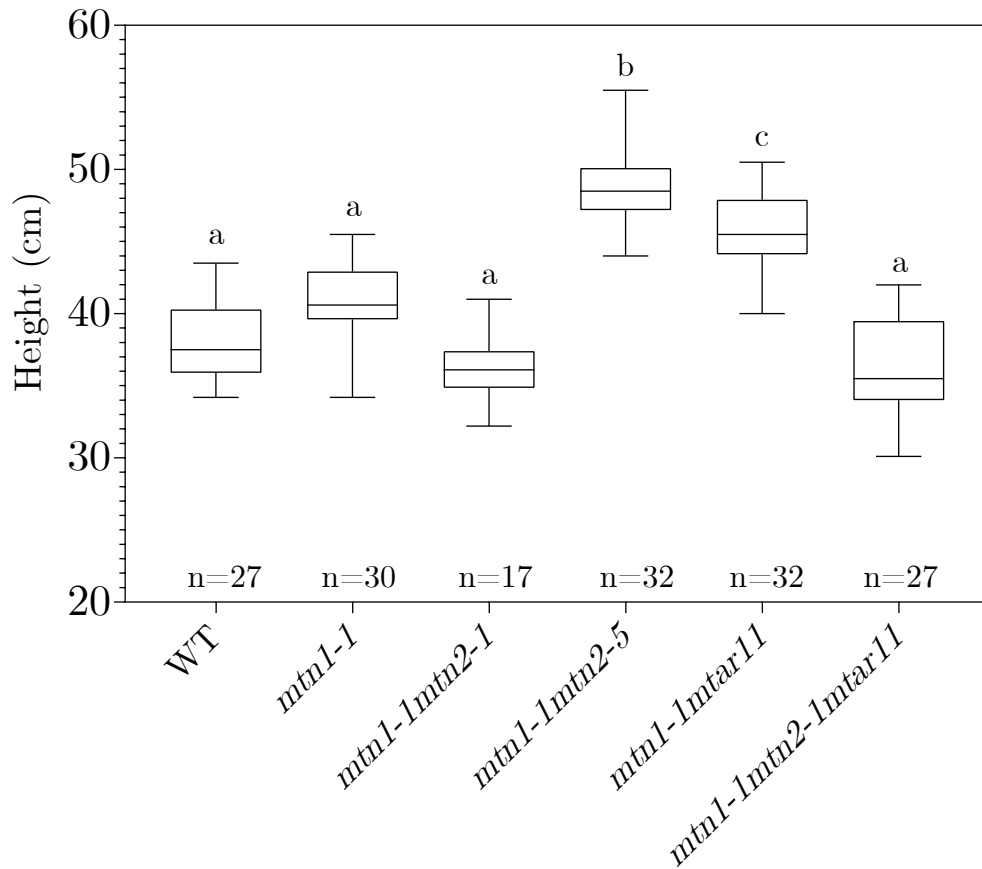
Figure 3.12: Plant inflorescence heights.

Once WT, *mtn1-1*, *mtn1-1mtar11*, *mtn1-1mtn2-5*, *mtn1-1mtn2-1*, and *mtn1-1mtn2-1mtar11* reach maturity and prior to senescence, the height of each plant was measured from the base of the rosette to the highest apical bud cluster. The number of replicates per genotype is marked under the data points. After a one-way ANOVA, letters represent statistical significance from Tukey's HSD post hoc test ($p < 0.05$).

Reproductive Development

In addition to the delay in transitioning to flowering, *mtn1-1mtn2-1* plants have an array of reproductive abnormalities (Waduwara-Jayabahu et al., 2012). The double mutant produces approximately twice as many siliques as WT (Figure 3.13*a*), however these siliques are generally empty and short (Figure 3.13*b*). These plants have very minimal amounts of viable seed, but with the addition of the *mtar11* mutation, fertility is restored (Figure 3.13*c*). *mtn1-1mtn2-1mtar11* plants produce approximately 25 times the amount of viable seed *mtn1-1mtn2-1* produces, although this is still a considerable amount lower than WT (Figure 3.13*c*). In addition, *mtn1-1mtn2-1mtar11* plants have longer and fewer siliques than *mtn1-1mtn2-1* (Figure 3.13*a, b*).

The *mtar11* mutation has a significant effect on both seed yield and silique length. *mtn1-1mtar11* plants have a greater seed yield than WT, *mtn1-1*, or *mtn1-1mtn2-5* (Figure 3.13*c*). Given that *mtn1-1mtn2-5* plants are taller than *mtn1-1mtar11*, there was a possibility that more siliques are produced. This correlation is not the case as *mtn1-1mtar11* produces more siliques that are longer than *mtn1-1mtn2-5* siliques (Figure 3.13*a, b*). Taken together, *mtar11* has a positive impact on seed yield and plant reproduction.

Internode Development

Proper internode development is a crucial part of the reproductive maturation of a plant, as controlling internode elongation during flowering allows the plant to customize its vertical form (McKim, 2020). The plant architecture of *mtn1-1mtn2-1* is very abnormal based on Waduwara-Jayabahu's (2012) observations. Not only does the stem twist but its increased branching and shortened plant height results in a bushy plant architecture (Waduwara-Jayabahu, 2012). Since the floral shoot apical meristem controls plant architecture and these observations point to its impairment, MTA accumulation likely inhibits the formation of a normal plant architecture. This other facet of reproductive development was investigated by measuring the first ten internode lengths between siliques on the primary branch.
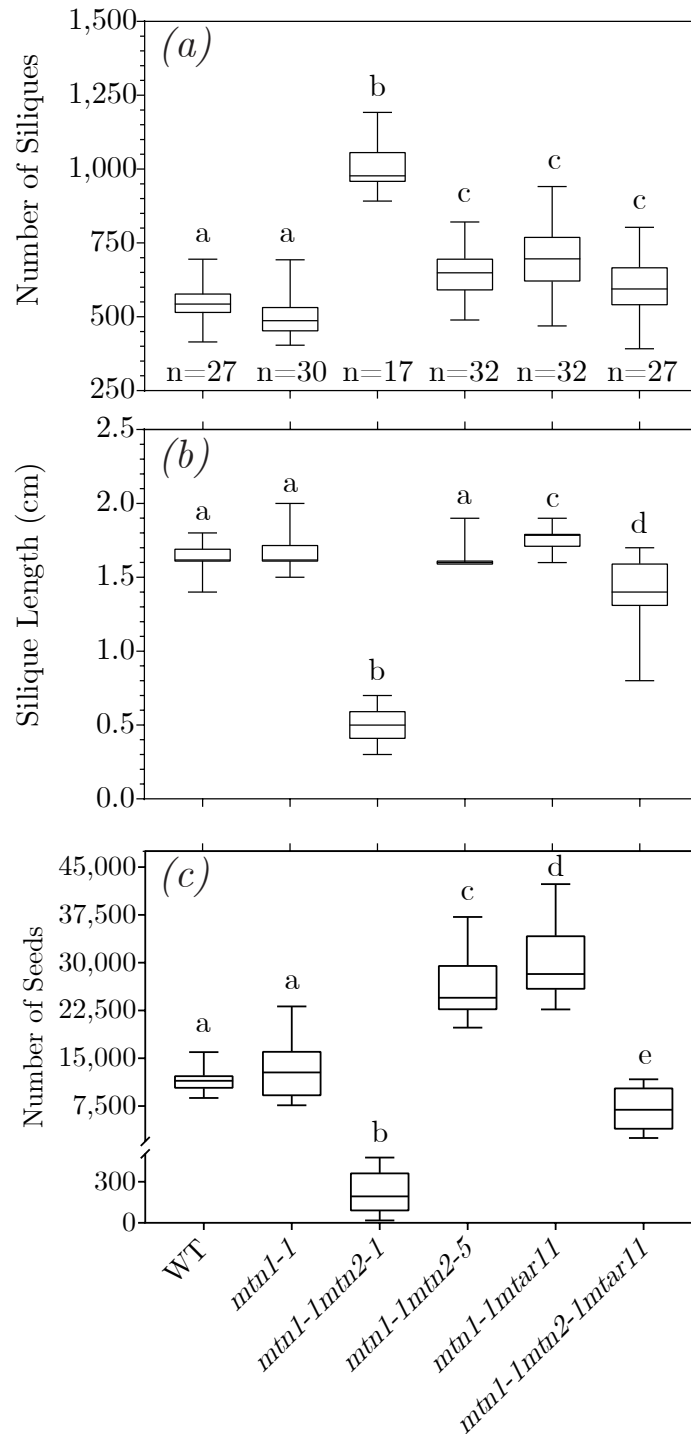
Figure 3.13: ***mtar11* increases seed yield and restore infertility of *mtn1-1mtn2-1* plants.**

Before complete senescence, WT, *mtn1-1*, *mtn1-1mtar11*, *mtn1-1mtn2-5*, *mtn1-1mtn2-1*, and *mtn1-1mtn2-1mtar11* siliques were counted *(a)*, and the average length of the fruiting body was measured *(b)*. Plants were then left to dry in isolation until seeds were harvested. Two

Figure 3.13 *(previous page)*: *mtar11* **increases seed yield and restore infertility of *mtn1-1mtn2-1* plants.**
weeks after harvesting, using the weight of approximately 300 seeds for each genotype, seeds were weighed and quantified. The viability of these seeds were tested on 1/2 MS and the % germination are as follows: WT 99%, *mtn1-1* 97%, *mtn1-1mtar11* 100%, *mtn1-1mtn2-1* 100%, *mtn1-1mtn2-5* 100%, and *mtn1-1mtn2-1mtar11* 99%. The number of replicates per genotype is marked under the data points in *(a)* and coincides with the data in *(b)* and *(c)*. Letters represent statistical significance from Tukey's HSD post hoc test after a one-way ANOVA ($p < 0.05$).

WT plants show a consistent internode pattern, with the first few internodes quite spread out and then becoming shorter when reaching the tenth internode (Figure 3.14*a*). *mtn1-1mtn2-1* plants deviate from this architecture, producing a synergistic phenotype of extremely long internodes interspersed with short internodes (Figure 3.14*b*). This abnormal internode elongation is consistent with previous results of a shortened plant stature (Figure 3.12). There is no consistent internode pattern associated with the *mtn1-1mtn2-1* plants as was observed in WT. *mtn1-1mtn2-1mtar11* plants recover the WT internode spacing by reducing the extreme internode changes and making internode lengths more consistent (Figure 3.14*c*). These plants have a similar internode patterning as WT, though the inconsistencies between plants make the similarities less apparent.

In agreement, *mtn1-1mtn2-1* internode measurements distinctly cluster away from WT and *mtn1-1mtn2-1mtar11* plants (Figure 3.15). In addition, the variation between plants are exemplified in *mtn1-1mtn2-1* as these plants are scattered along the Y-axis (PC2). In contrast, both WT and *mtn1-1mtn2-1mtar11* plants cluster relatively close to one spot on the Y-axis while *mtn1-1mtn2-1mtar11* is slightly variable across the X-axis (Figure 3.15). As depicted in the representative plants, *mtn1-1mtn2-1mtar11* plants have slighlty restored the abnormal plant architecture of *mtn1-1mtn2-1* as these plants cluster close to WT plants (Figure 3.15).
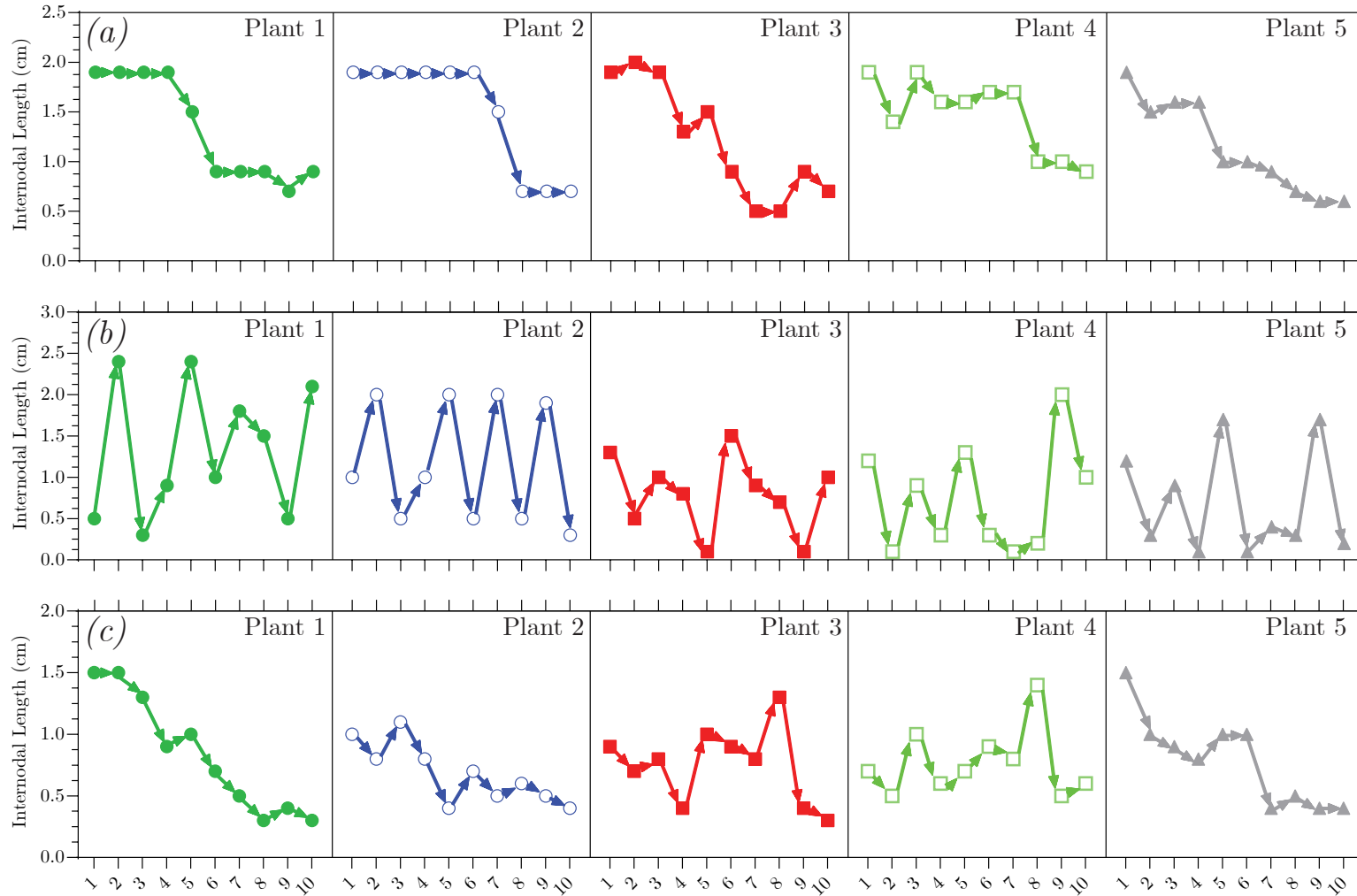
Figure 3.14: Abnormal plant architecture of *mtn1-1mtn2-1* plants.

After *(a)* WT, *(b) mtn1-1mtn2-1*, and *(c) mtn1-1mtn2-1mtar11* plants reached approximately 25 cm in height, the first ten internodes between siliques were measured on the primary inflorescence branch. The distribution of internode lengths of five representative plants is depicted based on internode and its size.
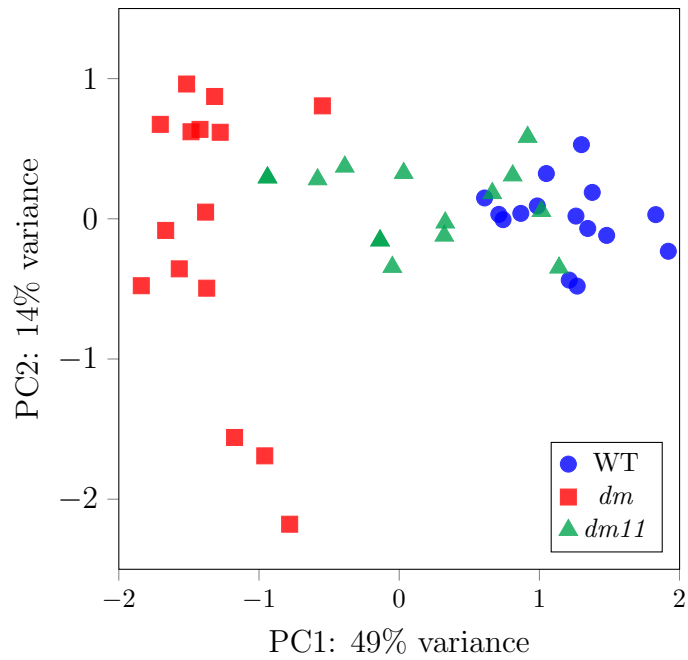
Figure 3.15: Clustering of internode development.

The first ten internodes between siliques were measured and summarized in a PCA for WT, *mtn1-1mtn2-1* (*dm*), and *mtn1-1mtn2-1mtar11* (*dm11*). Singular value decomposition with imputation was used to calculate the principal components. Principal component 1 (PC1) and component 2 (PC2) explain 49% and 14%, respectively. n = 20 for each genotype.

3.3.5 Inhibition of TOR activity impairs the cell cycle and induces endoreduplication

The TOR signaling network strongly influences several facets of plant development, ranging from controlling meristem development, regulating carbon, nitrogen, and sulfur metabolism, and balancing cell proliferation and differentiation (McCready et al., 2020). MTA negatively affects sulfur metabolism by reducing the abundance of sulfur-containing amino acids resulting in several phenotypic abnormalities. Therefore, the following hypothesis was tested, MTA's negative effect on sulfur metabolism and amino acid abundance have altered TOR activity. TOR activity in MTN-deficient plants was evaluated in rosette leaves five and six were developmentally matched approximately 21 DAS for WT, *mtn1-1mtn2-1*, *mtn1-1mtn2-5*, and *mtn1-1mtn2-1mtar11*. This leaf tissue was selected due to its high TOR activity (Brunkard et al., 2020) and the ease of collecting developmentally matched leaves from different genotypes.

In agreement with the reduction in meristem size due to exogenous MTA feeding, TOR activity was reduced due to MTA accumulation in the *mtn1-1mtn2-1* plant (Figure 3.16*a*). *mtn1-1mtn2-1* rosette leaves does not accumulate as much MTA as unopened buds (24-fold higher in buds; Waduwara-Jayabahu et al., 2012); nevertheless, MTA has a strong influence on TOR activity (Figure 3.16*b*). Remarkably, TOR activity in the *mtn1-1mtn2-1* background was restored with the addition of *mtar11* (Figure 3.16*a, b*).

The impairment of the cell cycle and the reduced TOR activity associated with MTN deficiency also influence the early induction of cells into the endocycle (Barrada et al., 2015). MTA inhibits the progression of the cell cycle at the G_2 checkpoint, leading to an additional hypothesis, MTA induces endoreduplication after the impairment of the cell cycle. By assessing the endoreduplication capacity of MTN-deficient mutants, a thorough characterization of a compromised cell cycle can be accomplished. The cell ploidy levels of the rosette leaves were evaluated by using the same leaf material as the TOR activity assay. As expected, both the loss of TOR activity and cell cycle progression results in endoreduplication as *mtn1-1mtn2-1* plants have an increased population of 16C and 32C cells compared to
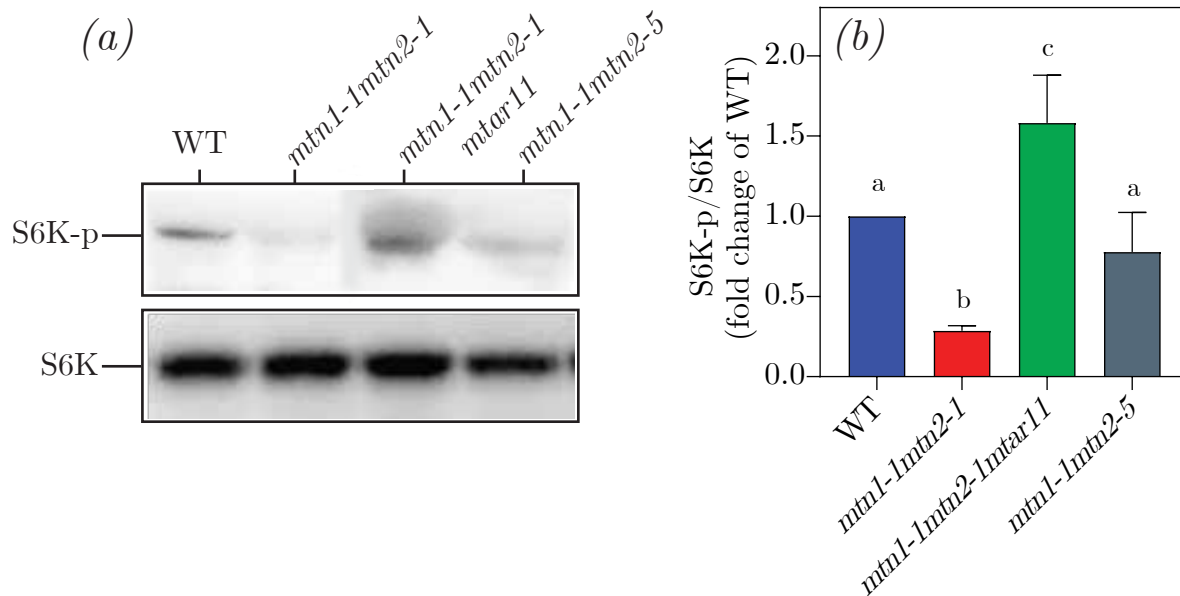
Figure 3.16: Recovery of TOR activity in *mtn1-mtn2-1mtar11*.

TOR activity was determined in 21-day old WT, *mtn1-1mtn2-1*, *mtn1-1mtn2-1mtar11*, and *mtn1-1mtn2-5* developmentally matched rosette leaves *(a)*. Relative TOR activity was determined using antibodies against S6K-p and S6K (approximate size: 52kDA) and *(b)* the calculated ratio of S6K-p/S6K expressed in fold change of WT. After a one-way ANOVA, letters represent statistical significance from Tukey's HSD post hoc test ($p < 0.05$). n = 4 per genotype. This analysis was performed by a collaborator, Dr. Yihan Dong (IBMP).
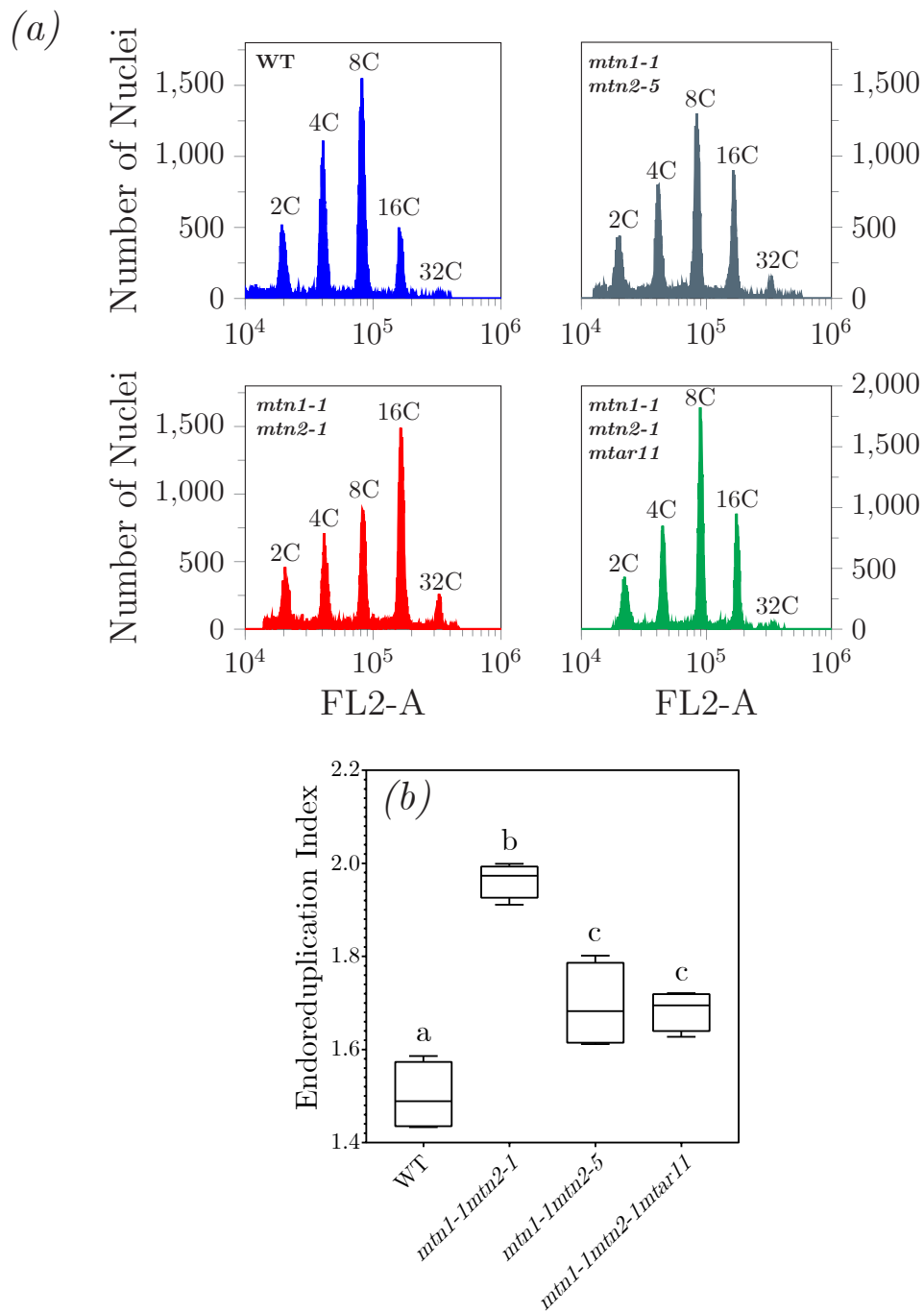
Figure 3.17: Endoreduplication is induced due to MTA accumulation.

Using flow cytometry, the cell ploidy of 21-day old WT, *mtn1-1mtn2-1*, *mtn1-1mtn2-1mtar11*, and *mtn1-1mtn2-5* developmentally matched rosette leaves were measured, which produced *(a)* histograms of fluorescence signals from propidium iodide stained nuclei for each genotype. Five major peaks in these representative histograms are from cells with ploidy levels at 2C, 4C, 8C, and 16C, 32C, respectively.

Figure 3.17 *(previous page)*: **Endoreduplication is induced due to MTA accumulation.**
(b) The endoreduplication index was calculated from the percentage of cells within each major peak. $EI = \frac{4C+(2\times8C)+(3\times16C)+(4\times32C)+(5\times64C)}{100}$. After a one-way ANOVA, letters represent statistical significance from Tukey's HSD post hoc test ($p < 0.05$). n = 4 per genotype.

WT and a substantial loss of 4C cells (Figure 3.17*a, b*). The WT ploidy profile is restored in *mtn1-1mtn2-1mtar11* as the levels of 4C and 8C cells match WT while the population of 16C cells matches *mtn1-1mtn2-5* plants (Figure 3.17*a*). As such, the endoreduplication indexes of both *mtn1-1mtn2-1mtar11* and *mtn1-1mtn2-5* are nearly identical (Figure 3.17*b*).

3.3.6 Decrease in root length upon MTA inhibition of TOR requires YAK1

TOR inhibition has been implicated in reducing the size of the meristematic zone of the root and inducing early differentiation of root cells (Montané and Menand, 2013). A known pathway of control on cell proliferation is YAK1 inhibition of CDK and CYC activity when TOR activity has been suppressed (See Figure 1.5 for schematic). In order to investigate the role of TOR and YAK1 on root growth, WT, *mtn1-1*, and *mtn1-1mtar11* were grown on media supplemented with proINDY, a YAK1 enzyme inhibitor. In addition, this media was also supplemented with either $MgSO_4$, MTA, and a TOR inhibitor, AZD-8055. The combination of these growth elements allows for the understanding of the effect of YAK1 when MTA or AZD-8055 has inhibited TOR activity.

The addition of proINDY to $MgSO_4$ supplemented media increases the overall root length 10 DAS for each genotype, with *mtn1-1mtar11* exhibiting the greatest increase compared to WT and *mtn1-1* (Figure 3.18, 3.19). When seedlings were provided with the TOR inhibitor, AZD-8055, a substantial reduction in root length was observed. Surprisingly, *mtn1-1mtar11* seedlings were relatively unresponsive to TOR inhibition and grow longer roots than WT and *mtn1-1* (Figure 3.18, Figure 3.19). proINDY treatment with the addition of either AZD-8055 or MTA had minimal effects on WT and *mtn1-1mtar11* root lengths. The only meaningful recovery was seen with *mtn1-1* seedlings grown on MTA and proINDY (Figure 3.18, 3.19).
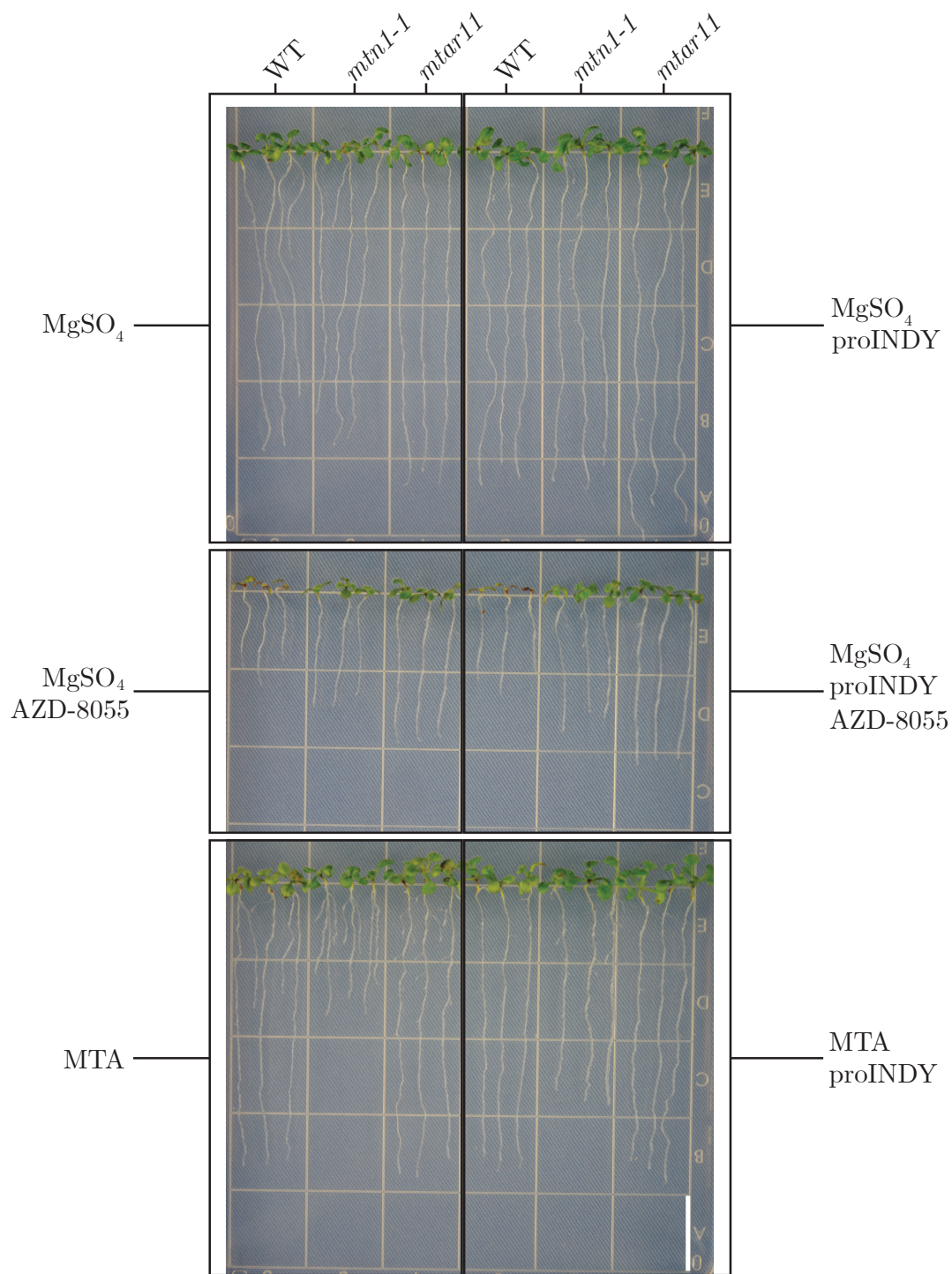
Figure 3.18: YAK1 dependent inhibition of root growth of MTA treated seedlings.

Representative seedlings of vertically grown WT, *mtn1-1*, and *mtn1-1mtar11* on sulfur-free media supplemented with either 500 μM MgSO$_4$, 20 μM proINDY, 1 μM AZD-8055, 650 μM MTA, or a combination. *mtar11*; *mtn1-1mtar11*. Images were taken 10 DAS. Scale bar = 1 cm.
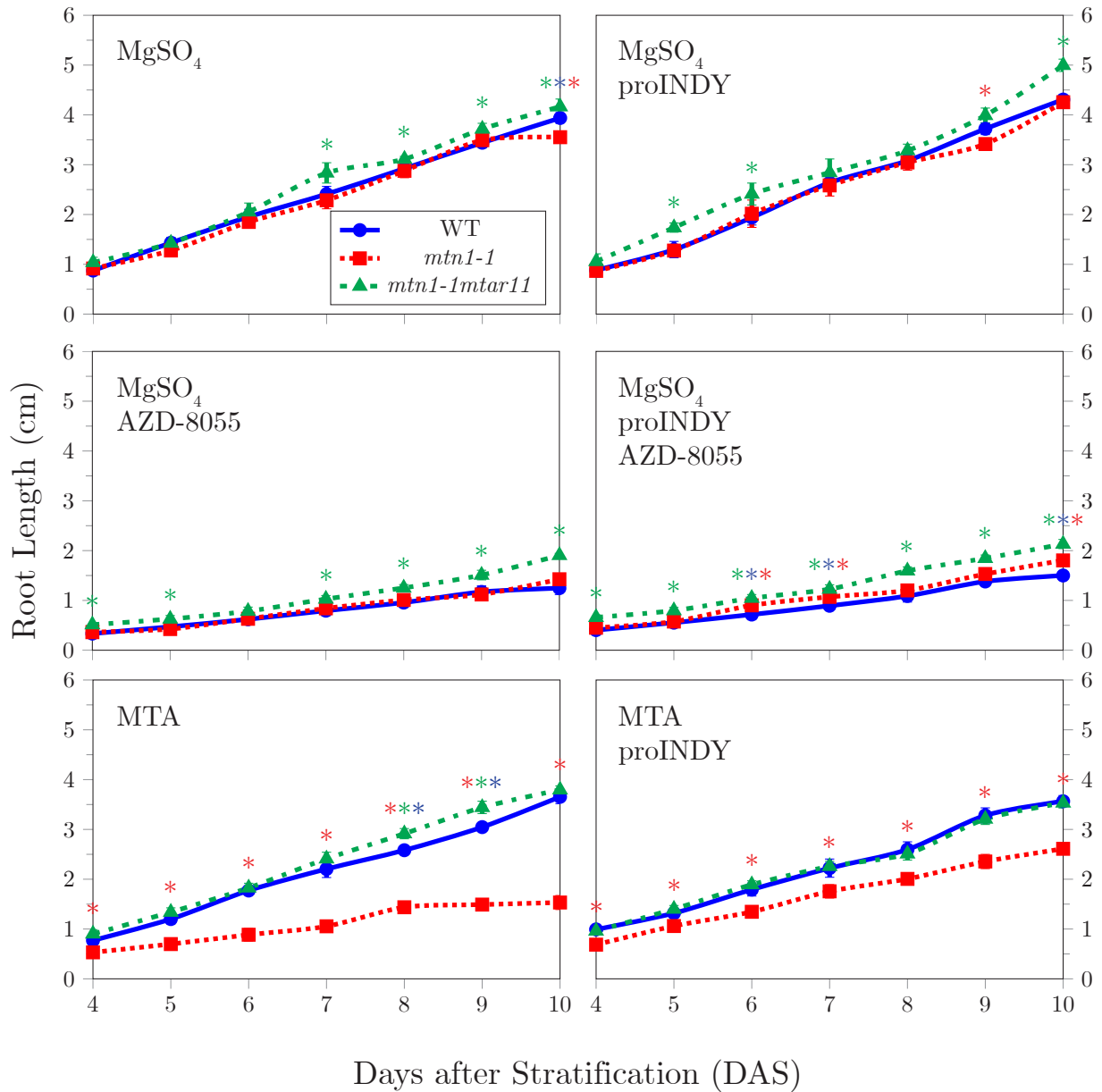
Figure 3.19: proINDY partially restores root length of *mtn1-1* on MTA.

WT, *mtn1-1*, and *mtn1-1mtar11* were grown vertically on sulfur-free media supplemented with either 500 μM MgSO$_4$, 20 μM proINDY, 1 μM AZD-8055, 650 μM MTA, or a combination. Images of the growth plates were taken every day, and the root lengths were measured on ImageJ. After a Tukey's HSD post hoc test after a two-way ANOVA (p < 0.0001), (*) represents statistical significance. The color of (*) represents significantly different genotypes. n = 10 per genotype per day.

3.3.7 Dramatic changes in phytohormone profiles of MTN-deficient mutants

Previous models explain the basis for MTA toxicity predicated that auxin levels increase with MTN deficiency. These models were built upon several lines of evidence, including preliminary IAA measurements (Waduwara-Jayabahu, 2012), auxin-related phenotypic changes in *mtn1-1mtn2-1*, increases in IAA biosynthesis pathway genes in transcriptomic datasets, and the proposed mechanism of suppression of the *mtar2* SNP (Tremblay, 2019). These previous indications led to the hypothesis that MTN deficiency results in increased auxin accumulation in the form of IAA.

The breakdown of MTA by MTN produces adenine as a by-product, and the inability to efficiently metabolize MTA in the *mtn1-1mtn2-1* would limit the available adenine (see Figure 1.2). Since adenine is used for cytokinin biosynthesis via the purine salvage pathway (Ashihara et al., 2018), the loss of MTN activity likely reduces adenine availability resulting in a decrease in active cytokinin. Considering that TOR activity is inhibited in MTN-deficient plants, any changes to the phytohormone profiles may further contribute to the phenotypic differences due to MTA.

Testing these hypotheses was approached in two ways. First, the accumulation of auxin was assessed under MTA pressure by evaluating the expression of the *DR5::n3GFP* (Liao et al., 2015) reporter specific for auxin on MTA. Second, phytohormone profiles of the rosette leaves and unopened floral buds of MTN-deficient mutants were measured.

DR5::n3GFP expression

Feeding MTA as the sole sulfur source for 7 DAS does not increase *DR5* expression, indicating that auxin does not accumulate in response to MTA, as would be predicted by previous models to explain the effects of MTA accumulation. In fact, *DR5* expression significantly decreases under these conditions (Figure 3.20a), and its expression is more dispersed when compared with *mtn1-1* seedlings grown on sulfur sufficient $MgSO_4$ media (Figure 3.20a).
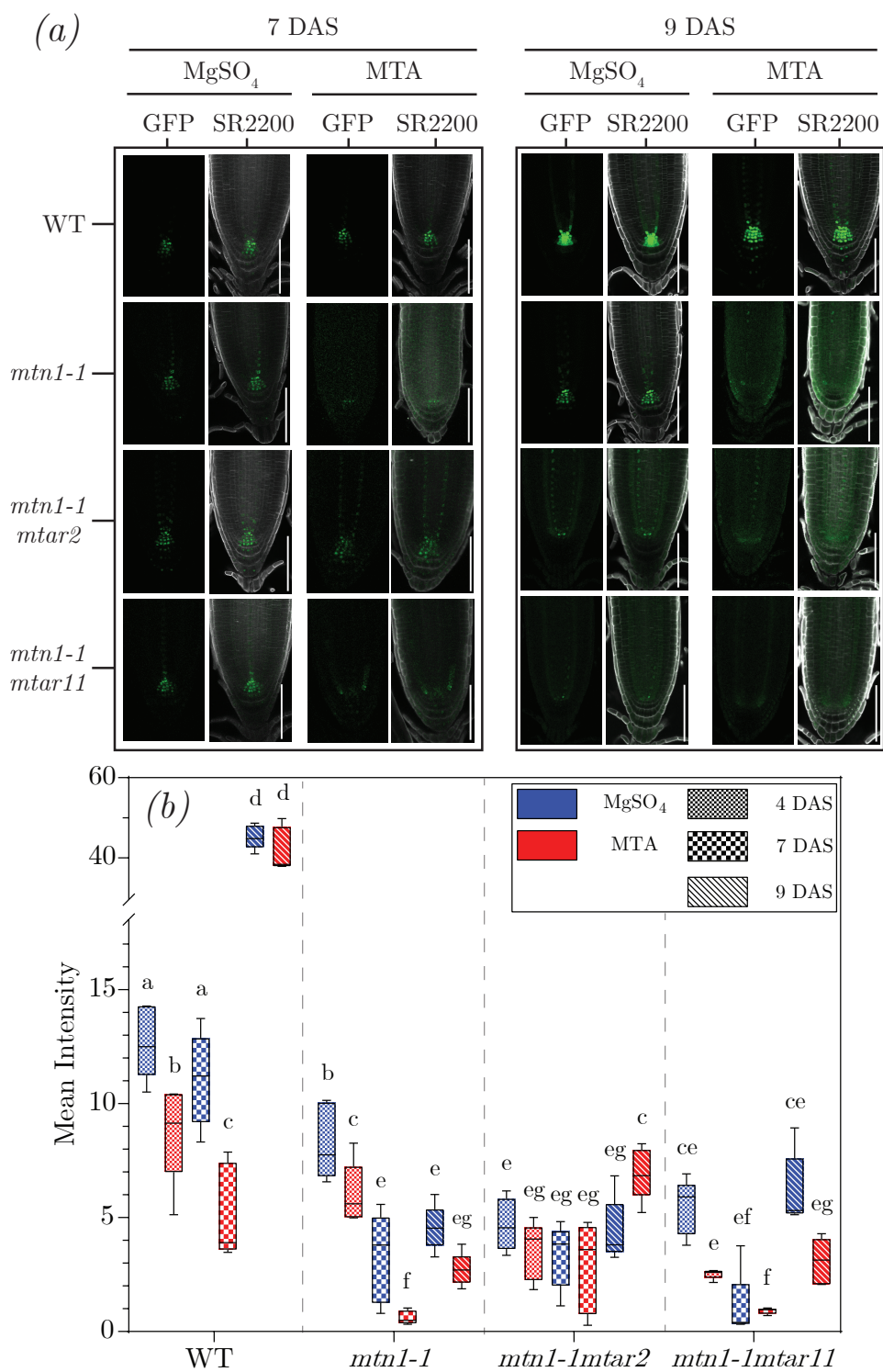
Figure 3.20: Exogenous MTA feeding abolishes auxin maxima at QC.

Representative images of *DR5::n3GFP* expression of WT, *mtn1-1*, *mtn1-1mtar2*, *mtn1-1mtar11* seedlings grown on 500 μM MgSO$_4$ and 650 μM MTA media for 7 and 9 DAS *(a)*.

Figure 3.20 *(previous page)*: **Exogenous MTA feeding abolishes auxin maxima at QC.**
SR2200 were used to stain seedlings and normalize the optical plane between replicates. *(b)* GFP expression was measured in ImageJ with a range of interest centered on the QC. After a two-way ANOVA, letters represent statistical significance from Tukey's HSD post hoc test ($p < 0.05$). Scale bar = 100 μm. n =10 for each genotype per day.

This expression pattern is consistent at 9 DAS as well. In contrast, *mtn1-1mtar2* seedlings do not have any evident changes in *DR5* expression (Figure 3.20*b*), but the distribution of the auxin reporter is more similar to WT on MTA (Figure 3.20*a*). The consistent decrease in *DR5* expression 4, 7, 9 DAS suggests auxin distribution is affected by MTA accumulation rather than an increase in auxin biosynthesis, as original thought (Figure 3.20*b*).

Furthermore, the slow deterioration of the auxin maxima at the QC of the MTN-deficient mutants by 9 DAS is quite evident (Figure 3.20*a*). This loss in auxin polarization is only apparent in seedlings relying on MTA as their sulfur source. The distribution of *DR5* expression also changes from being concentrated at the QC 7 DAS for both $MgSO_4$ and MTA to highly expressed in the stele by 9 DAS (Figure 3.20*a*).

Phytohormone profiles MTN-deficient mutants

In agreement with the *DR5* expression of seedlings grown on MTA media, IAA measurements of *mtn1-1mtn2-1* unopened buds were considerably lower than WT (Figure 3.21*a*). This decrease in IAA was also seen in the rosette leaves, although the reduction was not as substantial (Figure 3.21*a*). Despite this, *mtn1-1mtn2-1mtar11* plants have IAA concentration in their rosette leaves comparable to WT while also increasing IAA in their unopened buds compared to *mtn1-1mtn2-1*. This IAA profile of *mtn1-1mtn2-1* also coincides with its cytokinin profile as total cytokinin abundance was also substantially lower in the *mtn1-1mtn2-1* unopened floral buds and approximately half that of WT. The total cytokinin content slightly increased in *mtn1-1mtn2-1mtar11* (Figure 3.21*b*), similar to the IAA profile of these mutants.

The transcriptomic profile of *mtn1-1mtn2-1* was enriched with various stress markers indicating both oxidative and osmotic stress (Tremblay, 2019). The upregulation of these genes due to MTN deficiency may be due to the accumulation of ABA (Wang et al., 2018). However, ABA levels were lower in the double mutant unopened floral buds compared to WT, despite many stress-related genes being upregulated in this background (Figure 3.21*c*; Tremblay, 2019).

Another way to evaluate the physiological state of a plant is to calculate the ratios between these phytohormones (Samsonová et al., 2020; Figure 3.22). Despite the low ABA levels in *mtn1-1mtn2-1*, the stress response does dominate over growth-promoting processes as ABA/IAA and ABA/CK (Figure 3.22*a, b*) ratios are more prominent in the double mutant compared to that of WT in the unopened floral buds. This stress response is slightly restored in the *mtn1-1mtn2-1mtar11* background.
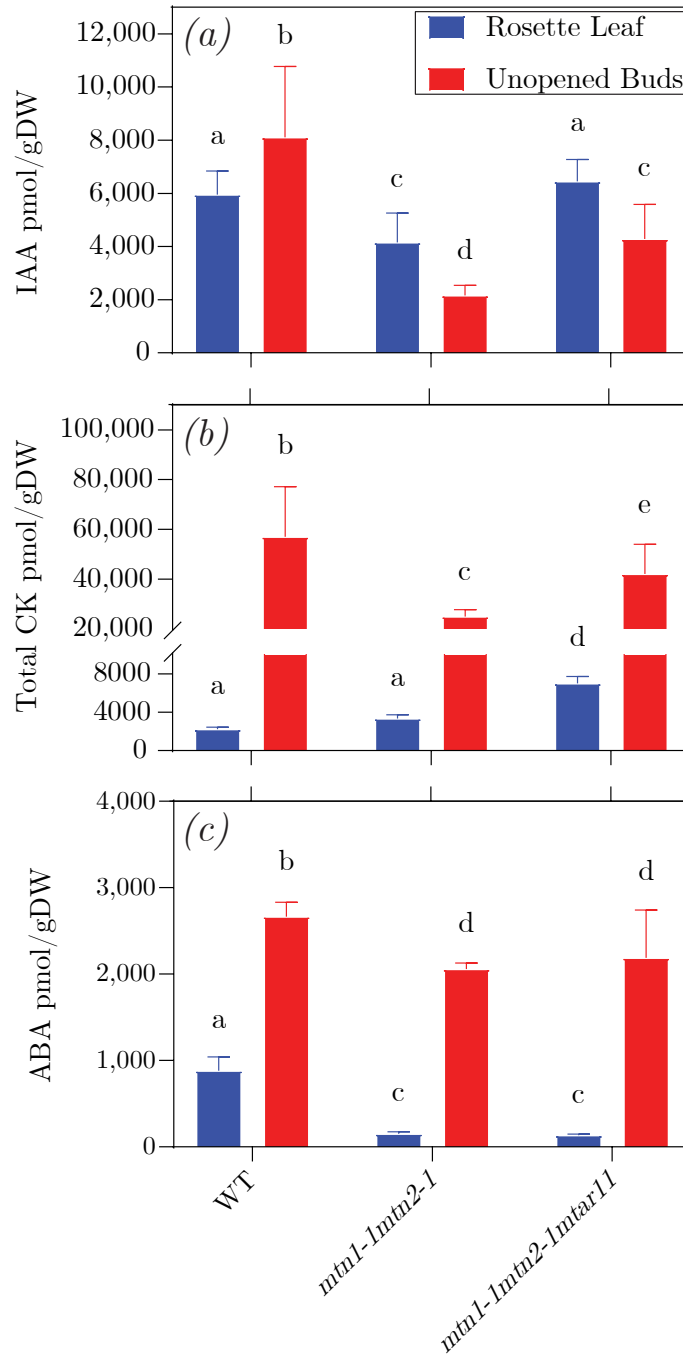
Figure 3.21: Altered phytohormone profiles of MTN-deficient mutants.

The unopened floral bud cluster and approximately 21-day old WT, *mtn1-1mtn2-1*, *mtn1-1mtn2-1mtar11*, and *mtn1-1mtn2-5* developmentally matched rosette leaves were harvested and the phytohormone profile of *(a)* auxin (IAA) *(b)* cytokinin (CK) and *(c)* ABA were measured by a collaborator, Dr. Anna Kisiała, (Trent University). Letters represent statistical significance from Tukey's HSD post hoc test ($p < 0.05$) after a two-way ANOVA. $n = 4$ for each genotype and tissue type.
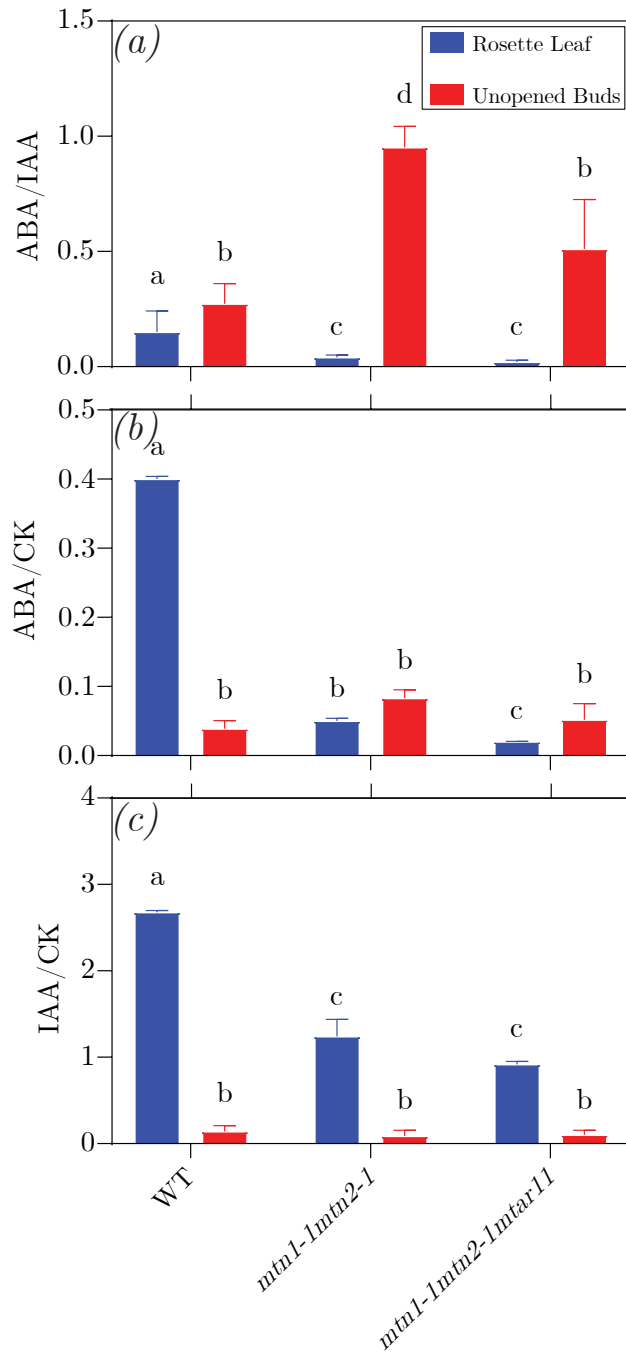
Figure 3.22: Physiologically stress state of MTN-deficient mutants based on phytohormone ratios.

From the phytohormone measurements, the ratios of *(a)* ABA/IAA *(b)* ABA/CK, and *(c)* IAA/CK were calculated for both unopened floral apical buds and rosette levels. Letters represent statistical significance from Tukey's HSD post hoc test ($p < 0.05$) after a two-way ANOVA. n = 4 for each genotype and tissue type.

3.4 Discussion

3.4.1 MTA accumulation inhibits TOR activity

The impact of MTA accumulation has been tissue-specific in previous research studying these MTN-deficient mutants as the Met salvage is utilized by specific cell types (i.e., phloem cells; Pommerrenig et al., 2011). Previous experiments using *mtn1-1mtn2-1* seedlings tend to result in variable changes as these seedlings do not accumulate toxic concentrations of MTA (Tremblay, 2019). Unfortunately, many fundamental techniques used to study plant physiology and cell division rely on seedlings as the tissue of choice to study the effects of different metabolites. Since *mtn1-1mtn2-1* could not directly correlate the effect of MTA on plant physiology, exogenous feeding of MTA to MTN-deficient mutants proved to be an informative alternative assay (Tremblay, 2019). This assay provided an unequivocal way to assess the growth of MTN-deficient seedlings and provided an excellent way to study the direct effects of MTA on root cells. Using this assay, increased MTA accumulation has a direct correlation with decreased cell proliferation. Not only does the meristem size decrease with MTA accumulation (Figure 3.2), but cells undergo premature elongation within the meristematic zone (Figure 3.3), and the number of meristematic cells substantially decreases (Figure 3.4).

The decreases in cell proliferation stem from the repression of TOR activity due to MTA accumulation (Figure 3.16). The decrease in TOR-dependent S6K phosphorylation also correlates with the increased effects of YAK1 on cell cycle inhibition as TOR mediated phosphorylation inhibits YAK1 activity (see schematic in Figure 1.5). Thus, the negative impact on the size of the meristematic zone is observed during low TOR activity (Barrada et al., 2019). In support of this, the shortened root length of *mtn1-1* seedlings on MTA is recovered with the addition of proINDY, a YAK1 inhibitor (Figure 3.18, 3.19). The YAK1 mechanism of cell cycle inhibition is disrupted by proINDY, thus, loss of TOR activity due to MTA has less of an effect on the root length of *mtn1-1* in the presence of proINDY. Since phosphorylated S6K directly interacts with YAK1 and inhibits its activity (Barrada et al., 2019), the inhibition of TOR activity due to MTA inhibits cell proliferation via YAK1.

The increased abundance of unphosphorylated S6K binds to the RBR-DP-EF2a/b complex and thus, prevents its dissociation resulting in an inhibited cell cycle (Henriques et al., 2010). By interfering with this mechanism, EF2a/b is unable to freely transcribe essential cell markers required for the S phase of the cell cycle. This mechanism is likely to be involved in the decrease of cell proliferation due to MTN deficiency. Taken together, the inhibition of TOR activity due to MTA accumulation likely arises from the repression of cell proliferation via the TOR-YAK1 signaling axis and the interaction with the RBR-DP-EF2a/b complex.

The direct mechanism of TOR inhibition by MTA toxicity is unknown. Given the many upstream inputs on TOR activity, pinpointing the exact interaction has proven to be complicated. Furthermore, it is possible that TOR regulation or its sensitivity to MTN deficiency differs in different tissues. An obvious source for this variation is the differing extent of MTA accumulated accross different tissue types (Waduwara-Jayabahu et al., 2012; Tremblay, 2019). The most likely primary effect of MTA on TOR activity is the decrease in amino acid abundance. *mtn1-1* seedlings grown on MTA as the sole sulfur source accumulate more Cys compared to when grown on sulfur sufficient media (i.e., $MgSO_4$). *mtn1-1mtn2-1* seedlings also show no misregulation of amino acid metabolism (Tremblay, 2019). It is only in the unopened buds where MTA accumulaiton caused a significant shift in amino acid metabolism by decreasing Cys and Met levels (Tremblay, 2019). The change in sulfur metabolism due to MTA is not like the *sir1-1* mutant (Dong et al., 2017), where sulfur assimilation is completely inhibited and TOR activity is abolished.

Given that there are only a few changes in amino acid abundances due to MTA, the next consideration as to why TOR activity decreased is physiological stress. It is quite apparent the stress profile found in the transcriptomes of *mtn1-mtn2-1* unopened buds is due to MTN deficiency and likely, cellular increases in MTA. It was initially thought that ABA was the culprit of this stress profile, and the ratios between ABA and the growth hormones auxin and cytokinin suggest this to be true (Figure 3.22). Considering that auxin and cytokinin are both positive effectors of TOR activity (Barrada et al., 2015) and levels of these phytohormones are low in the *mtn1-1mtn2-1* unopened floral buds (Figure 3.21), this large ABA ratio may be the basis for causing stress in an MTA background resulting in TOR activity to decrease.

3.4.2 MTA pressure induces the switch from cell proliferation to endoreduplication due to a stalled cell cycle

The regulation of two key checkpoints of the cell cycle is critical in determining whether cell division may proceed. Both the G_1 and G_2 checkpoints are gatekeepers of the continuation of the cell cycle and the eventual completion of cytokinesis. As previously described, the decision of a cell not to divide depends on whether there is a limited abundance of the relevant cell cycle markers at each checkpoint; CYCD for G_1/S and CYCB for G_2/M (Boudolf et al., 2004; del Pozo et al., 2006; Ahmad et al., 2019). The expression of these markers via reporters is one facet in evaluating the progression of the cell cycle. As such, it appears that MTA accumulation does not affect the entry into the cell cycle as both *CYCD3;1* and *CYCD3;3* expression are not affected by exogenous feeding of MTA in *mtn1-1* seedlings (Figure 3.7).

Both CYCDs bind to CDKA;1 and phosphorylate RBR in a targeted manner, resulting in the release of E2Fa-DP and E2Fb-DP from the RBR complex (Desvoyes et al., 2006). It is possible that the increase in unphosphorylated S6K due to a reduction in TOR activity may hinder this interaction and prevent entry into the cell cycle (Henriques et al., 2010). This involvement of TOR and S6K would require further investigation to determine the abundance of E2Fa/b in the *mtn1-1mtn2-1* background. These factors would theoretically accumulate as increased levels of unphosphorylated S6K would prevent the degradation of these factors by specific proteases and restrain cell division (Desvoyes et al., 2006; Henriques et al., 2010; del Pozo et al., 2006). Therefore, the entry into the cell cycle may have been inhibited by MTA however, more work is required to elucidate S6K's effect on restraining E2Fa/b activity at the G_1 checkpoint.

In contrast, there is strong evidence to suggest that MTA impairs the cell cycle at the G_2 checkpoint and prevents cells from entering cell division. The decrease in *CYCB1;2* expression (Figure 3.8) correlates with the reduction in cell numbers of the meristematic zone during exogenous feeding of MTA (Figure 3.4). The inability of cells to proliferate severely limits the growth capacity of the roots and the overall plant. Given this evidence, cells enter the cell cycle only to be stalled at the G_2 checkpoint by MTA accumulation.

The inhibition of meristematic cell proliferation by MTA is consistent with the induction of the endocycle. The upregulation of *SMR4* expression (Figure 3.9) with respect to the TOR-YAK1 mechanism also inhibits CDK activity. One downstream target CDKs is E2Fc (del Pozo et al., 2006). The resulting phosphorylation of E2Fc by CDK leads to its degradation and prevents endoreduplication (del Pozo et al., 2006). The impairment of CDK activity by increased *SMR4* expression would increase E2Fc levels, thereby actively repressing G_2/M transition cell marker genes and inducing the endocycle (Barrada et al., 2015; del Pozo et al., 2006). *E2Fc* overexpressing mutants suppress *CYCB1;1* and *CYCB1;2* expressions, resulting in cells transitioning to the endocycle (del Pozo et al., 2006). As such, *mtn1-1mtn2-1* rosettes have a much higher endoreduplication index than WT (Figure 3.17), solidifying the idea, cells that experience MTA pressure cannot divide and are stalled at the G_2 checkpoint.

3.4.3 Unexpected growth periodicity of the meristematic zone

The periodicity in root meristematic development was an unexpected outcome of assessing the effects of MTA on cell proliferation (Figure 3.2). There seems to be an intricate back and forth between cell elongation and proliferation in root development as root length increases linearly (Figure 3.19), but the root meristem length consistently changes (Figure 3.2). This is exemplified by the periodicity length of 2 days with WT between peaks compared to 3 days for *mtn1-1* just on $MgSO_4$ (Figure 3.2). *mtn1-1* does not accumulate enough MTA to have a substantial effect on root development on $MgSO_4$ (Tremblay, 2019). Nevertheless, there seems to be a subtle physiological difference in this mutant compared to WT seedlings. It is unclear as to the underlying cause of this change as this periodicity in meristem activity has not been characterized in the literature. Vertically grown roots may be influenced by external cues such as touch interaction with other seedlings, thereby changing meristematic growth direction in a process called root skewing (Hu et al., 2021). The increase in cell proliferation along the X and Z planes rather than the Y plane may contribute to the lack of increase in meristematic zone length (Hu et al., 2021). This is a common occurrence in root development, and by measuring the cell velocity as a root grows, a slight periodicity is observed (Hu et al., 2021).

3.4.4 Disruption of root stem cell homeostasis due to impaired cell proliferation and loss of auxin signaling

Since MTA accumulation impairs the cell cycle, the ability to maintain an adequate number of stem cells to produce different initial tissue cells has also been inhibited. Many elements are required to properly develop the apical meristem, all of which lead to maintaining a healthy population of stem cells (García-Gómez et al., 2021). The TOR signaling network responds to intrinsic/extrinsic signals like nutrient availability and stress response to regulate root development (Wu et al., 2019). More specifically, the interconnection between hormonal signaling, cell identity peptides, and regulators of cell division control the differentiation dynamics of the root stem cell niche (Barrada et al., 2015).

Hormones are fundamental cues for regulating cell proliferation, and in the case of auxin, an activator of cell proliferation (Brumos et al., 2018). Generally, an auxin maximum is located at the QC of the root apical meristem while slowly decreasing in concentration moving towards the transition zone (García-Gómez et al., 2021). Thus, forming a concentration gradient correlated with the rate of cell division of the respected root cells (García-Gómez et al., 2021). Exogenous MTA completely abolishes this auxin distribution within the root apical meristem and lacks an auxin maxima at the QC (Figure 3.20). *WOX5* and auxin would normally promote the accumulation of each other in a positive feedback loop at the QC (Gonzali et al., 2005; Di Mambro et al., 2017), but in the case of *mtn1-1* mutants on MTA, auxin was not concentrated at the QC based on *DR5* directed GFP expression (Figure 3.20).

Furthermore, high auxin concentrations would normally induce cell division at the root apical meristem, but *WOX5* indirectly maintains a quiescent state at the QC by inhibiting *CYCD3;3* expression early in root development (Forzani et al., 2014). In agreement with low *DR5* expression at the QC, *mtn1-1* seedlings also consistently maintain high *CYCD3;3* expression (Figure 3.7), increasing columella layers (Figure 3.5) even though cell proliferation is still inhibited at the G_2 checkpoint under MTA pressure. Hence, MTA accumulation has compromised root stem cell homeostasis in a cumulative manner as both cell proliferation of the meristematic zone has been impaired and auxin signaling is disrupted.

Given that polar auxin transport towards the QC is essential in maintaining an auxin maxima (Michniewicz et al., 2007), it is possible that the poor auxin transport seen in the *mtn1-1mtn2-1* rosette leaves translates to a defective polar transport in the root (Waduwara-Jayabahu et al., 2012). This additional mechanism may also inhibit the normal regulation of *WOX5* in MTN-deficient mutants resulting in misregulation of auxin and *CYCD3;3*. In addition, the diffuse *DR5* expression pattern (Figure 3.20) suggests that PIN localization and activity have been altered due to MTA toxicity, requiring further investigation.

3.4.5 Systematic repression of growth with increasing MTA

The TOR signaling network is widely considered the regulatory hub of managing the growth of plants. Even so, there are many other factors other than TOR that need to be considered. With respect to MTA toxicity, previous research characterized many systemic abnormalities associated with high MTA content in the unopened floral buds. Many of these systematic changes begin with the abnormalities of the metabolome, leading to the deprivation of important sulfur-containing metabolites like Cys, Met, and SAM (Tremblay, 2019). From here, dramatic changes to the methylome result in transcriptional changes in pathways related to stress, cell proliferation, and reproductivity (Tremblay, 2019).

By monitoring the growth of the MTN-deficient mutants, it is quite clear that increased MTA accumulation correlates with abnormal phenotypes, and the systematic changes observed in some of these pathways directly relate with MTA phenotypes. For example, *mtn1-1mtn2-1* seedlings exhibit very few developmental problems as they do not meet a theoretical threshold of MTN activity resulting in the accumulation of MTA, translating to very few trends in the transcriptome (Tremblay, 2019). Once the MTA threshold is surpassed in the rosette leaves (Waduwara-Jayabahu et al., 2012), additional developmental problems arise. Many vegetative phenotypes of *mtn1-1mtn2-1* are quite distinct from *mtn1-1* and *mtn1-1mtn2-5*, where the highest MTA content they encounter is only a fraction of *mtn1-1mtn2-1* (Waduwara-Jayabahu et al., 2012; Tremblay, 2019). The significant delay in the growth of *mtn1-1mtn2-1* is attributed to the lack of cell proliferation (Figure 3.17) and the changes in the phytohormone profile of rosette leaves

(Figure 3.21). Auxin and cytokinin levels are reduced considerably in this background, limiting the proliferation potential and delaying the vegetative growth of *mtn1-1mtn2-1*.

The developmental decision to transition to reproductive growth is also quite delayed in *mtn1-1mtn2-1* (Figure 3.11). There are three reasons why this may be. One of which is the loss of proliferation potential at the shoot apex slowing the development of a visible inflorescence stem. This would suggest that the shoot apical meristem has morphologically changed in preparation for bolting an inflorescence stem. Another possible cause is the interference of the CLAVATA/WUSCHEL negative feedback loop due to the change in phytohormones. MTA has inhibited cytokinin biosynthesis (Figure 3.21*b*) due to the lack of adenine produced by the MTN breakdown of MTA. This substantial loss of cytokinins in *mtn1-1mtn2-1* decreases the abundance of WUS in the shoot apical meristem, while a decrease in auxin (Figure 3.21*a*) limits *CLV3* expression. The lack of stem cells due to decreased *WUS* expression and the inability to differentiate due to a reduction in CLV3 would collectively disrupt shoot apical meristem maintenance and delay the transition to flowering.

The final possible explanation is the lack of transitional players in the shoot apical meristem including, FT, *SOC1*, and LFY. FLOWERING LOCUS C (FLC) would normally repress these elements, but in the Col-0 background, a non-functional *FRIGIDA* gene due to a naturally occurring deletion results in low FLC levels (Deng et al., 2011; Shindo et al., 2005). The abnormal vascular development in *mtn1-1mtn2-1* may hinder the transport of FT from the rosette leaves to the shoot apical meristem. It is also possible that the transport of FT from phloem companion cells, where it is translated, to phloem sieve tubes via the plasmodesmata has been impaired by the accumulation of callose resulting from increased stress responses in the *mtn1-1mtn2-1* background. Additionally, SOC1 transcriptionally activates *LFY* though, LFY's interaction with WUS is required to promote the transition to flowering (Lee and Lee, 2010).

Another piece of evidence implicating an impaired shoot apical meristem is the inconsistent internode lengths in the *mtn1-1mtn2-1* inflorescence stem (Figure 3.14). In this case, the interaction between *STM* and *BEL1-like* (*BELL*) homeobox genes, *PENNYWISE* (*PNY*), and *POUNDFOOLISH* (*PNF*) regulate early internode patterning events while STM-PNY

interaction promotes meristem formation (Kanrar et al., 2006). The extremely short internodes interspersed with long internodes observed in the *mtn1-1mtn2-1* are consistent with PNY, PNF, and STM mutants (Kanrar et al., 2006). This would also implicate the involvement of STM in the shoot apical meristem phenotypes of MTA toxicity. This would be consistent with the impairment of the CLAVATA/WUSCHEL negative feedback loop as STM inhibits CLV1 activity while also inducing cytokinin biosynthesis (Landrein et al., 2015). The exact mechanism of STM activity suppression by MTA remains unknown.

Several other development defects arise due to MTA accumulation once the plant transitions into reproductive growth (Waduwara-Jayabahu et al., 2012). Here, MTA accumulates a considerable amount in the unopened floral buds compared to seedlings and WT unopened floral buds (Tremblay, 2019). The lack of fertility in the *mtn1-1mtn2-1* mutant can be attributed to both pollen and ovule developmental impairments (Waduwara-Jayabahu et al., 2012). The cause of these impairments is likely hormonal, as both auxin and cytokinin influence pollen and ovule development. The loss of auxin signaling in *mtn1-1mtn2-1* buds resulted in the abnormal ovules observed in previous studies and the poor pollen development and lack of dehiscences in the anthers.

3.4.6 *mtar11* mutation releases the inhibition of growth and reproductivity caused by MTA toxicity

The causative mutation in *mtar11* located in *bZIP29* unlocks the plant's ability to grow during restrictive conditions like the one experienced by MTN-deficient mutants (Figure 3.10 - 3.16). The characterization of this mutation is consistent with the *dkml* mutant as both allow for permissive growth, resulting in plants that produce larger organs (Lozano-Sotomayor et al., 2016). The primary mechanism of suppression seems to be *mtar11*'s interaction with the TOR signaling network. A recent study has identified that interaction between bZIP29 and the TOR complex in Arabidopsis exists within a cell culture (Van Leene et al., 2019). How the TOR complex regulates bZIP29's activity remains unknown. Even so, the *mtar11* mutation may change bZIP29's protein interactions, and thus, this mutation may alter bZIP29s interaction within the TOR signaling network.

There are several pieces of evidence gathered in this study to suggest this mechanism of suppression. First is the recovery of TOR activity in the *mtn1-1mtn2-1mtar11* plant (Figure 3.16), which suggests that bZIP29 is involved in positive feedback interaction with the TOR complex. In this model, TOR activity is reduced due to MTA accumulation by unknown effectors upstream of the signaling network, increasing bZIP29's involvement in suppressing growth. Assuming TOR's activity has been suppressed, bZIP29 reduces growth by its involvement in cell proliferation and further represses TOR activity with its interaction. This feedback loop is disrupted by introducing the *mtar11* mutation in bZIP29. This model only holds if bZIP29 is not involved in sulfur metabolism and stress response, both of which may be the upstream effectors of TOR. There is no evidence that bZIP29 is involved in those mechanism pathways thus far.

Another indication that supports this model is that *mtn1-1mtar11* grows a longer root on a TOR inhibitor, AZD-8055, than WT and *mtn1-1* (Figure 3.18, 3.19). This outcome advocates bZIP29's involvement in restricting growth in a TOR-dependent manner. By disrupting the inhibition of growth by MTA toxicity, *mtar11* mutation rescues both fertility and growth in the *mtn1-1mtn2-1* mutant. Furthermore, the *mtar11* mutation also slightly recovers the abnormal phytohormone profile of *mtn1-1mtn2-1* (Figure 3.21). Again, this is most likely mediated by disrupting the positive feedback loop and recovering TOR activity.

Considering that the *mtar11* mutation is also associated with domesticated species, the disruption of this positive feedback model may have been inadvertently selected by humans. The increase in plant height (Figure 3.12), fruit size, and fertility (Figure 3.13*b*, *c*) of the *mtn1-1mtar11* plants make an amino acid change at the *mtar11* residue more favorable for selection. As such, *mtar11* proved favourability as one mechanism to suppress MTA toxicity.

While the evolutionary significance of the *mtar11* mutation is interesting, an additional unexpected resulted occurred when *mtar11* was introduced into *mtn1-1mtn2-1*. The progeny of *mtn1-1mtn2-1mtar11* plants exhibited evidence of genetic restoration (Lolle et al., 2005; detailed in Appendix A1: Figure A.1). It is likely that the *mtar11* mutation has significantly affected a number of fundamental cellular mechanisms resulting in this very rare event.

Chapter 4

Conclusion

4.1 Amino acid changes in specific genes may be linked to the domestication process of plants

Domestication of plants is a multi-generational process in which humans significantly influence plant life cycles to establish a predictable supply of resources (Zeder, 2015). The domestication of a plant begins after the selection of traits that are favorable to humans. Usually, the initial selection involves genetic changes to genes involved in seed size and yield, plant architecture, and seed dispersal mechanisms. These genetic changes are typically random mutations found in the wild and are selected for during the cultivation of the plant. While the phenotypic traits that separate a domesticated plant from a wild ancestor may be obvious, the genetic differences are subtle, especially early in the process (Olsen and Wendel, 2013). Many domestic populations have also undergone successive natural alterations, resulting in the selection of several variants. However, the domestication traits that initially separated wild and domesticated populations are fixed.

With the understanding of the genetic pathways that control plant traits and combining advanced molecular techniques like genome-wide association studies, several novel signatures of selection have been identified in domesticated plants (Olsen and Wendel, 2013). These studies have revealed various underlying causative changes leading to plant domestication, including amino substitutions, gene duplications, transposon activation, and polyploid (Akhunov et al., 2010; Huang et al., 2012). One of the most interesting aspects of plant domestication is the enrichment of regulatory genes targeted, unknowingly, by human selection and resulting in the propagation of changes throughout the transcriptome (He et al., 2011).

bZIP29 or its homologs are not known as a causative element associated with the domestication of plants. However, after careful characterization of the phenotypes caused by the *mtar11* mutation, it is plausible that *bZIP29* may have been involved in the domestication of certain plants. As stated, a few conditions are required for a gene to be considered a determinate of domestication. The three important ones include altering a gene that causes favorable phenotypes for human selection, mutations are associated with domesticated plant

species, and the gene in question has a broad range of downstream targets. Considering these conditions, I propose that certain protein alterations to bZIP29 and its homologs result in domestication traits, like greater seed yield.

When considering the first condition, it is evident that changes to bZIP29 in Arabidopsis have an apparent positive effect on root growth, seed yield, plant height, and a marginal impact on silique length (Chapter 2; Figure 2.2, 2.3). Two independent lines of evidence confirm this observation. The *dkml* knock-out mutant located in *bZIP29* has similar effects on plant height and silique length (Lozano-Sotomayor et al., 2016), while overexpression of *bZIP29* triggers dominant repression of growth and cell number (Van Leene et al., 2016). Regarding the second condition, careful residue analysis of amino acid changes in 461 homologs of bZIP29 across 173 plant species and 88 domesticated plants, associated amino acid changes like the *mtar11* mutation to domesticated plants (Chapter 2; Figure 2.7). Furthermore, this analysis found several other novel residues which suggest changes at these sites are functionally significant and may result in a domestication trait. By assessing the phylogenetic inheritance of these changes and, more specifically, at the *mtar11* site (Chapter 2; Figure 2.8), it is apparent that the selection of these changes occurred independently of other members of the same taxonomic order. Most likely, resulting in the convergent evolution of domesticated species (Chapter 2; Figure 2.9).

The final consideration is whether or not bZIP29 has a broad range of downstream targets. This condition is based on changes to a single gene resulting in a wide range of positive phenotypic changes associated with domesticated plant species. bZIP29 is a transcription factor that regulates a wide range of genes involved in plant development and cell proliferation (Van Leene et al., 2016). More importantly, it appears that bZIP29 may have a pleiotropic effect on growth based on its interactions with other bZIPs or other proteins. The most significant evidence which associates bZIP29s overall impact on the plant's physiology is the complete genetic dominance of the *mtar11* mutation (Chapter 2; Table 2.4). The influence of a single *mtar11* allele conferring positive growth effects suggests its influence on domestication traits.

4.2 A unifying model bridging the impact of MTA on sulfur metabolism and growth regulation

The results reported in this thesis, and previous investigations of the effects of MTN deficiency, are assembled here into a model to explain the possible effects of MTA accumulation on plant physiology and bridge the gap between sulfur metabolism and plant growth (Figure 4.1). The foundation of this model stems from the identification of the causative *mtar11* mutation in *bZIP29*. Several experiments were derived from the known literature describing bZIP29's function and used to evaluate different aspects of plant development. These experiments ranged from assessing meristem maintenance and cell proliferation in the root, TOR activity in rosette leaves, to plant reproductivity in the *mtn1-1mtn2-1mtar11* mutant. While this model tries to encompass the overall physiological effects of MTA, several tissue or cell-specific effects may be overlooked for the simplicity of the model as MTA pressure differs between tissue types (Waduwara-Jayabahu et al., 2012; Tremblay, 2019). Nevertheless, the significant pathways that implicate sulfur metabolism, TOR growth regulation, meristem maintenance, and phytohormone homeostasis that MTA impacts are depicted in this unifying model.

This model begins with the impact of MTN deficiency on sulfur metabolism as its the primary catalyst of phenotypes associated with MTA accumulation (Figure 4.1*a*). Previous investigations have carefully characterized the effect of MTA accumulation in the severe *mtn1-1mtn2-1* mutant. These studies proposed two direct consequences of MTA accumulation. The first is MTA's feedback inhibition of sulfur assimilation prior to Cys biosynthesis (Tremblay, 2019), and the second, MTA's feedback inhibition of enzyme reactions involving NA, Spd, Spm, and Tspm biosynthesis enzymes (Waduwara-Jayabahu et al., 2012). While the evidence for feedback inhibition of Cys and NA biosynthesis due to MTA pressure is very convincing, the same is not true about polyamine biosynthesis. The effect of a depleted NA pool is quite evident in the phenotypes of the *mtn1-1mtn2-1* mutant, as several tissues of this plant become chlorotic. Interestingly, the *mtar11* mutation does not affect this biochemical pathway as *mtn1-1mtn2-1mtar11* plants are also chlorotic. The lack of sufficient NA levels inhibits the plant's capacity to chelate metal ions from the soil. However, this is unlikely the

primary deterrent of growth due to MTA as *mtn1-1mtn2-1mtar11* is able to overcome this deficiency and recover other phenotypes of *mtn1-1mtn2-1* (e.g., bolting time, fertility).

On the other hand, the depletion of Cys abundance in the unopened apical buds of *mtn1-1mtn2-1* has a significant ripple effect on both Met and SAM levels, resulting in a depleted amino acid pool (Figure 4.1*a*). Tremblay (2019) proposed that sulfur flux away from Cys biosynthesis was instead used to produce GLS. A recent study suggested a retrograde flow of sulfur from GLS back to Cys production during sulfur deprivation (Sugiyama et al., 2021). It is unclear how *mtar2* affects this flux change, as this mutation does not deter IAA production from the overaccumulation of GLS (Chapter 3; Figure 3.20).

Unfortunately, the impairment of sulfur metabolism due to MTA fails to implicate the growth defects of *mtn1-1mtn2-1* directly. This missing link suggests that a global mechanism like the TOR signaling network is directly involved in sensing the impairments of sulfur metabolism and restraining growth accordingly (Forzani and Meyer, 2019). Therefore, the second major component of this model incorporates the TOR signaling network and seeks to describe the majority of growth defects resulting from MTA accumulation (Figure 4.1*b*). This component of the model is supported as TOR activity in *mtn1-1mtn2-1* is less than half of WT based on S6K phosphorylation (Chapter 3; Figure 3.16). Furthermore, the *mtar11* mutation in *mtn1-1mtn2-1* not only recovers TOR activity but significantly increases over 1.5 fold ($p < 0.05$) compared to WT (Chapter 3; Figure 3.16).

This remarkable increase of TOR activity in *mtn1-1mtn2-1mtar11* presents an interesting hypothesis, the negative growth regulation due to reduced TOR activity in MTN-deficient mutants is due to a novel interaction between bZIP29 and the TOR complex (Figure 4.1*c*). I propose that the decrease of TOR activity in *mtn1-1mtn2-1* increases bZIP29's involvement in suppressing growth and restricting TOR activity via its feedback interaction (Figure 4.1*c*). This hypothesis was initially tested by growing *mtn1-1mtar11* seedlings on a TOR activity inhibitor, AZD-8055, resulting in longer seedling length than WT and *mtn1-1* (Chapter 3; Figure 3.18, 3.19). Therefore, most of the inhibition of growth due to MTA accumulation is attributed to a decrease in TOR activity with bZIP29 as a significant contributor to restricting plant growth.
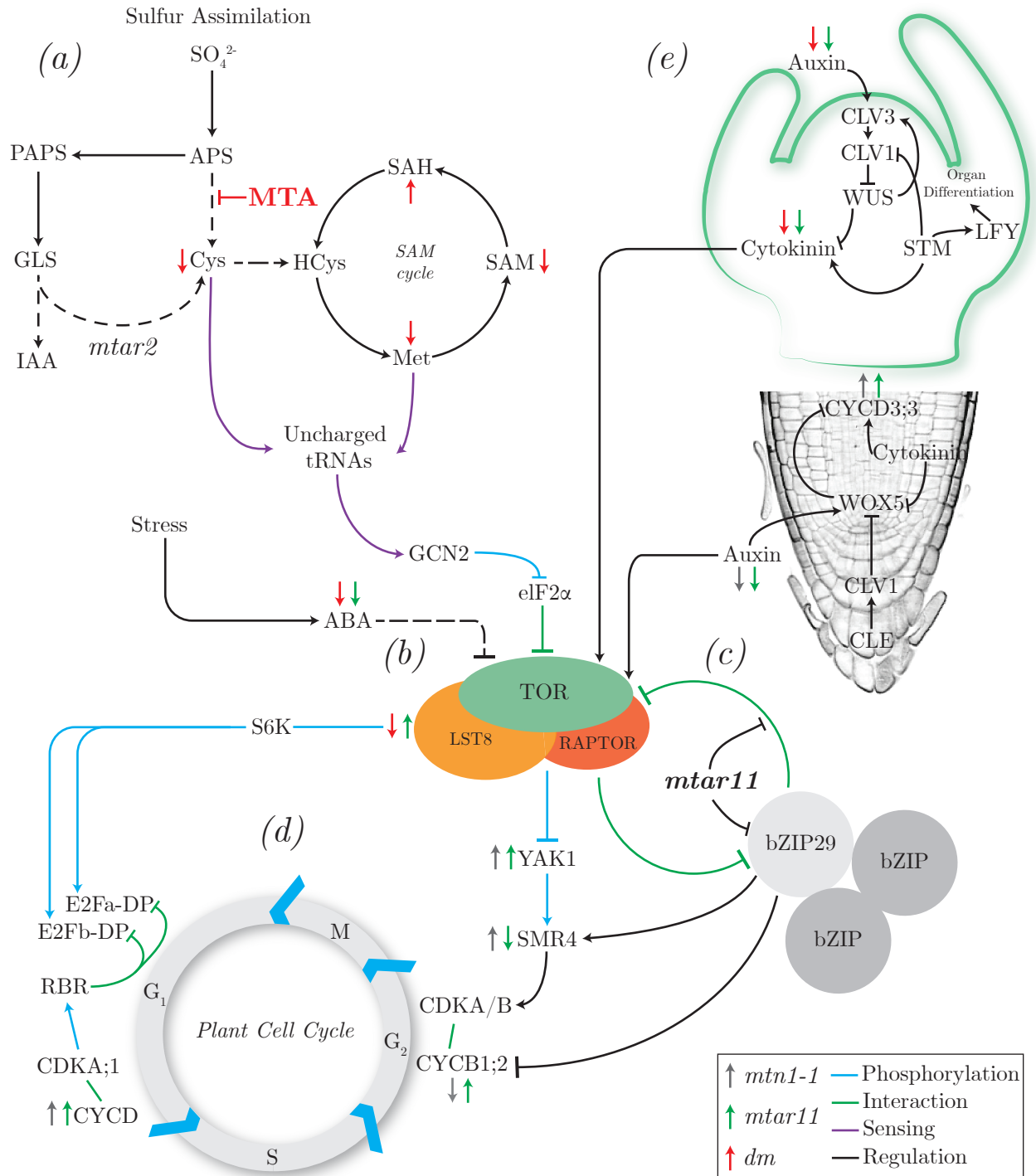
Figure 4.1: Unifying model for the impact of MTA accumulation on sulfur metabolsim and plant growth.

In *(a)*, MTA reprograms sulfur assimilation by changing sulfur flux away from Cys and Met biosynthesis towards PAPS and GLS production. The lack of Cys and Met biosynthesis contributes to the pool of uncharged tRNAs that GCN2 recognizes and phosphorylates eIF2α.

Figure 4.1 *(previous page)*: **Unifying model for the impact of MTA accumulation on sulfur metabolsim and plant growth.**

The TOR complex senses the upstream effectors like ABA from stress and amino acid deficiency from GCN2 and regulates its activity based on those signals *(b)*. MTA suppresses TOR activity via amino acid deficiency and increases in ABA stress. Part of TOR's response is its feedback interaction with bZIP29 in a theorized bZIP regulatory hub *(c)*. MTA pressure stalls cells at the G_2 checkpoint with bZIP29 and TOR downstream factors regulating the cell cycle *(d)*. MTA accumulation changes the phytohormone profiles auxin and cytokinin, resulting in loss of meristem homeostasis *(e)*. Arrows depicting relative changes were plotted for *mtn1-1*, *mtn1-1mtar11* (*mtar11*), and *mtn1-1mtn2-1* (*dm*). These changes are relative to WT.

One weakness of this proposed model is the lack of an explanation for how the TOR network senses the impairments of sulfur metabolism with increased MTA pressure. I propose that the amino acid deficiency in the *mtn1-1mtn2-1* plants due to their impaired sulfur metabolism is the likely link to the impaired TOR signaling network. There is evidence that GCN2 kinase is involved in sensing uncharged tRNAs due to reduced amino acid metabolism. GCN2's only target in Arabidopsis is eIF2α, and upon the accumulation and binding of uncharged tRNAs to GCN2, eIF2α is phosphorylated and results in the dissociation of the ribosomal complex, and translation ceases (Li et al., 2013; Zhang et al., 2008). Additionally, GCN2 is also a sensor of both nitrogen and carbon precursors of Cys (Dong et al., 2017). It is noteworthy to point out that TOR tightly regulates the dissociation and biogenesis of ribosomes, and thus, GCN2's phosphorylation of eIF2α and eIF2α's interaction with TOR is likely key in communicating the impairments of sulfur metabolism due to MTA accumulation.

Another aspect of MTA accumulation is the significant decrease in cell proliferation of MTN-deficient roots and rosette leaves (Figure 4.1*d*). MTA accumulation does not affect the cell's ability to enter the cell but significantly affects the G_2 checkpoint. The reduction in *CYCB1;2* expression of *mtn1-1* seedlings on MTA growth media suggests that cells stall at the G_2/M phase transition (Chapter 3; Figure 3.8). It seems that the primary pathway preventing cell division in the presence of MTA pressure is the TOR-YAK1 cell cycle control axis. Under low TOR activity, YAK1 induces the activity of SMR4 (Chapter 3; Figure 3.9), which in turn inhibits CDKB activity and prevents cells from transitioning to the mitotic phase. When *mtn1-1* seedlings are grown on media with MTA as the sole sulfur source, a significant decrease in root length occurs due to the MTA pressure. Adding a YAK1 enzyme

inhibitor, proINDY, to this media not only suppresses the short root phenotype of *mtn1-1* but also reduces the lateral root growth (Chapter 3; Figure 3.18). In addition, the loss of S6K phosphorylation due to the loss of TOR activity may prevent the disassociation of the E2Fa/b factors from the RBR complex (Henriques et al., 2010), resulting in an additional mechanism of inhibition of cell proliferation under MTA pressure (Figure 4.1*d*). A consequence of an impaired cell cycle is the induction of the endocycle. As such, *mtn1-mtn2-1* plants have an increased endoreduplication index (Chapter 3; Figure 3.17), signifying that cells that experience MTA pressure become stalled.

MTA accumulation also inhibits meristem maintenance exhibited by the slow transition from vegetative to reproductive growth in the shoot apical meristem of *mtn1-1mtn2-1* and the loss of stem cell homeostasis in the root apical meristem of *mtn1-1* in the presence of MTA. Auxin significantly upregulates *CLV3* transcription in the shoot apical meristem and *WOX5* in the root apical meristem, while WUS systematically suppresses auxin signaling in the central zone of the shoot apical meristem (Figure 4.1*e*; Ma et al., 2019). On the other hand, cytokinin induces the expression of *WUS* in the shoot and suppresses the expression of *WOX5* in the root apical meristem (Figure 4.1*e*; Luo et al., 2018). While an auxin maxima is required for the proper function of the root apical meristem, an increase in auxin concentration is detrimental to the shoot apical meristem (Pfeiffer et al., 2016).

Auxin measurements in the unopened apical buds of *mtn1-1mtn2-1* mutants reveal that the low auxin is not the reason for the abnormal phenotypes stemming from the shoot apical meristem (Chapter 3; Figure 3.21). Instead, the lack of cytokinin content at the shoot apical meristem is the likely culprit. The lack of concentrated cytokinin in the central zone of the shoot meristem would reduce *WUS* expression and disrupt the positive feedback loop used to sustain its expression (Figure 4.1*e*). By limiting its expression in the *mtn1-1mtn2-1*, stem cells within the central zone would theoretically differentiate prematurely, increasing the number of rosette leaves, flowers, and bushy plant architecture (Ma et al., 2019; Chapter 3; Figure 3.11, 3.14). Furthermore, the decrease in abundance of both auxin and cytokinin in the unopened buds of *mtn1-1mtn2-1* inhibits the normal development of male and female productive organs resulting in the substantial loss of fertility (Chapter 3; Figure 3.13).

In the root apical meristem, the lack of an auxin maximum in *mtn1-1* seedlings when grown on MTA media results in the loss of stem cell homeostasis. Auxin is vital in maintaining *WOX5* expression, but in MTN-deficient mutants, the loss of *WOX5* expression due to no auxin maxima results in the abolishment of a quiescent state at the QC (Chapter 3; Figure 3.20). In normal conditions, WOX5 would maintain a quiescent state by limiting *CYCD3;3* expression and cell division at the root apical meristem (Figure 4.1*e*). The increase in *CYCD3;3* in the root apical meristem of *mtn1-1* is evidence of decreased *WOX5* expression in MTN-deficient seedlings (Chapter 3; Figure 3.7).

The phytohormone profile provided unexpected insight into the stressed physiological state suggested by previous transcriptomic studies of the effects of MTA pressure (Tremblay, 2019) is a result of heightened ratios of ABA to the growth of phytohormones, auxin, and cytokinin (Chapter 3; Figure 3.22). While the concentration of ABA in *mtn1-1mtn2-1* unopened buds is sustainably lower than WT (Chapter 3; Figure 3.21), it does not necessarily indicate the plant is not experiencing stress. In this case, both auxin and cytokinin levels are much lower than ABA, resulting in a high ABA ratio (Chapter 3; Figure 3.21). This heightened ratio may suggest a stress signal in the plant and likely negatively affect TOR activity.

The component that unifies this model is *mtar11*, specifically the function of bZIP29 in plant development (Figure 4.1*c*). Unfortunately, this model fails to encompass the plethora of processes associated with bZIP29. This transcription factor targets genes involved in stress and osmosensory responses and regulates several core cell cycle genes (Van Leene et al., 2016). bZIP29 has many interactions with other proteins and bZIP transcription factors resulting in a pleiotropic function in plant development. In fact, an argument can be made regarding bZIP functioning within a large regulatory complex independent of the TOR regulatory hub, given the substantial number of protein-protein and protein-DNA interactions associated with bZIPs (Figure 4.1*c*). For this study, only the effect of the *mtar11* mutation on bZIP29's function in cell proliferation and its interaction with the TOR network was investigated under MTA pressure. This functional characterization of the *mtar11* mutation revealed that the *mtar11* releases the inhibition of growth and reproductively caused by MTA accumulation.

4.3 Future Analyses

Two additional directions could further the bioinformatic analysis of amino changes and their association with domesticated plant species. The first is to assess if mutations to a gene that produces no advantageous phenotypes (i.e., plant growth, seed yield) are associated with domesticated species. This analysis would function as a negative control and determine if this pipeline is correctly tuned where only significant changes that separate wild and domesticated species are identified. The location of the *mtar2* mutation in NSP1 would be one locus that can be tested as no advantageous phenotypes have been characterized in that plant under normal conditions. By using bZIP29 as a proof of concept, novel genetic signatures can be identified, providing a genetic explanation as to why certain plant species are domesticated. This second direction would extend beyond a single locus and involve assessing genomic signatures across multiple genomes and their association with domesticated traits.

In order to advance the investigation into the effects of MTA accumulation on plant physiology, four additional directions could be taken. The first is identifying and characterizing the remaining *mtars*; this includes *mtar5*, *mtar8*, and *mtar10*. The causative mutation in *mtar8* is located in *CLV1* though, the mechanism of suppression has yet to be characterized. Surprisingly, *mtar8* suppresses specific abnormal phenotypes of *mtn1-1mtn2-1* and restores fertility. More work is required to identify the causative mutation in *mtar10* but the likely SNP involved is located in *PP2A subunit A3* (AT1G13320), which is involved in ABA signaling and regulation of phosphorylation. The *mtar5* SNP is located in *ABA3* (AT1G16540), which catalyzes the final step in ABA biosynthesis and is involved in sulfur mobilization in plants. More work is required to prove the SNP in *ABA3* is the causative mutation in *mtar5*. Both of these mutations in ABA-related genes may reduce the stress response associated with MTA accumulation. The characterization of these mechanisms of suppression will further add to the explanation of MTA accumulation and contribute to the model proposed in Figure 4.1.

The next direction involves conducting a transcriptomic experiment with the *mtn1-1mtn2-1mtar11* to uncover novel physiological pathways that have changed due to the *mtar11* mutation. This should be done in unopened flower buds to match previous RNA-seq

experiments, and other data gather in this work involving unopened buds. The stress profile in the previous RNA-seq experiments likely masked some of the direct effects of MTA. Thus, using a less stressed genetic background in *mtn1-1mtn2-1mtar11*, additional novel pathways may be discovered. In addition, a metabolomics study would support findings in this study as well as the RNA-seq experiment. This metabolomics study is currently underway with the help of collaborators, Drs. Neil Emery and Anna Kisiała (Trent University, Peterborough, Canada).

The third direction is to continue to explore the possible upstream effectors of TOR which are sensitive to MTA accumulation, resulting in the loss of TOR activity in the *mtn1-1mtn2-1* mutant. One avenue that is currently being undertaken involves characterizing the effects of a T-DNA insertion in GCN2. By knocking out GCN2 activity in *mtn1-1mtn2-1*, eIF2α is unable to communicate with the TOR complex about the lack of amino acids and disrupted ribosome biogenesis in this MTN-deficient mutant. This disconnect in communicating a lack of amino acids would theoretically leave TOR activity unaffected in *mtn1-1mtn2-1* and thus, attenuate some of the negative growth phenotypes associated with MTA accumulation.

The final avenue which requires further investigation is the genetic restoration of the WT MTN2 allele in *mtn1-1mtn2-1mtar11* plants. This homozygous mutant produced progeny that replaced the *mtn2-1* mutant allele with a WT copy of *MTN2*. This investigation would aim to determine if the restoration of the *MTN2* allele is due to genetic restoration proposed by Lolle et al. (2005) or via outcrossing. *gl1-1*, a stable recessive visible marker, was introduced to the *mtn1-1mtn2-1mtar11* background by a former Senior Honors Thesis student to assess if outcrossing occurs in this background (Simpson, 2021). This visible marker would be absent in the progeny of plants that relied on outcrossing. Furthermore, attempts should be made to find and identify the RNA cache that facilitated this non-mendelian inheritance of *MTN2*. The search for the RNA cache requires the correct tissue type and assay to detect it accurately. Unfortunately, recent attempts to locate the RNA cache have been unsuccessful.

Bibliography

Abe, M., Kosaka, S., Shibuta, M., Nagata, K., Uemura, T., Nakano, A., and Kaya, H. (2019). Transient activity of the florigen complex during the floral transition in *Arabidopsis thaliana*. *Development*, 146(7).

Ahmad, Z., Magyar, Z., Bögre, L., and Papdi, C. (2019). Cell cycle control by the target of rapamycin signalling pathway in plants. *J. Exp. Bot.*, 70(8):2275–2284.

Akhunov, E. D., Akhunova, A. R., Anderson, O. D., Anderson, J. A., Blake, N., Clegg, M. T., Coleman-Derr, D., Conley, E. J., Crossman, C. C., Deal, K. R., Dubcovsky, J., Gill, B. S., Gu, Y. Q., Hadam, J., Heo, H., Huo, N., Lazo, G. R., Luo, M.-C., Ma, Y. Q., Matthews, D. E., McGuire, P. E., Morrell, P. L., Qualset, C. O., Renfro, J., Tabanao, D., Talbert, L. E., Tian, C., Toleno, D. M., Warburton, M. L., You, F. M., Zhang, W., and Dvorak, J. (2010). Nucleotide diversity maps reveal variation in diversity among wheat genomes and chromosomes. *BMC Genomics*, 11(1):702.

An, H., Roussot, C., Suarez-Lopez, P., Corbesier, L., Vincent, C., Pineiro, M., Hepworth, S., Mouradov, A., Justin, S., Turnbull, C., and Coupland, G. (2004). CONSTANS acts in the phloem to regulate a systemic signal that induces photoperiodic flowering of *Arabidopsis*. *Development*, 131(15):3615–3626.

Anderson, G. H., Veit, B., and Hanson, M. R. (2005). The *Arabidopsis AtRaptor* genes are essential for post-embryonic plant growth. *BMC Biol.*, 3(1):12.

Araki, S., Ito, M., Soyano, T., Nishihama, R., and Machida, Y. (2004). Mitotic cyclins stimulate the activity of c-Myb-like factors for transactivation of G2/M phase-specific genes in tobacco. *J. Biol. Chem.*, 279(31):32979–32988.

Ashihara, H., Stasolla, C., Fujimura, T., and Crozier, A. (2018). Purine salvage in plants. *Phytochemistry*, 147:89–124.

Augstein, F. and Carlsbecker, A. (2018). Getting to the Roots: A Developmental Genetic View of Root Anatomy and Function From *Arabidopsis* to Lycophytes .

Barbosa, I. C. R., Hammes, U. Z., and Schwechheimer, C. (2018). Activation and Polarity Control of PIN-FORMED Auxin Transporters by Phosphorylation. *Trends Plant Sci.*, 23(6):523–538.

Barrada, A., Djendli, M., Desnos, T., Mercier, R., Robaglia, C., Montané, M.-H., and Menand, B. (2019). A TOR-YAK1 signaling axis controls cell cycle, meristem activity and plant growth in *Arabidopsis*. *Development*, 146(3):dev171298.

Barrada, A., Montané, M.-H., Robaglia, C., and Menand, B. (2015). Spatial Regulation of Root Growth: Placing the Plant TOR Pathway in a Developmental Perspective. *Int. J. Mol. Sci.*, 16(8):19671–19697.

Bednarek, P., Piślewska-Bednarek, M., Svatoš, A., Schneider, B., Doubský, J., Mansurova, M., Humphry, M., Consonni, C., Panstruga, R., Sanchez-Vallet, A., Molina, A., and Schulze-Lefert, P. (2009). A Glucosinolate Metabolism Pathway in Living Plant Cells Mediates Broad-Spectrum Antifungal Defense. *Science (80-.).*, 323(5910):101 LP – 106.

Bekele, F. and Phillips-Mora, W. (2019). Cacao (*Theobroma cacao* L.) Breeding. In Al-Khayri, J. M., Jain, S. M., and Johnson, D. V., editors, *Adv. Plant Breed. Strateg. Ind. Food Crop.*, pages 409–487. Springer International Publishing, Cham.

Bencivenga, S., Simonini, S., Benková, E., and Colombo, L. (2012). The Transcription Factors BEL1 and SPL Are Required for Cytokinin and Auxin Signaling During Ovule Development in *Arabidopsis*. *Plant Cell*, 24(7):2886 LP – 2897.

Benfey, P. N. and Scheres, B. (2000). Root development. *Curr. Biol.*, 10(22):R813–5.

Berkopec, A. (2007). HyperQuick algorithm for discrete hypergeometric distribution. *J. Discret. Algorithms*, 5(2):341–347.

Bhagavan, N. and Ha, C.-E. (2015). *Essentials of Medical Biochemistry*. Academic Press, Cambridge, Massachusettes, USA, 2nd edition.

Blázquez, M. A. and Weigel, D. (2000). Integration of floral inductive signals in *Arabidopsis*. *Nature*, 404(6780):889–892.

Blom, N., Gammeltoft, S., and Brunak, S. (1999). Sequence and structure-based prediction of eukaryotic protein phosphorylation sites. *J. Mol. Biol.*, 294(5):1351–1362.

Boudolf, V., Vlieghe, K., Beemster, G. T. S., Magyar, Z., Torres Acosta, J. A., Maes, S., Van Der Schueren, E., Inzé, D., and De Veylder, L. (2004). The plant-specific cyclin-dependent kinase CDKB1;1 and transcription factor E2Fa-DPa control the balance of mitotically dividing and endoreduplicating cells in *Arabidopsis*. *Plant Cell*, 16(10):2683–2692.

Brand, U., Fletcher, J. C., Hobe, M., Meyerowitz, E. M., and Simon, R. (2000). Dependence of Stem Cell Fate in *Arabidopsis* on a Feedback Loop Regulated by *CLV3* Activity. *Science (80-.).*, 289(5479):617 LP – 619.

Broad Institute (2019). Picard tools. `http://broadinstitute.github.io/picard/`.

Brumos, J., Robles, L. M., Yun, J., Vu, T. C., Jackson, S., Alonso, J. M., and Stepanova, A. N. (2018). Local Auxin Biosynthesis Is a Key Regulator of Plant Development. *Dev. Cell*, 47(3):306–318.e5.

Brunkard, J. O., Xu, M., Scarpin, M. R., Chatterjee, S., Shemyakina, E. A., Goodman, H. M., and Zambryski, P. (2020). TOR dynamically regulates plant cell–cell transport. *Proc. Natl. Acad. Sci.*, 117(9):5049 LP – 5058.

Bulankova, P., Akimcheva, S., Fellner, N., and Riha, K. (2013). Identification of *Arabidopsis* Meiotic Cyclins Reveals Functional Diversification among Plant Cyclin Genes. *PLOS Genet.*, 9(5):e1003508.

Burkart, G. M. and Brandizzi, F. (2021). A Tour of TOR Complex Signaling in Plants. *Trends Biochem. Sci.*, 46(5):417–428.

Bürstenbinder, K., Rzewuski, G., Wirtz, M., Hell, R., and Sauter, M. (2007). The role of methionine recycling for ethylene synthesis in *Arabidopsis*. *Plant J.*, 49(2):238–249.

Bürstenbinder, K., Waduwara, I., Schoor, S., Moffatt, B. A., Wirtz, M., Minocha, S. C., Oppermann, Y., Bouchereau, A., Hell, R., and Sauter, M. (2010). Inhibition of 5'-methylthioadenosine metabolism in the Yang cycle alters polyamine levels, and impairs seedling growth and reproduction in *Arabidopsis*. *Plant J.*, 62(6):977–88.

Capella-Gutiérrez, S., Silla-Martínez, J. M., and Gabaldón, T. (2009). trimAl: a tool for automated alignment trimming in large-scale phylogenetic analyses. *Bioinformatics*, 25(15):1972–1973.

Capra, J. A. and Singh, M. (2007). Predicting functionally important residues from sequence conservation. *Bioinformatics*, 23(15):1875–1882.

Cardarelli, M. and Cecchetti, V. (2014). Auxin polar transport in stamen formation and development: how many actors?

Chaïr, H., Traore, R. E., Duval, M. F., Rivallan, R., Mukherjee, A., Aboagye, L. M., Van Rensburg, W. J., Andrianavalona, V., Pinheiro de Carvalho, M. A. A., Saborio, F., Sri Prana, M., Komolong, B., Lawac, F., and Lebot, V. (2016). Genetic diversification and dispersal of taro (*Colocasia esculenta* (l.) schott). *PLOS ONE*, 11(6):1–19.

Cheng, Y., Dai, X., and Zhao, Y. (2006). Auxin biosynthesis by the YUCCA flavin monooxygenases controls the formation of floral organs and vascular tissues in *Arabidopsis*. *Genes Dev.*, 20(13):1790–1799.

Cingolani, P., Patel, V. M., Coon, M., Nguyen, T., Land, S. J., Ruden, D. M., and Lu, X. (2012). Using Drosophila melanogaster as a Model for Genotoxic Chemical Mutational Studies with a New Program, SnpSift. *Front. Genet.*, 3:35.

Clark, S. E., Jacobsen, S. E., Levin, J. Z., and Meyerowitz, E. M. (1996). The *CLAVATA* and *SHOOT MERISTEMLESS* loci competitively regulate meristem activity in *Arabidopsis*. *Development*, 122(5):1567–1575.

Clark, S. E., Williams, R. W., and Meyerowitz, E. M. (1997). The *CLAVATA1* Gene Encodes a Putative Receptor Kinase That Controls Shoot and Floral Meristem Size in *Arabidopsis*. *Cell*, 89(4):575–585.

Clay, N. K. and Nelson, T. (2005). *Arabidopsis thickvein* Mutation Affects Vein Thickness and Organ Vascularization, and Resides in a Provascular Cell-Specific Spermine Synthase Involved in Vein Definition and in Polar Auxin Transport. *Plant Physiol.*, 138(2):767 LP – 777.

Coen, E. S. and Meyerowitz, E. M. (1991). The war of the whorls: genetic interactions controlling flower development. *Nature*, 353(6339):31–37.

Collins, C., Maruthi, N. M., and Jahn, C. E. (2015). CYCD3 D-type cyclins regulate cambial cell proliferation and secondary growth in *Arabidopsis*. *J. Exp. Bot.*, 66(15):4595–4606.

Crooks, G. E., Hon, G., Chandonia, J.-M., and Brenner, S. E. (2004). WebLogo: a sequence logo generator. *Genome Res.*, 14(6):1188–1190.

Cucinotta, M., Di Marzo, M., Guazzotti, A., de Folter, S., Kater, M. M., and Colombo, L. (2020). Gynoecium size and ovule number are interconnected traits that impact seed yield. *J. Exp. Bot.*, 71(9):2479–2489.

Curie, C., Panaviene, Z., Loulergue, C., Dellaporta, S. L., Briat, J.-F., and Walker, E. L. (2001). Maize yellow stripe1 encodes a membrane protein directly involved in Fe(III) uptake. *Nature*, 409(6818):346–349.

del Pozo, J. C., Diaz-Trivino, S., Cisneros, N., and Gutierrez, C. (2006). The Balance between Cell Division and Endoreplication Depends on E2FC-DPB, Transcription Factors Regulated by the Ubiquitin-SCF^{SKP2A} Pathway in *Arabidopsis*. *Plant Cell*, 18(9):2224 LP – 2235.

Deng, W., Ying, H., Helliwell, C. A., Taylor, J. M., Peacock, W. J., and Dennis, E. S. (2011). FLOWERING LOCUS C (FLC) regulates development pathways throughout the life cycle of *Arabidopsis*. *Proc. Natl. Acad. Sci. U. S. A.*, 108(16):6680–6685.

Deprost, D., Truong, H.-N., Robaglia, C., and Meyer, C. (2005). An *Arabidopsis* homolog of RAPTOR/KOG1 is essential for early embryo development. *Biochem. Biophys. Res. Commun.*, 326(4):844–850.

Desvoyes, B., Ramirez-Parra, E., Xie, Q., Chua, N.-H., and Gutierrez, C. (2006). Cell Type-Specific Role of the Retinoblastoma/E2F Pathway during *Arabidopsis* Leaf Development. *Plant Physiol.*, 140(1):67 LP – 80.

Di Mambro, R., De Ruvo, M., Pacifici, E., Salvi, E., Sozzani, R., Benfey, P. N., Busch, W., Novak, O., Ljung, K., Di Paola, L., Marée, A. F. M., Costantino, P., Grieneisen, V. A., and Sabatini, S. (2017). Auxin minimum triggers the developmental switch from cell division to cell differentiation in the *Arabidopsis* root. *Proc. Natl. Acad. Sci.*, 114(36):E7641 LP – E7649.

Dolan, L., Janmaat, K., Willemsen, V., Linstead, P., Poethig, S., Roberts, K., and Scheres, B. (1993). Cellular organisation of the *Arabidopsis thaliana* root. *Development*, 119(1):71–84.

Dong, P., Xiong, F., Que, Y., Wang, K., Yu, L., Li, Z., and Maozhi, R. (2015). Expression profiling and functional analysis reveals that TOR is a key player in regulating photosynthesis and phytohormone signaling pathways in *Arabidopsis* .

Dong, Y., Silbermann, M., Speiser, A., Forieri, I., Linster, E., Poschet, G., Allboje Samami, A., Wanatabe, M., Sticht, C., Teleman, A. A., Deragon, J.-M., Saito, K., Hell, R., and Wirtz, M. (2017). Sulfur availability regulates plant growth via glucose-TOR signaling. *Nat. Commun.*, 8(1):1174.

Dreyfus, C., Lemaire, D., Mari, S., Pignol, D., and Arnoux, P. (2009). Crystallographic snapshots of iterative substrate translocations during nicotianamine synthesis in archaea. *Proc. Natl. Acad. Sci.*, 106(38):16180 LP – 16184.

Eddy, S. R. (2004). Where did the BLOSUM62 alignment score matrix come from? *Nat. Biotechnol.*, 22(8):1035–1036.

Edgar, R. C. (2010). Search and clustering orders of magnitude faster than BLAST. *Bioinformatics*, 26(19):2460–2461.

Endrizzi, K., Moussian, B., Haecker, A., Levin, J. Z., and Laux, T. (1996). *The SHOOT MERISTEMLESS* gene is required for maintenance of undifferentiated cells in *Arabidopsis* shoot and floral meristems and acts at a different regulatory level than the meristem genes *WUSCHEL* and *ZWILLE*. *Plant J.*, 10(6):967–979.

Evangelou, M., Rendon, A., Ouwehand, W. H., Wernisch, L., and Dudbridge, F. (2012). Comparison of Methods for Competitive Tests of Pathway Analysis. *PLoS One*, 7(7):e41018.

Forzani, C., Aichinger, E., Sornay, E., Willemsen, V., Laux, T., Dewitte, W., and Murray, J. A. H. (2014). WOX5 suppresses CYCLIN D activity to establish quiescence at the center of the root stem cell niche. *Curr. Biol.*, 24(16):1939–1944.

Forzani, C., Duarte, G. T., Van Leene, J., Clément, G., Huguet, S., Paysant-Le-Roux, C., Mercier, R., De Jaeger, G., Leprince, A.-S., and Meyer, C. (2019). Mutations of the AtYAK1 Kinase Suppress TOR Deficiency in *Arabidopsis*. *Cell Rep.*, 27(12):3696–3708.e5.

Forzani, C. and Meyer, C. (2019). Exploring the nine realms of TOR. *Nat. Plants*, 5(3):251–252.

García-Gómez, M. L., Garay-Arroyo, A., García-Ponce, B., Sánchez, M. d. l. P., and Álvarez-Buylla, E. R. (2021). Hormonal Regulation of Stem Cell Proliferation at the *Arabidopsis thaliana* Root Stem Cell Niche .

Gidda, S. K., Miersch, O., Levitin, A., Schmidt, J., Wasternack, C., and Varin, L. (2003). Biochemical and molecular characterization of a hydroxyjasmonate sulfotransferase from *Arabidopsis thaliana*. *J. Biol. Chem.*, 278(20):17895–17900.

Gigolashvili, T. and Kopriva, S. (2014). Transporters in plant sulfur metabolism. *Front. Plant Sci.*, 5:442.

Gonzali, S., Novi, G., Loreti, E., Paolicchi, F., Poggi, A., Alpi, A., and Perata, P. (2005). A turanose-insensitive mutant suggests a role for WOX5 in auxin homeostasis in *Arabidopsis thaliana*. *Plant J.*, 44(4):633–645.

He, Z., Zhai, W., Wen, H., Tang, T., Wang, Y., Lu, X., Greenberg, A. J., Hudson, R. R., Wu, C.-I., and Shi, S. (2011). Two Evolutionary Histories in the Genome of Rice: the Roles of Domestication Genes. *PLOS Genet.*, 7(6):e1002100.

Henriques, R., Magyar, Z., Monardes, A., Khan, S., Zalejski, C., Orellana, J., Szabados, L., de la Torre, C., Koncz, C., and Bögre, L. (2010). *Arabidopsis* S6 kinase mutants display chromosome instability and altered RBR1–E2F pathway activity. *EMBO J.*, 29(17):2979–2993.

Hesse, H. and Hoefgen, R. (2003). Molecular aspects of methionine biosynthesis. *Trends Plant Sci.*, 8(6):259–262.

Higuchi, M., Pischke, M. S., Mähönen, A. P., Miyawaki, K., Hashimoto, Y., Seki, M., Kobayashi, M., Shinozaki, K., Kato, T., Tabata, S., Helariutta, Y., Sussman, M. R., and Kakimoto, T. (2004). *In planta* functions of the *Arabidopsis* cytokinin receptor family. *Proc. Natl. Acad. Sci. U. S. A.*, 101(23):8821 LP – 8826.

Hirotsu, N., Murakami, N., Kashiwagi, T., Ujiie, K., and Ishimaru, K. (2010). Protocol: a simple gel-free method for SNP genotyping using allele-specific primers in rice and other plant species. *Plant Methods*, 6(1):12.

Hu, Y., Omary, M., Hu, Y., Doron, O., Hoermayer, L., Chen, Q., Megides, O., Chekli, O., Ding, Z., Friml, J., Zhao, Y., Tsarfaty, I., and Shani, E. (2021). Cell kinetics of auxin transport and activity in *Arabidopsis* root growth and skewing. *Nat. Commun.*, 12(1):1657.

Huang, X., Zhao, Y., Wei, X., Li, C., Wang, A., Zhao, Q., Li, W., Guo, Y., Deng, L., Zhu, C., Fan, D., Lu, Y., Weng, Q., Liu, K., Zhou, T., Jing, Y., Si, L., Dong, G., Huang, T., Lu, T., Feng, Q., Qian, Q., Li, J., and Han, B. (2012). Genome-wide association study of flowering time and grain yield traits in a worldwide collection of rice germplasm. *Nat. Genet.*, 44(1):32–39.

Hyodo, H. and Tanaka, K. (1986). Inhibition of 1-Aminocyclopropane-l-carboxylic Acid Synthase Activity by Polyamines, Their Related Compounds and Metabolites of S-adenosylmethionine. *Plant Cell Physiol.*, 27(3):391–398.

Hyodo, H., Yamakawa, S., Takeda, Y., Tsuduki, M., Yokota, A., Nishitani, K., and Kohchi, T. (2003). Active gene expression of a xyloglucan endotransglucosylase/hydrolase gene, *XTH9*, in inflorescence apices is related to cell elongation in *Arabidopsis thaliana*. *Plant Mol. Biol.*, 52(2):473–482.

Imai, A., Akiyama, T., Kato, T., Sato, S., Tabata, S., Yamamoto, K. T., and Takahashi, T. (2004). Spermine is not essential for survival of *Arabidopsis*. *FEBS Lett.*, 556(1-3):148–152.

Imai, A., Hanzawa, Y., Komura, M., Yamamoto, K. T., Komeda, Y., and Takahashi, T. (2006). The dwarf phenotype of the *Arabidopsis acl5* mutant is suppressed by a mutation in an upstream ORF of a *bHLH* gene. *Development*, 133(18):3575–3585.

Inzé, D. and De Veylder, L. (2006). Cell Cycle Regulation in Plant Development. *Annu. Rev. Genet.*, 40(1):77–105.

Iqbal, N., Khan, N. A., Ferrante, A., Trivellini, A., Francini, A., and Khan, M. I. R. (2017). Ethylene Role in Plant Growth, Development and Senescence: Interaction with Other Phytohormones. *Front. Plant Sci.*, 8:475.

Ito, M., Araki, S., Matsunaga, S., Itoh, T., Nishihama, R., Machida, Y., Doonan, J. H., and

Watanabe, A. (2001). G2/M-Phase–Specific Transcription during the Plant Cell Cycle Is Mediated by c-Myb–Like Transcription Factors. *Plant Cell*, 13(8):1891 LP – 1905.

James, G. V., Patel, V., Nordström, K. J. V., Klasen, J. R., Salomé, P. A., Weigel, D., and Schneeberger, K. (2013). User guide for mapping-by-sequencing in *Arabidopsis*. *Genome Biol.*, 14(6):R61.

Kanrar, S., Onguka, O., and Smith, H. M. S. (2006). *Arabidopsis* inflorescence architecture requires the activities of KNOX-BELL homeodomain heterodimers. *Planta*, 224(5):1163–1173.

Kantar, M. B., Nashoba, A. R., Anderson, J. E., Blackman, B. K., and Rieseberg, L. H. (2017). The Genetics and Genomics of Plant Domestication. *Bioscience*, 67(11):971–982.

Kardailsky, I., Shukla, V. K., Ahn, J. H., Dagenais, N., Christensen, S. K., Nguyen, J. T., Chory, J., Harrison, M. J., and Weigel, D. (1999). Activation Tagging of the Floral Inducer *FT*. *Science (80-.).*, 286(5446):1962 LP – 1965.

Katoh, K. and Standley, D. M. (2013). MAFFT multiple sequence alignment software version 7: improvements in performance and usability. *Mol. Biol. Evol.*, 30(4):772–780.

Kim, J. and Guan, K.-L. (2011). Amino Acid Signaling in TOR Activation. *Annu. Rev. Biochem.*, 80(1):1001–1032.

Kinoshita, A. and Richter, R. (2020). Genetic and molecular basis of floral induction in *Arabidopsis thaliana*. *J. Exp. Bot.*, 71(9):2490–2504.

Kinoshita-Tsujimura, K. and Kakimoto, T. (2011). Cytokinin receptors in sporophytes are essential for male and female functions in *Arabidopsis thaliana*. *Plant Signal. Behav.*, 6(1):66–71.

Kobayashi, Y., Kaya, H., Goto, K., Iwabuchi, M., and Araki, T. (1999). A Pair of Related Genes with Antagonistic Roles in Mediating Flowering Signals. *Science (80-.).*, 286(5446):1960 LP – 1962.

Koornneef, M., Hanhart, C. J., and van der Veen, J. H. (1991). A genetic and physiological analysis of late flowering mutants in *Arabidopsis thaliana*. *Mol. Gen. Genet. MGG*, 229(1):57–66.

Krueger, F. (2012). Trim Galore! `https://github.com/FelixKrueger/TrimGalore`.

Lageix, S., Lanet, E., Pouch-Pélissier, M.-N., Espagnol, M.-C., Robaglia, C., Deragon, J.-M., and Pélissier, T. (2008). *Arabidopsis* eIF2α kinase GCN2 is essential for growth in stress conditions and is activated by wounding. *BMC Plant Biol.*, 8:134.

Landrein, B., Kiss, A., Sassi, M., Chauvet, A., Das, P., Cortizo, M., Laufs, P., Takeda, S., Aida, M., Traas, J., Vernoux, T., Boudaoud, A., and Hamant, O. (2015). Mechanical stress contributes to the expression of the *STM* homeobox gene in *Arabidopsis* shoot meristems. *Elife*, 4:e07811.

Lee, J. and Lee, I. (2010). Regulation and function of SOC1, a flowering pathway integrator. *J. Exp. Bot.*, 61(9):2247–2254.

Legris, M., Klose, C., Burgie, E. S., Rojas, C. C. R., Neme, M., Hiltbrunner, A., Wigge, P. A., Schäfer, E., Vierstra, R. D., and Casal, J. J. (2016). Phytochrome B integrates light and temperature signals in *Arabidopsis*. *Science (80-.).*, 354(6314):897 LP – 900.

Leigh, J. W., Lapointe, F.-J., Lopez, P., and Bapteste, E. (2011). Evaluating phylogenetic congruence in the post-genomic era. *Genome Biol. Evol.*, 3:571–587.

Letunic, I. and Bork, P. (2021). Interactive Tree Of Life (iTOL) v5: an online tool for phylogenetic tree display and annotation. *Nucleic Acids Res.*, 49(W1):W293–W296.

Leustek, T., Martin, M. N., Bick, J.-A., and Davies, J. P. (2000). PATHWAYS AND REGULATION OF SULFUR METABOLISM REVEALED THROUGH MOLECULAR AND GENETIC STUDIES. *Annu. Rev. Plant Physiol. Plant Mol. Biol.*, 51:141–165.

Li, H. and Durbin, R. (2009). Fast and accurate short read alignment with Burrows-Wheeler transform. *Bioinformatics*, 25(14):1754–1760.

Li, J., Krichevsky, A., Vaidya, M., Tzfira, T., and Citovsky, V. (2005). Uncoupling of the functions of the *Arabidopsis* VIP1 protein in transient and stable plant genetic transformation by *Agrobacterium*. *Proc. Natl. Acad. Sci. U. S. A.*, 102(16):5733 LP – 5738.

Li, M., AuYeung, W., and Lam, H. (2013). The GCN2 homologue in *Arabidopsis thaliana* interacts with uncharged tRNA and uses *Arabidopsis* eIF2α molecules as direct substrates. *Plant Biol.*, 15(1):13–18.

Li, X., Cai, W., Liu, Y., Li, H., Fu, L., Liu, Z., Xu, L., Liu, H., Xu, T., and Xiong, Y. (2017). Differential TOR activation and cell proliferation in *Arabidopsis* root and shoot apexes. *Proc. Natl. Acad. Sci.*, 114(10):2765–2770.

Li, X. and Zhang, Y. (2016). Suppressor Screens in *Arabidopsis* BT - Plant Signal Transduction: Methods and Protocols. pages 1–8. Springer New York, New York, NY.

Liao, C.-Y., Smet, W., Brunoud, G., Yoshida, S., Vernoux, T., and Weijers, D. (2015). Reporters for sensitive and quantitative measurement of auxin response. *Nat. Methods*, 12(3):207–210.

Lindsey, B. E. r., Rivero, L., Calhoun, C. S., Grotewold, E., and Brkljacic, J. (2017). Standardized Method for High-throughput Sterilization of *Arabidopsis* Seeds. *J. Vis. Exp.*, (128).

Liu, X., Afrin, T., and Pajerowska-Mukhtar, K. M. (2019). *Arabidopsis* GCN2 kinase contributes to ABA homeostasis and stomatal immunity. *Commun. Biol.*, 2(1):302.

Lolle, S. J., Victor, J. L., Young, J. M., and Pruitt, R. E. (2005). *Genome-wide non-mendelian inheritance of extra-genomic information in Arabidopsis*, volume 434.

Lozano-Sotomayor, P., Chávez Montes, R. A., Silvestre-Vañó, M., Herrera-Ubaldo, H., Greco, R., Pablo-Villa, J., Galliani, B. M., Diaz-Ramirez, D., Weemen, M., Boutilier, K., Pereira, A., Colombo, L., Madueño, F., Marsch-Martínez, N., and de Folter, S. (2016). Altered expression of the bZIP transcription factor *DRINK ME* affects growth and reproductive development in *Arabidopsis thaliana*. *Plant J.*, 88(3):437–451.

Luo, L., Zeng, J., Wu, H., Tian, Z., and Zhao, Z. (2018). A Molecular Framework for Auxin-Controlled Homeostasis of Shoot Stem Cells in *Arabidopsis*. *Mol. Plant*, 11(7):899–913.

Ma, Y., Miotk, A., Šutiković, Z., Ermakova, O., Wenzl, C., Medzihradszky, A., Gaillochet, C., Forner, J., Utan, G., Brackmann, K., Galván-Ampudia, C. S., Vernoux, T., Greb, T., and Lohmann, J. U. (2019). WUSCHEL acts as an auxin response rheostat to maintain apical stem cells in *Arabidopsis*. *Nat. Commun.*, 10(1):5093.

Mair, A., Pedrotti, L., Wurzinger, B., Anrather, D., Simeunovic, A., Weiste, C., Valerio, C., Dietrich, K., Kirchler, T., Nägele, T., Vicente Carbajosa, J., Hanson, J., Baena-González, E., Chaban, C., Weckwerth, W., Dröge-Laser, W., and Teige, M. (2015). SnRK1-triggered switch of bZIP63 dimerization mediates the low-energy response in plants. *Elife*, 4:e05828.

Massonnet, C., Tisné, S., Radziejwoski, A., Vile, D., De Veylder, L., Dauzat, M., and Granier, C. (2011). New insights into the control of endoreduplication: endoreduplication could be driven by organ growth in *Arabidopsis* leaves. *Plant Physiol.*, 157(4):2044–2055.

Masubelele, N. H., Dewitte, W., Menges, M., Maughan, S., Collins, C., Huntley, R., Nieuwland, J., Scofield, S., and Murray, J. A. H. (2005). D-type cyclins activate division in the root apex to promote seed germination in *Arabidopsis*. *Proc. Natl. Acad. Sci.*, 102(43):15694 LP – 15699.

Mayer, K. F. X., Schoof, H., Haecker, A., Lenhard, M., Jürgens, G., and Laux, T. (1998). Role of WUSCHEL in Regulating Stem Cell Fate in the *Arabidopsis* Shoot Meristem. *Cell*, 95(6):805–815.

McCready, K., Spencer, V., and Kim, M. (2020). The Importance of TOR Kinase in Plant Development. *Front. Plant Sci.*, 11:16.

McKenna, A., Hanna, M., Banks, E., Sivachenko, A., Cibulskis, K., Kernytsky, A., Garimella, K., Altshuler, D., Gabriel, S., Daly, M., and DePristo, M. A. (2010). The Genome Analysis Toolkit: a MapReduce framework for analyzing next-generation DNA sequencing data. *Genome Res.*, 20(9):1297–1303.

McKim, S. M. (2020). Moving on up – controlling internode growth. *New Phytol.*, 226(3):672–678.

Menand, B., Desnos, T., Nussaume, L., Berger, F., Bouchez, D., Meyer, C., and Robaglia, C. (2002). Expression and disruption of the *Arabidopsis* TOR (target of rapamycin) gene. *Proc. Natl. Acad. Sci.*, 99(9):6422 LP – 6427.

Michniewicz, M., Zago, M. K., Abas, L., Weijers, D., Schweighofer, A., Meskiene, I., Heisler, M. G., Ohno, C., Zhang, J., Huang, F., Schwab, R., Weigel, D., Meyerowitz, E. M., Luschnig, C., Offringa, R., and Friml, J. (2007). Antagonistic Regulation of PIN Phosphorylation by PP2A and PINOID Directs Auxin Flux. *Cell*, 130(6):1044–1056.

Miyazaki, J. H. and Yang, S. F. (1987). The methionine salvage pathway in relation to ethylene and polyamine biosynthesis. *Physiol. Plant.*, 69(2):366–370.

Mizuno, D., Higuchi, K., Sakamoto, T., Nakanishi, H., Mori, S., and Nishizawa, N. K. (2003). Three Nicotianamine Synthase Genes Isolated from Maize Are Differentially Regulated by Iron Nutritional Status. *Plant Physiol.*, 132(4):1989 LP – 1997.

Mondal, S., Das, Y. B., and Chatterjee, S. P. (1996). Methionine production by microorganisms. *Folia Microbiol. (Praha).*, 41(6):465–472.

Montané, M.-H. and Menand, B. (2013). ATP-competitive mTOR kinase inhibitors delay plant growth by triggering early differentiation of meristematic cells but no developmental patterning change. *J. Exp. Bot.*, 64(14):4361–4374.

Moreau, M., Azzopardi, M., Clément, G., Dobrenel, T., Marchive, C., Renne, C., Martin-Magniette, M.-L., Taconnat, L., Renou, J.-P., Robaglia, C., and Meyer, C. (2012). Mutations in the *Arabidopsis* Homolog of LST8/GβL, a Partner of the Target of Rapamycin Kinase, Impair Plant Growth, Flowering, and Metabolic Adaptation to Long Days. *Plant Cell*, 24(2):463 LP – 481.

Murashige, T. and Skoog, F. (1962). A Revised Medium for Rapid Growth and Bio Assays with Tobacco Tissue Cultures. *Physiol. Plant.*, 15(3):473–497.

Musielak, T. J., Schenkel, L., Kolb, M., Henschen, A., and Bayer, M. (2015). A simple and versatile cell wall staining protocol to study plant reproduction. *Plant Reprod.*, 28(3):161–169.

Nimchuk, Z. L., Tarr, P. T., Ohno, C., Qu, X., and Meyerowitz, E. M. (2011). Plant stem cell signaling involves ligand-dependent trafficking of the CLAVATA1 receptor kinase. *Curr. Biol.*, 21(5):345–352.

Noir, S., Marrocco, K., Masoud, K., Thomann, A., Gusti, A., Bitrian, M., Schnittger, A., and Genschik, P. (2015). The Control of *Arabidopsis thaliana* Growth by Cell Proliferation and Endoreplication Requires the F-Box Protein FBL17. *Plant Cell*, 27(5):1461–1476.

Oh, S.-I., Park, J., Yoon, S., Kim, Y., Park, S., Ryu, M., Nam, M. J., Ok, S. H., Kim, J.-K., Shin, J.-S., and Kim, K.-N. (2008). The *Arabidopsis* calcium sensor calcineurin B-like 3 inhibits the 5'-methylthioadenosine nucleosidase in a calcium-dependent manner. *Plant Physiol.*, 148(4):1883–1896.

Ok, S. H., Cho, J. H., Oh, S.-I., Choi, M. N., Ma, J.-Y., Shin, J.-S., and Kim, K.-N. (2015). Calcineurin B-like 3 calcium sensor associates with and inhibits 5'-methylthioadenosine nucleosidase 2 in *Arabidopsis*. *Plant Sci.*, 238:228–240.

Okada, K., Ueda, J., Komaki, M. K., Bell, C. J., and Shimura, Y. (1991). Requirement of the Auxin Polar Transport System in Early Stages of *Arabidopsis* Floral Bud Formation. *Plant Cell*, 3(7):677 LP – 684.

O'Leary, B. M., Oh, G. G. K., Lee, C. P., and Millar, A. H. (2020). Metabolite Regulatory Interactions Control Plant Respiratory Metabolism via Target of Rapamycin (TOR) Kinase Activation[OPEN]. *Plant Cell*, 32(3):666–682.

Olsen, K. M. and Wendel, J. F. (2013). A Bountiful Harvest: Genomic Insights into Crop Domestication Phenotypes. *Annu. Rev. Plant Biol.*, 64(1):47–70.

Park, S.-Y., Fung, P., Nishimura, N., Jensen, D. R., Fujii, H., Zhao, Y., Lumba, S., Santiago, J., Rodrigues, A., Chow, T.-f. F., Alfred, S. E., Bonetta, D., Finkelstein, R., Provart, N. J.,

Desveaux, D., Rodriguez, P. L., McCourt, P., Zhu, J.-K., Schroeder, J. I., Volkman, B. F., and Cutler, S. R. (2009). Abscisic Acid Inhibits Type 2C Protein Phosphatases via the PYR/PYL Family of START Proteins. *Science (80-.).*, 324(5930):1068 LP – 1071.

Pattyn, J., Vaughan-Hirsch, J., and Van de Poel, B. (2021). The regulation of ethylene biosynthesis: a complex multilevel control circuitry. *New Phytol.*, 229(2):770–782.

Petersson, S. V., Johansson, A. I., Kowalczyk, M., Makoveychuk, A., Wang, J. Y., Moritz, T., Grebe, M., Benfey, P. N., Sandberg, G., and Ljung, K. (2009). An auxin gradient and maximum in the *Arabidopsis* root apex shown by high-resolution cell-specific analysis of IAA distribution and synthesis. *Plant Cell*, 21(6):1659–1668.

Petricka, J. J., Winter, C. M., and Benfey, P. N. (2012). Control of *Arabidopsis* Root Development. *Annu. Rev. Plant Biol.*, 63(1):563–590.

Pfeiffer, A., Janocha, D., Dong, Y., Medzihradszky, A., Schöne, S., Daum, G., Suzaki, T., Forner, J., Langenecker, T., Rempel, E., Schmid, M., Wirtz, M., Hell, R., and Lohmann, J. U. (2016). Integration of light and metabolic signals for stem cell activation at the shoot apical meristem. *Elife*, 5:e17023.

Pitzschke, A., Djamei, A., Teige, M., and Hirt, H. (2009). VIP1 response elements mediate mitogen-activated protein kinase 3-induced stress gene expression. *Proc. Natl. Acad. Sci.*, 106(43):18414 LP – 18419.

Pommerrenig, B., Feussner, K., Zierer, W., Rabinovych, V., Klebl, F., Feussner, I., and Sauer, N. (2011). Phloem-Specific Expression of Yang Cycle Genes and Identification of Novel Yang Cycle Enzymes in *Plantago* and *Arabidopsis*. *Plant Cell*, 23(5):1904 LP – 1919.

R Core Team (2020). *R: A Language and Environment for Statistical Computing.* R Foundation for Statistical Computing, Vienna, Austria.

Ravanel, S., Block, M. A., Rippert, P., Jabrin, S., Curien, G., Rébeillé, F., and Douce, R. (2004). Methionine Metabolism in Plants. *J. Biol. Chem.*, 279(21):22548–22557.

Ravanel, S., Gakière, B., Job, D., and Douce, R. (1998). The specific features of methionine biosynthesis and metabolism in plants. *Proc. Natl. Acad. Sci.*, 95(13):7805 LP – 7812.

Richard, C., Lescot, M., Inzé, D., and De Veylder, L. (2002). Effect of auxin, cytokinin, and sucrose on cell cycle gene expression in *Arabidopsis thaliana* cell suspension cultures. *Plant Cell. Tissue Organ Cult.*, 69(2):167–176.

Saito, K. (2004). Sulfur Assimilatory Metabolism. The Long and Smelling Road. *Plant Physiol.*, 136(1):2443 LP – 2450.

Samsonová, Z., Kiran, N. S., Novák, O., Spyroglou, I., Skalák, J., Hejátko, J., and Gloser, V. (2020). Steady-State Levels of Cytokinins and Their Derivatives May Serve as a Unique Classifier of *Arabidopsis* Ecotypes. *Plants*, 9(1).

Sarkar, A. K., Luijten, M., Miyashima, S., Lenhard, M., Hashimoto, T., Nakajima, K., Scheres, B., Heidstra, R., and Laux, T. (2007). Conserved factors regulate signalling in *Arabidopsis thaliana* shoot and root stem cell organizers. *Nature*, 446(7137):811–814.

Sauter, M., Moffatt, B., Saechao, M., Hell, R., and Wirtz, M. (2013). Methionine salvage and S-adenosylmethionine: essential links between sulfur, ethylene and polyamine biosynthesis. *Biochem. J.*, 451(2):145–154.

Schneider, C. A., Rasband, W. S., and Eliceiri, K. W. (2012). NIH Image to ImageJ: 25 years of image analysis. *Nat. Methods*, 9(7):671–675.

Schoch, C. L., Ciufo, S., Domrachev, M., Hotton, C. L., Kannan, S., Khovanskaya, R., Leipe, D., Mcveigh, R., O'Neill, K., Robbertse, B., Sharma, S., Soussov, V., Sullivan, J. P., Sun, L., Turner, S., and Karsch-Mizrachi, I. (2020). NCBI Taxonomy: a comprehensive update on curation, resources and tools. *Database (Oxford).*, 2020:baaa062.

Schuler, M., Rellán-Álvarez, R., Fink-Straube, C., Abadía, J., and Bauer, P. (2012). Nicotianamine Functions in the Phloem-Based Transport of Iron to Sink Organs, in Pollen Development and Pollen Tube Growth in *Arabidopsis*. *Plant Cell*, 24(6):2380–2400.

Sekowska, A., Ashida, H., and Danchin, A. (2019). Revisiting the methionine salvage pathway and its paralogues. *Microb. Biotechnol.*, 12(1):77–97.

Shi, B. and Vernoux, T. (2019). Chapter Four - Patterning at the shoot apical meristem and phyllotaxis. In Grossniklaus, U. B. T. C. T. i. D. B., editor, *Plant Dev. Evol.*, volume 131, pages 81–107. Academic Press.

Shi, L., Wu, Y., and Sheen, J. (2018). TOR signaling in plants: conservation and innovation. *Development*, 145(13):dev160887.

Shindo, C., Aranzana, M. J., Lister, C., Baxter, C., Nicholls, C., Nordborg, M., and Dean, C. (2005). Role of FRIGIDA and FLOWERING LOCUS C in Determining Variation in Flowering Time of *Arabidopsis*. *Plant Physiol.*, 138(2):1163–1173.

Simpson, I. (2021). Investigating the elusive cached rna transcript and its role in *MTN2* restoration in *Arabidopsis thaliana* [unpublished undergraduate honors thesis]. Bachelor's thesis, University of Waterloo.

Šimura, J., Antoniadi, I., Široká, J., Tarkowská, D., Strnad, M., Ljung, K., and Novák, O. (2018). Plant Hormonomics: Multiple Phytohormone Profiling by Targeted Metabolomics. *Plant Physiol.*, 177(2):476–489.

Smith, F. W., Ealing, P. M., Hawkesford, M. J., and Clarkson, D. T. (1995). Plant members of a family of sulfate transporters reveal functional subtypes. *Proc. Natl. Acad. Sci. U. S. A.*, 92(20):9373–9377.

Smyth, D. R., Bowman, J. L., and Meyerowitz, E. M. (1990). Early flower development in *Arabidopsis*. *Plant Cell*, 2(8):755–767.

Speiser, A., Silbermann, M., Dong, Y., Haberland, S., Uslu, V. V., Wang, S., Bangash, S. A. K., Reichelt, M., Meyer, A. J., Wirtz, M., and Hell, R. (2018). Sulfur Partitioning between Glutathione and Protein Synthesis Determines Plant Growth. *Plant Physiol.*, 177(3):927 LP – 937.

Stamatakis, A. (2014). RAxML version 8: a tool for phylogenetic analysis and post-analysis of large phylogenies. *Bioinformatics*, 30(9):1312–1313.

Steeves, T. A. and Sussex, I. M. (1989). *Patterns in Plant Development*. Cambridge University Press, Cambridge, 2 edition.

Sugiyama, R., Li, R., Kuwahara, A., Nakabayashi, R., Sotta, N., Mori, T., Ito, T., Ohkama-Ohtsu, N., Fujiwara, T., Saito, K., Nakano, R. T., Bednarek, P., and Hirai, M. Y. (2021). Retrograde sulfur flow from glucosinolates to cysteine in *Arabidopsis*. *Proc. Natl. Acad. Sci.*, 118(22):e2017890118.

Takahashi, H., Kopriva, S., Giordano, M., Saito, K., and Hell, R. (2011). Sulfur Assimilation in Photosynthetic Organisms: Molecular Functions and Regulations of Transporters and Assimilatory Enzymes. *Annu. Rev. Plant Biol.*, 62(1):157–184.

Terceros, G. C., Resentini, F., Cucinotta, M., Manrique, S., Colombo, L., and Mendes, M. A. (2020). The Importance of Cytokinins during Reproductive Development in *Arabidopsis* and Beyond. *Int. J. Mol. Sci.*, 21(21):8161.

Thomson, B., Zheng, B., and Wellmer, F. (2017). Floral Organogenesis: When Knowing Your ABCs Is Not Enough. *Plant Physiol.*, 173(1):56–64.

Torres-Schumann, S., Ringli, C., Heierli, D., Amrhein, N., and Keller, B. (1996). In vitro binding of the tomato bZIP transcriptional activator VSF-1 to a regulatory element that controls xylem-specific gene expression. *Plant J.*, 9(3):283–296.

Traa, A. (2019). Elucidating the Mechanism(s) by which MTA Accumulation May Cause Infertility in *Arabidopsis thaliana* Sulfur Metabolism Mutants [Unpublished undergraduate honors thesis]. Bachelor's thesis, University of Waterloo.

Tremblay, B. J.-M. (2019). Investigating the Impact of 5′-Methylthioadenosine Accumulation in *Arabidopsis thaliana*. Master's thesis, University of Waterloo.

Trivedi, R. and Nagarajaram, H. A. (2019). Amino acid substitution scoring matrices specific to intrinsically disordered regions in proteins. *Sci. Rep.*, 9(1):16380.

Ubeda-Tomás, S., Beemster, G. T. S., and Bennett, M. J. (2012). Hormonal regulation of root growth: integrating local activities into global behaviour. *Trends Plant Sci.*, 17(6):326–331.

Urbancsok, J., Bones, A. M., and Kissen, R. (2017). Glucosinolate-Derived Isothiocyanates Inhibit *Arabidopsis* Growth and the Potency Depends on Their Side Chain Structure. *Int. J. Mol. Sci.*, 18(11):2372.

van den Berg, C., Willemsen, V., Hendriks, G., Weisbeek, P., and Scheres, B. (1997). Short-range control of cell differentiation in the *Arabidopsis* root meristem. *Nature*, 390(6657):287–289.

Van Leene, J., Blomme, J., Kulkarni, S. R., Cannoot, B., De Winne, N., Eeckhout, D., Persiau, G., Van De Slijke, E., Vercruysse, L., Vanden Bossche, R., Heyndrickx, K. S., Vanneste, S., Goossens, A., Gevaert, K., Vandepoele, K., Gonzalez, N., Inzé, D., and De Jaeger, G. (2016). Functional characterization of the *Arabidopsis* transcription factor bZIP29 reveals its role in leaf and root development. *J. Exp. Bot.*, 67(19):5825–5840.

Van Leene, J., Han, C., Gadeyne, A., Eeckhout, D., Matthijs, C., Cannoot, B., De Winne, N., Persiau, G., Van De Slijke, E., Van de Cotte, B., Stes, E., Van Bel, M., Storme, V., Impens, F., Gevaert, K., Vandepoele, K., De Smet, I., and De Jaeger, G. (2019). Capturing the phosphorylation and protein interaction landscape of the plant TOR kinase. *Nat. Plants*, 5(3):316–327.

Van Leene, J., Hollunder, J., Eeckhout, D., Persiau, G., Van De Slijke, E., Stals, H., Van Isterdael, G., Verkest, A., Neirynck, S., Buffel, Y., De Bodt, S., Maere, S., Laukens, K., Pharazyn, A., Ferreira, P. C. G., Eloy, N., Renne, C., Meyer, C., Faure, J.-D., Steinbrenner, J., Beynon, J., Larkin, J. C., Van de Peer, Y., Hilson, P., Kuiper, M., De Veylder, L., Van Onckelen, H., Inzé, D., Witters, E., and De Jaeger, G. (2010). Targeted interactomics reveals a complex core cell cycle machinery in *Arabidopsis thaliana*. *Mol. Syst. Biol.*, 6(1):397.

Veyel, D., Sokolowska, E. M., Moreno, J. C., Kierszniowska, S., Cichon, J., Wojciechowska, I., Luzarowski, M., Kosmacz, M., Szlachetko, J., Gorka, M., Méret, M., Graf, A., Meyer,

E. H., Willmitzer, L., and Skirycz, A. (2018). PROMIS, global analysis of PROtein-metabolite interactions using size separation in *Arabidopsis thaliana*. *J. Biol. Chem.*, 293(32):12440–12453.

Vik, D., Mitarai, N., Wulff, N., Halkier, B. A., and Burow, M. (2018). Dynamic Modeling of Indole Glucosinolate Hydrolysis and Its Impact on Auxin Signaling .

Waduwara-Jayabahu, C. I. (2012). *Significance of Methylthioadenosine Metabolism to Plant Growth and Development*. PhD thesis, University of Waterloo.

Waduwara-Jayabahu, I., Oppermann, Y., Wirtz, M., Hull, Z. T., Schoor, S., Plotnikov, A. N., Hell, R., Sauter, M., and Moffatt, B. A. (2012). Recycling of Methylthioadenosine Is Essential for Normal Vascular Development and Reproduction in *Arabidopsis*. *Plant Physiol.*, 158(4):1728 LP – 1744.

Wang, J., Tian, C., Zhang, C., Shi, B., Cao, X., Zhang, T.-Q., Zhao, Z., Wang, J.-W., and Jiao, Y. (2017a). Cytokinin Signaling Activates WUSCHEL Expression during Axillary Meristem Initiation. *Plant Cell*, 29(6):1373–1387.

Wang, L., Li, H., Zhao, C., Li, S., Kong, L., Wu, W., Kong, W., Liu, Y., Wei, Y., Zhu, J.-K., and Zhang, H. (2017b). The inhibition of protein translation mediated by AtGCN1 is essential for cold tolerance in *Arabidopsis thaliana*. *Plant. Cell Environ.*, 40(1):56–68.

Wang, P., Zhao, Y., Li, Z., Hsu, C.-C., Liu, X., Fu, L., Hou, Y.-J., Du, Y., Xie, S., Zhang, C., Gao, J., Cao, M., Huang, X., Zhu, Y., Tang, K., Wang, X., Tao, W. A., Xiong, Y., and Zhu, J.-K. (2018). Reciprocal Regulation of the TOR Kinase and ABA Receptor Balances Plant Growth and Stress Response. *Mol. Cell*, 69(1):100–112.e6.

Watanabe, M., Chiba, Y., and Hirai, M. Y. (2021). Metabolism and Regulatory Functions of O-Acetylserine, S-Adenosylmethionine, Homocysteine, and Serine in Plant Development and Environmental Responses .

Wirtz, M., Droux, M., and Hell, R. (2004). O-acetylserine (thiol) lyase: an enigmatic enzyme of plant cysteine biosynthesis revisited in *Arabidopsis thaliana*. *J. Exp. Bot.*, 55(404):1785–1798.

Wirtz, M. and Hell, R. (2006). Functional analysis of the cysteine synthase protein complex from plants: Structural, biochemical and regulatory properties. *J. Plant Physiol.*, 163(3):273–286.

Wu, Y., Shi, L., Li, L., Fu, L., Liu, Y., Xiong, Y., and Sheen, J. (2019). Integration of nutrient, energy, light, and hormone signalling via TOR in plants. *J. Exp. Bot.*, 70(8):2227–2238.

Wu, Y., Zhao, Q., Gao, L., Yu, X.-M., Fang, P., Oliver, D. J., and Xiang, C.-B. (2010). Isolation and characterization of low-sulphur-tolerant mutants of *Arabidopsis*. *J. Exp. Bot.*, 61(12):3407–3422.

Xiong, Y., McCormack, M., Li, L., Hall, Q., Xiang, C., and Sheen, J. (2013). Glucose-TOR signalling reprograms the transcriptome and activates meristems. *Nature*, 496(7444):181–186.

Yadegari, R. and Drews, G. N. (2004). Female Gametophyte Development. *Plant Cell*, 16(suppl 1):S133 LP – S141.

Yang, L., Wang, Z., and Hua, J. (2019). Measuring Cell Ploidy Level in *Arabidopsis thaliana* by Flow Cytometry. *Methods Mol. Biol.*, 1991:101–106.

Yang, W., Cortijo, S., Korsbo, N., Roszak, P., Schiessl, K., Gurzadyan, A., Wightman, R., Jönsson, H., and Meyerowitz, E. (2021). Molecular mechanism of cytokinin-activated cell division in *Arabidopsis*. *Science (80-.)*., 371(6536):1350 LP – 1355.

Yi, D., Alvim Kamei, C. L., Cools, T., Vanderauwera, S., Takahashi, N., Okushima, Y., Eekhout, T., Yoshiyama, K. O., Larkin, J., Van den Daele, H., Conklin, P., Britt, A., Umeda, M., and De Veylder, L. (2014). The *Arabidopsis* SIAMESE-RELATED cyclin-dependent kinase inhibitors SMR5 and SMR7 regulate the DNA damage checkpoint in response to reactive oxygen species. *Plant Cell*, 26(1):296–309.

Yuan, W., Guo, S., Gao, J., Zhong, M., Yan, G., Wu, W., Chao, Y., and Jiang, Y. (2017). General Control Nonderepressible 2 (GCN2) Kinase Inhibits Target of Rapamycin Complex 1 in Response to Amino Acid Starvation in *Saccharomyces cerevisiae*. *J. Biol. Chem.*, 292(7):2660–2669.

Zeder, M. A. (2015). Core questions in domestication research. *Proc. Natl. Acad. Sci. U. S. A.*, 112(11):3191–3198.

Zhang, W., Swarup, R., Bennett, M., Schaller, G., and Kieber, J. (2013). Cytokinin Induces Cell Division in the Quiescent Center of the *Arabidopsis* Root Apical Meristem. *Curr. Biol.*, 23(20):1979–1989.

Zhang, Y., Wang, Y., Kanyuka, K., Parry, M. A., Powers, S. J., and Halford, N. G. (2008). GCN2-dependent phosphorylation of eukaryotic translation initiation factor-2α in *Arabidopsis*. *J. Exp. Bot.*, 59(11):3131–3141.

Zhao, Z., Andersen, S. U., Ljung, K., Dolezal, K., Miotk, A., Schultheiss, S. J., and Lohmann, J. U. (2010). Hormonal control of the shoot stem-cell niche. *Nature*, 465(7301):1089–1092.

Zia, A. and Moses, A. M. (2011). Ranking insertion, deletion and nonsense mutations based on their effect on genetic information. *BMC Bioinformatics*, 12:299.

Appendices

A.1 Genetic Restoration

Lolle et al. (2005) observed an unusual restoration rate among Arabidopsis plants harboring homozygous for recessive mutant *HOTHEAD* (*hth*) alleles. These alleles were not present in their parent's genome but were seen in previous generations (Lolle et al., 2005). These plants genetically restored WT alleles from a sequestered source of extra-genomic information. The spontaneous reappearance of WT alleles was driven by a template sequestered in an RNA cache. It was proposed that the genomic information in the form of RNA copies can modify DNA sequences in a template-directed manner (Lolle et al., 2005). It appears that the RNA cache is tapped into during periods of physiological stress brought on by environmental fluctuations or nutrient limitations.

A similar restoration event was observed in the *mtn1-1mtn2-1mtar11* line. After the initial isolation of the *mtn1-1mtn2-1mtar11* from the initial cross of *mtn1-1 $\frac{MTN2}{mtn2-1}$* to *mtn1-1mtar11*, a few cauline leaves from these plants were harvested to confirm their genotypes. Two of these plants had leaves with a WT copy of *MTN2*, indicating that genetic restoration has occurred in this plant line. Unfortunately, these plants were discarded at the time due to the uncertainty of the origin of the tissue (i.e., tissue was collected from the wrong plants).

In order to replicate this restoration event, an *mtn1-1 $\frac{MTN2}{mtn2-1}$ mtar11* plant (Line.3.9) was segregated to find *mtn1-1mtn2-1mtar11* again. The progeny from L3.9 produced 11 *mtn1-1mtn2-1mtar11* plants (Figure A.1*a*). For these 11 plants, newly emerging and old rosette leaves were selected in addition to a cauline leaf. These plants had no restoration events as they were homozygous for all three mutant alleles (i.e., *mtn1-1*, *mtn2-1*, and *mtar11*). Several other cauline leaves were assessed on a single plant in case genomic restoration did not occur in the three original tissue types. However, no restoration was observed as these cauline leaves were *mtn1-1mtn2-1mtar11* (data not shown).

As a final attempt to reproduce our original observation, the progeny of two *mtn1-1mtn2-1mtar11* plants from L3.9 were assessed, L3.9.7 and L3.9.14. The first indication that restoration had occurred in both L3.9.7 and L3.9.14 was the segregation pattern of their progenies. *mtn1-1mtn2-1mtar11* plants have chlorotic true leaves when grown on 1/2MS,

but the phenotype was segregating with several seedlings resembling WT. For the L3.9.14 line, 32 of these seedlings were genotyped for *MTN2*, resulting in a normal segregation ratio of 1:2:1 (Figure A.1*b*). It is evident that the L3.9.14 plant was restored prior to generating these progenies given this ratio.
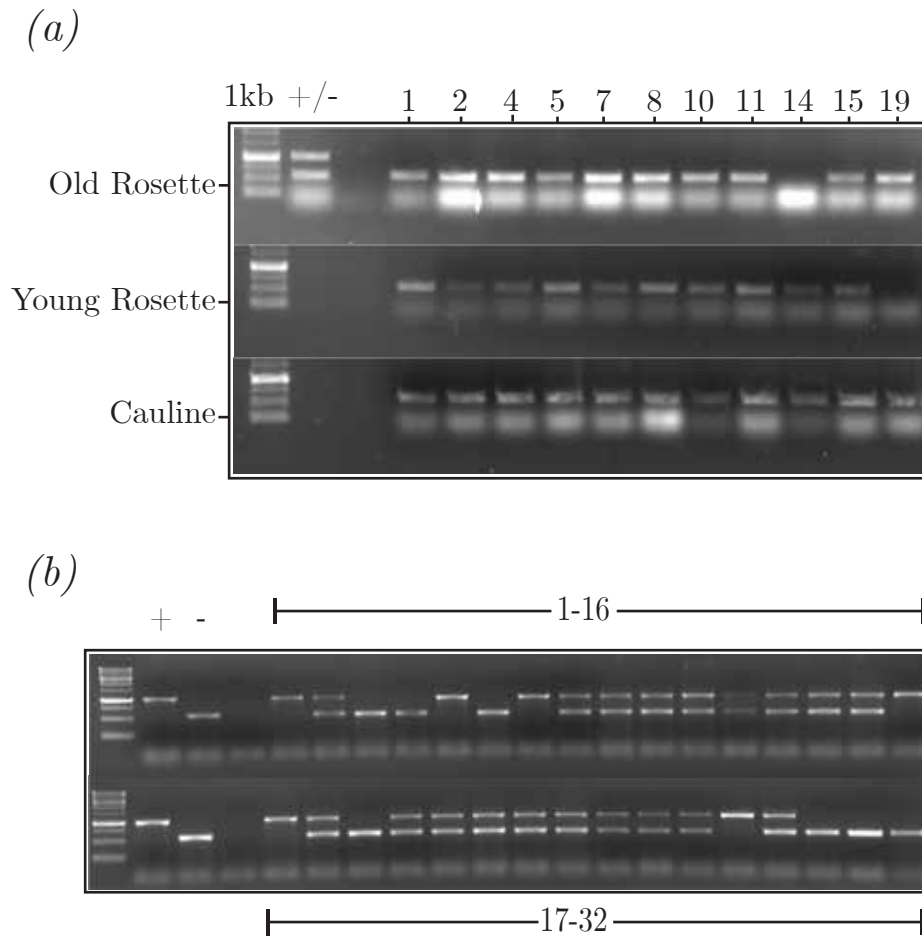
Figure A.1: *MTN2* **PCR results.**

The gel results of the *MTN2* PCR genotyping. The lower band is represents the *mtn2-1* allele while the upper band is the WT allele. In *(a)*, the different leaf tissue of the progeny plants of L3.9. In *(b)*, leaf tissue of young rosettes of L3.9.14.

A.2 Plant species list

Table A 1: Plant species in the curated database of bZIP29 homologs.
Each plant species in the curated database of *bZIP29* homologs was manually classified as either wild (W) or domesticated (D) after a thorough literature search.

Organism	Label	Order	Common Name	Status (W/D)	Reference
Abrus precatorius	*A. precatorius*	Fabales	Rosary Pea	W	`dx.doi.org/10.4103%2Fijccm.IJCCM_320_16`
Acer yangbiense	*A. yangbiense*	Sapindales	Chinese Maple	W	`doi.org/10.1093/gigascience/giz085`
Actinidia chinensis var. chinensis	*A. chinensis var. chinensis*	Ericales	Kiwi	D	`doi.org/10.1016/B978-0-12-803066-0.00004-6`
Actinidia rufa	*A. rufa*	Ericales	Kiwi fruit	W	`doi.org/10.1007/s42161-019-00349-9`

Organism	Label	Order	Common Name	Status (W/D)	Reference
Amborella trichopoda	*A. trichopoda*	Other		W	`www.iucnredlist.org/species/126024907/136825145`
Aquilegia coerulea	*A. coerulea*	Ranunculales	Colorado blue columbine	W	`www.fs.fed.us/wildflowers/beauty/columbines/naturalhistory.shtml`
Arabidopsis lyrata subsp. lyrata	*A. lyrata subsp. lyrata*	Brassicales	Lyre-leaved rock-cress	W	`doi.org/10.1186/1471-2148-10-98`
Arabidopsis thaliana	*A. thaliana*	Brassicales	Thale cress	W	`dx.doi.org/10.1007%2Fs12374-012-0438-7`
Arabis nemorensis	*A. nemorensis*	Brassicales		W	`doi.org/10.1111/j.1526-100X.2010.00668.x`

Organism	Label	Order	Common Name	Status (W/D)	Reference
Arachis duranensis	*A. duranensis*	Fabales		W	`doi.org/10.1038/ng.3517`
Arachis hypogaea	*A. hypogaea*	Fabales	Peanut	D	`doi.org/10.1038/s41588-019-0402-2`
Arachis ipaensis	*A. ipaensis*	Fabales		W	`doi.org/10.1038/ng.3517`
Artemisia annua	*A. annua*	Asterales	Sweet wormwood	D	Journal of Scientific and Industrial Research 59(1):1-11
Beta vulgaris subsp. vulgaris	*B. vulgaris subsp. vulgaris*	Caryophyllales	Sugar beet	D	`doi.org/10.1038/nature12817`
Brassica cretica	*B. cretica*	Brassicales		W	`doi.org/10.1038/sj.hdy.6800027`
Brassica napus	*B. napus*	Brassicales	Rapeseed	D	`doi.org/10.1038/ng.3634`

Organism	Label	Order	Common Name	Status (W/D)	Reference
Brassica oleracea	*B. oleracea*	Brassicales		W	`doi.org/10.1038/ncomms4930`
Brassica oleracea var. oleracea	*B. oleracea var. oleracea*	Brassicales	Cabbage Variety	D	`doi.org/10.1007/s10722-017-0516-2`
Brassica rapa	*B. rapa*	Brassicales	Field Mustard	D	`doi.org/10.1038/ng.3634`
Cajanus cajan	*C. cajan*	Fabales	Pigeon pea	D	`doi.org/10.1038/nbt.2022`
Camelina sativa	*C. sativa*	Brassicales	False flax	D	`doi.org/10.1038/s41598-021-83629-8`
Camellia sinensis	*C. sinensis*	Ericales	Tea tree Camellia	W	`dx.doi.org/10.3389%2Ffpls.2017.02270`
Cannabis sativa	*C. sativa*	Rosales	Marijuana	D	`doi.org/10.1038/s41438-020-0295-3`

Organism	Label	Order	Common Name	Status (W/D)	Reference
Capsella rubella	*C. rubella*	Brassicales	The pink shepherd's-purse	W	`doi.org/10.1038/ng.2669`
Capsicum annuum	*C. annuum*	Solanales	Peppers	D	`doi.org/10.1038/s41438-019-0132-8`
Capsicum baccatum	*C. baccatum*	Solanales	Locoto	D	`doi.org/10.1038/s41438-019-0132-8`
Capsicum chinense	*C. chinense*	Solanales	Habanero pepper	D	`doi.org/10.1038/s41438-019-0132-8`
Carica papaya	*C. papaya*	Brassicales	Papaya	D	`doi.org/10.1038/s41438-019-0205-8`
Carpinus fangiana	*C. fangiana*	Fagales	Hornbeam	W	`doi.org/10.1038/s41597-020-0370-5`
Castanea mollissima	*C. mollissima*	Fagales	Chinese chestnut	D	`doi.org/10.1038/s41467-020-17111-w`

Organism	Label	Order	Common Name	Status (W/D)	Reference
Cephalotus follicularis	*C. follicularis*	Other	Albany pitcher plant	W	`doi.org/10.1111/ 1467-8748.00379`
Chenopodium quinoa	*C. quinoa*	Caryophyllales	Quinoa	D	`doi.org/10.1038/ s41598-018-36693-6`
Cicer arietinum	*C. arietinum*	Fabales	Chickpea	D	`doi.org/10.1111/ nph.14010`
Cinnamomum micranthum f. kanehirae	*C. micranthum*	Other	Stout camphor tree	W	`doi.org/10.1515/ hf-2016-0133`
Citrus x clementina	*C. clementina*	Sapindales	Clementine	D	`doi.org/10.1038/ s41438-019-0195-6`
Citrus sinensis	*C. sinensis*	Sapindales	Sweet Orange	D	`doi.org/10.1038/ s41438-019-0195-6`

Organism	Label	Order	Common Name	Status (W/D)	Reference
Citrus unshiu	*C. unshiu*	Sapindales	Tangerine	D	`doi.org/10.1038/` `s41438-019-0195-6`
Coffea arabica	*C. arabica*	Gentianales	Arabian coffee	D	`doi.org/10.1007/` `s10722-021-01139-y`
Coffea eugenioides	*C. eugenioides*	Gentianales	African Coffee	W	`doi.org/10.1007/` `s004380050965`
Colocasia esculenta	*C. esculenta*	Alismatales	Taro	D	`doi.org/10.1038/` `srep20546`
Corchorus capsularis	*C. capsularis*	Malvales	White jute	D	`doi.org/10.1007/` `s13562-012-0165-7`
Corchorus olitorius	*C. olitorius*	Malvales	Jute mallow	D	`doi.org/10.1007/` `s10722-016-0438-4`
Cucumis melo	*C. melo*	Cucurbitales	Melon	D	`doi.org/10.1038/` `s41438-020-0305-5`

Organism	Label	Order	Common Name	Status (W/D)	Reference
Cucumis melo var. makuwa	*C. melo var. makuwa*	Cucurbitales	Oriental melon	D	`doi.org/10.1038/ s41597-019-0244-x`
Cucumis sativus	*C. sativus*	Cucurbitales	Cucumber	D	`doi.org/10.1111/j. 1365-313x.2012. 05017.x`
Cucurbita maxima	*C. maxima*	Cucurbitales		D	`doi.org/10.1111/ pbi.12860`
Cucurbita moschata	*C. moschata*	Cucurbitales	Crookneck pumpkin	D	`doi.org/10.1111/ pbi.12860`
Cucurbita pepo subsp. pepo	*C. pepo subsp. pepo*	Cucurbitales		D	`doi.org/10.1023/A: 1024464831595`
Cuscuta australis	*C. australis*	Solanales	Australian dotter	W	`doi.org/10.1038/ s41467-018-04721-8`

Organism	Label	Order	Common Name	Status (W/D)	Reference
Cymbidium ensifolium	*C. ensifolium*	Asparagales	Golden-thread orchid	D	`doi.org/10.1038/s41438-018-0052-z`
Cynara cardunculus var. scolymus	*C. cardunculus var. scolymus*	Asterales	Artichoke	D	`doi.org/10.1093/aob/mcm127`
Daucus carota subsp. sativus	*D. carota subsp. sativus*	Other	Carrot	D	`doi.org/10.3390/genes11080906`
Dendrobium catenatum	*D. catenatum*	Asparagales		D	`doi.org/10.1038/s41438-018-0052-z`
Dorcoceras hygrometricum	*D. hygrometricum*	Lamiales		W	`doi.org/10.1073/pnas.1505811112`
Durio zibethinus	*D. zibethinus*	Malvales	Durian	D	`doi.org/10.1038/ng.3972`
Elaeis guineensis	*E. guineensis*	Arecales	Afican oil palm	D	`doi.org/10.1038/nature12309`

Organism	Label	Order	Common Name	Status (W/D)	Reference
Erythranthe guttata	*E. guttata*	Lamiales	Seep monkey flower	W	doi.org/10.1371/ journal.pone. 0101463
Eucalyptus grandis	*E. grandis*	Myrtales	Flooded gum	W	doi.org/10.1038/ nature13308
Eutrema salsugineum	*E. salsugineum*	Brassicales		W	doi.org/10.1073/ pnas.1209954109
Fragaria vesca subsp. vesca	*F. vesca subsp. vesca*	Rosales	Wild strawberry	W	doi.org/10.5073/ JABFQ.2013.086.006
Genlisea aurea	*G. aurea*	Lamiales		W	doi.org/10.1038/ s41598-017-11999-z
Glycine max	*G. max*	Fabales	Soybean	D	doi.org/10.1038/ nbt.3096
Glycine soja	*G. soja*	Fabales	Wild Soybean	W	doi.org/10.1038/ nbt.3096

Organism	Label	Order	Common Name	Status (W/D)	Reference
Gossypium arboreum	_G. arboreum_	Malvales	Tree cotton	D	doi.org/10.1186/ s42397-018-0011-0doi. org/10.1038/hdy. 1954.20
Gossypium aridum	_G. aridum_	Malvales		W	doi.org/10.1038/ng. 2371
Gossypium armourianum	_G. armourianum_	Malvales	Wild cotton	W	doi.org/10.1186/ s42397-018-0011-0
Gossypium australe	_G. australe_	Malvales		W	doi.org/10.1111/ pbi.13249
Gossypium barbadense	_G. barbadense_	Malvales	Sea Island cotton	W	doi.org/10.1111/j. 1525-142X.2008. 00272.x
Gossypium darwinii	_G. darwinii_	Malvales	Darwin's cotton	W	doi.org/10.2307/ 2446640

Organism	Label	Order	Common Name	Status (W/D)	Reference
Gossypium davidsonii	*G. davidsonii*	Malvales		W	`doi.org/10.1038/ng.2371`
Gossypium gossypioides	*G. gossypioides*	Malvales		W	`www.iucnredlist.org/species/71774439/173931754`
Gossypium harknessii	*G. harknessii*	Malvales	San Marcos hibiscus	W	`www.iucnredlist.org/species/71774483/173932153#taxonomy`
Gossypium hirsutum	*G. hirsutum*	Malvales	Upland cotton	D	`doi.org/10.1111/j.1525-142X.2008.00272.x`
Gossypium klotzschianum	*G. klotzschianum*	Malvales		W	`doi.org/10.1038/ng.2371`

Organism	Label	Order	Common Name	Status (W/D)	Reference
Gossypium laxum	*G. laxum*	Malvales		W	`doi.org/10.1038/ng.2371`
Gossypium lobatum	*G. lobatum*	Malvales		W	`www.iucnredlist.org/species/71774683/174152905`
Gossypium mustelinum	*G. mustelinum*	Malvales		W	`dx.doi.org/10.1111%2Fjipb.12084`
Gossypium raimondii	*G. raimondii*	Malvales		W	`doi.org/10.1038/ng.2371`
Gossypium schwendimanii	*G. schwendimanii*	Malvales		W	`dx.doi.org/10.2305/IUCN.UK.2018-1.RLTS.T71774903A71774929.en`

Organism	Label	Order	Common Name	Status (W/D)	Reference
Gossypium tomentosum	*G. tomentosum*	Malvales	Hawaiian cotton	W	`doi.org/10.1002/j.1537-2197.1992.tb13735.x`
Gossypium trilobum	*G. trilobum*	Malvales		W	`www.iucnredlist.org/species/71774980/183188719`
Handroanthus impetiginosus	*H. impetiginosus*	Lamiales	Pink Trumpet Tree	W	`doi.org/10.1093/gigascience/gix125`
Helianthus annuus	*H. annuus*	Asterales	Common Sunflower	D	`doi.org/10.1007/s00122-011-1619-3`
Herrania umbratica	*H. umbratica*	Malvales	Colombian cocoa tree	W	`dx.doi.org/10.2305/IUCN.UK.2020-3.RLTS.T38907A177763193.es`

Organism	Label	Order	Common Name	Status (W/D)	Reference

Hevea brasiliensis	*H. brasiliensis*	Malpighiales	Rubber Tree	D	`doi.org/10.1111/j.`
					`1536-7150.1993.`
					`tb02573.xdoi.org/`
					`10.1016/`
					`0160-9327(77)`
					`90172-7`

Hibiscus syriacus	*H. syriacus*	Malvales	Common Hibiscus	D	`plants.ces.ncsu.`
					`edu/plants/`
					`hibiscus-syriacus/`

Ipomoea nil	*I. nil*	Solanales	Japanese morning glory	D	`doi.org/10.1093/` `jhered/est046`

Ipomoea triloba	*I. triloba*	Solanales	Littlebell	W	`dx.doi.org/10.1371%`
					`2Fjournal.pone.`
					`0062707`

Organism	Label	Order	Common Name	Status (W/D)	Reference
Jatropha curcas	*J. curcas*	Malpighiales	Barbados Nut	W	`doi-org.proxy.lib.uwaterloo.ca/10.1016/j.tplants.2016.08.008`
Juglans regia	*J. regia*	Fagales	Walnut	D	`doi.org/10.1111/tpj.13207`
Kingdonia uniflora	*K. uniflora*	Ranunculales	Kingdonia	W	`doi.org/10.1016/j.isci.2020.101124`
Lactuca saligna	*L. saligna*	Asterales	Willowleaf lettuce	W	`doi.org/10.1038/s41467-017-02445-9`
Lactuca sativa	*L. sativa*	Asterales	Lettuce	D	`doi.org/10.1038/s41467-017-02445-9`
Lupinus albus	*L. albus*	Fabales	White lupin	D	`doi.org/10.1038/s41598-020-76197-w`

Organism	Label	Order	Common Name	Status (W/D)	Reference
Lupinus angustifolius	*L. angustifolius*	Fabales	Narrowleaf lupine	D	`doi.org/10.1038/` `s41598-020-76197-w`
Macleaya cordata	*M. cordata*	Ranunculales	Five-seeded plume-poppy	D	`doi.org/10.1038/` `s41598-018-30560-0`
Malus baccata	*M. baccata*	Rosales	Chinese crab apple	W	`doi.org/10.1038/` `s41588-020-00723-9`
Malus domestica	*M. domestica*	Rosales	Apple	D	`doi.org/10.1038/` `s41588-020-00723-9`
Manihot esculenta	*M. esculenta*	Malpighiales	Cassava	D	`doi.org/10.1073/` `pnas.96.10.5586`
Medicago truncatula	*M. truncatula*	Fabales	Barrel clover	W	`dx.doi.org/10.1105%` `2Ftpc.13.3.458`

Organism	Label	Order	Common Name	Status (W/D)	Reference
Microthlaspi erraticum	*M. erraticum*	Brassicales		W	`doi.org/10.3389/ fpls.2020.00943`
Mikania micrantha	*M. micrantha*	Asterales	Bitter vine	W	`doi.org/10.1038/ s41467-019-13926-4`
Momordica charantia	*M. charantia*	Cucurbitales	Bitter groud	D	`doi.org/10.1038/ s41438-020-0305-5`
Morella rubra	*M. rubra*	Fagales	Chinese bayberry	D	`dx.doi.org/10.1371% 2Fjournal.pone. 0139840`
Morus notabilis	*M. notabilis*	Rosales		W	`doi.org/10.1038/ s41598-017-10079-6`
Mucuna pruriens	*M. pruriens*	Fabales	Velvet bean	D	`doi.org/10.1038/ srep11078`

Organism	Label	Order	Common Name	Status (W/D)	Reference
Musa acuminata subsp. malaccensis	*M. acuminata subsp. malaccensis*	Other	Wild banana	W	`doi.org/10.1006/ anbo.2001.1542`
Nelumbo nucifera	*N. nucifera*	Other	Indian lotus	D	`dx.doi.org/10.1186% 2Fgb-2013-14-5-r41`
Nicotiana attenuata	*N. attenuata*	Solanales	Coyote Tobacco	W	`doi.org/10.1007/ BF02033207`
Nicotiana sylvestris	*N. sylvestris*	Solanales	Woodland tobacco	W	`doi.org/10.1016/j. plantsci.2006.01. 005`
Nicotiana tabacum	*N. tabacum*	Solanales	Tobacco	D	`doi.org/10.1073/ pnas.1813796115`
Nicotiana tomentosiformis	*N. tomentosiformis*	Solanales	Wild Tobacco	W	`doi.org/10.1186/ gb-2013-14-6-r60`

Organism	Label	Order	Common Name	Status (W/D)	Reference
Nymphaea colorata	*N. colorata*	Nymphaeales	Blue petal water lily	D	`doi.org/10.1038/ s41586-019-1852-5`
Nymphaea thermarum	*N. thermarum*	Nymphaeales	Pygmy Rwandan water lily	W	`doi.org/10.1093/ aob/mcu235`
Nyssa sinensis	*N. sinensis*	Other	Chinese tupelo	W	`www.exbury.co.uk/ Nyssa`
Olea europaea var. sylvestris	*O. europaea var. sylvestris*	Lamiales	European olive	W	`doi.org/10.1093/ aob/mcp105`
Papaver somniferum	*P. somniferum*	Ranunculales	Opium Poppy	D	`doi.org/10.1038/ s41438-020-00435-5`
Parasponia andersonii	*P. andersonii*	Rosales		W	`www.theplantlist. org/1.1/browse/A/ Cannabaceae/Trema/`

Organism	Label	Order	Common Name	Status (W/D)	Reference
Phalaenopsis equestris	*P. equestris*	Asparagales	The Horse Phalaenopsis	D	doi.org/10.1038/ng.3149
Phaseolus vulgaris	*P. vulgaris*	Fabales	Common Bean	D	doi.org/10.1038/ng.3008
Phoenix dactylifera	*P. dactylifera*	Arecales	Date palm	D	doi.org/10.1038/ncomms3274
Phtheirospermum japonicum	*P. japonicum*	Lamiales		W	doi.org/10.1038/s42003-020-01143-5
Pistacia vera	*P. vera*	Sapindales	Pistachio	D	doi.org/10.1038/s41598-020-62108-6
Populus alba	*P. alba*	Malpighiales	White poplar	W	doi.org/10.1007/s11295-012-0574-8
Populus euphratica	*P. euphratica*	Malpighiales	Euphrates poplar	D	doi.org/10.1007/s13595-011-0119-6

Organism	Label	Order	Common Name	Status (W/D)	Reference
Populus trichocarpa	*P. trichocarpa*	Malpighiales	Black cottonwood	W	`doi.org/10.1038/ng.3075`
Prosopis alba	*P. alba*	Fabales	White Mesquite	W	`doi.org/10.1093/forestry/cpw032`
Prunus armeniaca	*P. armeniaca*	Rosales	Armenian plum	D	`doi.org/10.1111/mec.13772`
Prunus avium	*P. avium*	Rosales	Sweet cherry	D	`doi.org/10.1038/s41438-020-0281-9`
Prunus dulcis	*P. dulcis*	Rosales	Almond	D	`doi.org/10.1111/mec.12129`
Prunus mume	*P. mume*	Rosales	Chinese plum tree	D	`doi.org/10.1038/s41467-018-04093-z`
Prunus persica	*P. persica*	Rosales	Peach	D	`doi.org/10.1038/ng.2586`

Organism	Label	Order	Common Name	Status (W/D)	Reference
Prunus yedoensis var. nudiflora	*P. yedoensis var. nudiflora*	Rosales	Flowering Cherry Tree	W	`doi.org/10.1016/j.japb.2019.09.006`
Punica granatum	*P. granatum*	Myrtales	Pomegranate	W	`www.ncbi.nlm.nih.gov/pmc/articles/PMC3832175/`
Pyrus ussuriensis x Pyrus communis	*P. ussuriensis x P. communis*	Rosales	Ussurian pear	D	`doi.org/10.1186/s13059-018-1452-y`
Pyrus x bretschneideri	*Pyrus x bretschneideri*	Rosales	Chinese white pear	D	`doi.org/10.1186/s13059-018-1452-y`
Quercus lobata	*Q. lobata*	Fagales	Valley Oak	W	`dx.doi.org/10.2305/IUCN.UK.2017-2.RLTS.T61983021A61983023.en`

Organism	Label	Order	Common Name	Status (W/D)	Reference
Quercus suber	*Q. suber*	Fagales	Cork Oak	D	`dx.doi.org/10.2305/ IUCN.UK.2017-3. RLTS. T194237A2305530.en`
Raphanus sativus	*R. sativus*	Brassicales	Radish	D	`doi.org/10.1038/ srep10835`
Rhamnella rubrinervis	*R. rubrinervis*	Rosales		W	`globalplantcouncil. org/ a-new-evergreen-/ species-of-rhamnac/ eae-found-in-guangxi/`
Rhodamnia argentea	*R. argentea*	Myrtales	Malletwood	W	`apps.des.qld.gov. au/species-search/ details/?id=13402`
Rhododendron simsii	*R. simsii*	Ericales	Indian Azalea	D	`doi.org/10.1038/ s41467-020-18771-4`

Organism	Label	Order	Common Name	Status (W/D)	Reference
Rhododendron williamsianum	*R. williamsianum*	Ericales	Williams rhododen-dron	W	`www.gardendesign.com/rhododendron/species.html`
Ricinus communis	*R. communis*	Malpighiales	Castor bean	D	`doi.org/10.1186/1471-2229-10-13`
Rosa chinensis	*R. chinensis*	Rosales	Chinese Rose	W	`doi.org/10.1038/s41588-018-0110-3`
Salix brachista	*S. brachista*	Malpighiales	Cushion Willow	W	`doi.org/10.1038/s41467-019-13128-y`
Salvia splendens	*S. splendens*	Lamiales	Scarlet sage	D	`doi.org/10.1093/gigascience/giy068`
Senna tora	*S. tora*	Fabales		W	`bioversityinternational.org/news/detail/women-farming-wild-/species-in-west-africa/`

Organism	Label	Order	Common Name	Status (W/D)	Reference
Sesamum indicum	*S. indicum*	Lamiales	Sesame	D	`doi.org/10.1023/A:1025029903549`
Solanum chilense	*S. chilense*	Solanales	Wild tomato	W	`doi.org/10.3390/agronomy10101481`
Solanum lycopersicum	*S. lycopersicum*	Solanales	Tomato	D	`doi.org/10.3390/agronomy10101481`
Solanum tuberosum	*S. tuberosum*	Solanales	Potato	D	`doi.org/10.1073/pnas.1714380114`
Spatholobus suberectus	*S. suberectus*	Fabales		W	`doi.org/10.1038/s41597-019-0110-x`
Spinacia oleracea	*S. oleracea*	Caryophyllales	Spinach	D	`doi.org/10.1038/ncomms15275`
Striga asiatica	*S. asiatica*	Lamiales	Asiatic witchweed	W	`doi.org/10.1017/S0043174500059725`

Organism	Label	Order	Common Name	Status (W/D)	Reference
Striga asiatica	*S. asiatica*	Lamiales	Asiatic witchweed	W	`dx.doi.org/10.1111%` `2Fmpp.12058`
Syzygium oleosum	*S. oleosum*	Myrtales	Blue Cherry	W	`tuckerbush.com.au/` `blue-lilly-pilly-/` `syzygium-oleosum/`
Tamarix hispida	*T. hispida*	Caryophyllales	Kashgar tamarisk	W	`dx.doi.org/10.3390%` `2Fplants9010086`
Tanacetum cinerariifolium	*T. cinerariifolium*	Asterales	Dalmatian chrysanthemum	W	`doi.org/10.1371/` `journal.pone.` `0105265`
Tarenaya hassleriana (Cleome hassleriana)	*T. hassleriana*	Brassicales	Spider flower	W	`dx.doi.org/10.1105%` `2Ftpc.113.113480`
Thalictrum thalictroides	*T. thalictroides*	Ranunculales	Rue anemone	D	`dx.doi.org/10.1073%` `2Fpnas.1203686109`

Organism	Label	Order	Common Name	Status (W/D)	Reference
Theobroma cacao	*T. cacao*	Malvales	Cacao tree	D	`doi.org/10.1038/sj.hdy.6800156`
Trema orientale	*T. orientale*	Rosales	Charcoal-tree	W	`doi.org/10.1038/s41438-020-0295-3`
Trifolium pratense	*T. pratense*	Fabales	Red Clover	D	`doi.org/10.1038/s41598-020-64989-z`
Trifolium subterraneum	*T. subterraneum*	Fabales	Subterranean clover	D	`doi.org/10.1038/srep30358`
Tripterygium wilfordii	*T. wilfordii*	Other	Thunder duke vine	W	`doi.org/10.1038/s41467-020-14776-1`
Vigna angularis	*V. angularis*	Fabales	Adzuki bean	D	`dx.doi.org/10.1534%2Fgenetics.107.078451`
Vigna radiata var. radiata	*V. radiata var. radiata*	Fabales	Mung bean	D	`doi.org/10.1093/aob/mcm048`

Organism	Label	Order	Common Name	Status (W/D)	Reference
Vigna unguiculata	*V. unguiculata*	Fabales	Black-eyed pea	D	`doi.org/10.1038/` `s41598-018-24349-4`
Vitis riparia	*V. riparia*	Vitales	Riverbank Grape	W	`dx.doi.org/10.1093%` `2Faob%2Fmcp298`
Vitis vinifera	*V. vinifera*	Vitales	Common Grape Vine	D	`doi.org/10.1073/` `pnas.1709257114`
Ziziphus jujuba	*Z. jujuba*	Rosales	Jujube	D	`doi.org/10.1371/` `journal.pgen.` `1006433`
Zostera marina	*Z. marina*	Alismatales	Common eelgrass	D	`doi.org/10.1038/` `s41598-017-18782-0`
			Wild Count	85	
			Domesticated Count	88	